Technical Report
916

Volume 2: Appendices A through D

Multifrequency Measurements of Radar Ground Clutter at 42 Sites

Volume 1 contains Principal Results.
Volume 3 contains Appendix E.

J.B. Billingsley
J.F. Larrabee

15 November 1991

Lincoln Laboratory
MASSACHUSETTS INSTITUTE OF TECHNOLOGY
LEXINGTON, MASSACHUSETTS

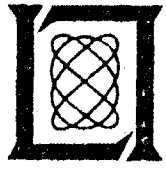

Prepared for the Department of the Air Force
under Contract F19628-90-C-0002.

This report is based on studies performed at Lincoln Laboratory, a center for research operated by Massachusetts Institute of Technology. The work was sponsored by the Department of the Air Force under Contract F19628-90-C-0002.

The ESD Public Affairs Office has reviewed this report, and it is releasable to the National Technical Information Service, where it will be available to the general public, including foreign nationals.

This technical report has been reviewed and is approved for publication.

FOR THE COMMANDER

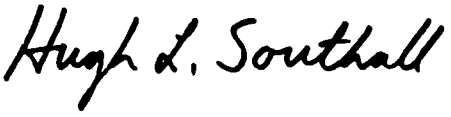

Hugh L. Southall, Lt. Col., USAF
Chief, ESD Lincoln Laboratory Project Office

Non-Lincoln Recipients

PLEASE DO NOT RETURN

Permission is given to destroy this document when it is no longer needed.

DISCLAIMER NOTICE

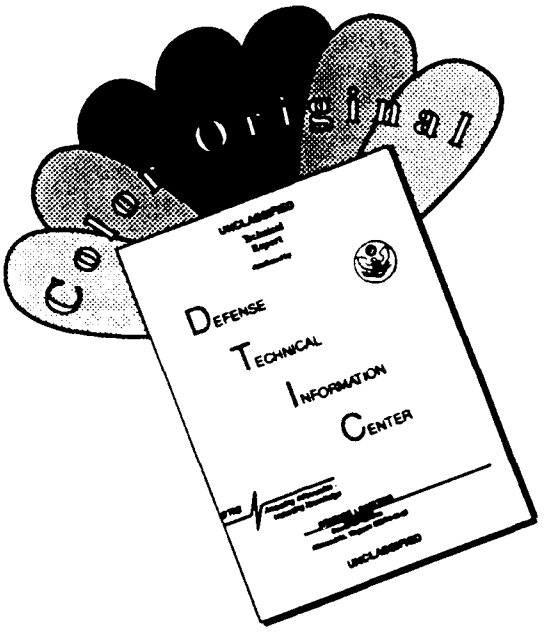

THIS DOCUMENT IS BEST QUALITY AVAILABLE. THE COPY FURNISHED TO DTIC CONTAINED A SIGNIFICANT NUMBER OF COLOR PAGES WHICH DO NOT REPRODUCE LEGIBLY ON BLACK AND WHITE MICROFICHE.

MASSACHUSETTS INSTITUTE OF TECHNOLOGY
LINCOLN LABORATORY

MULTIFREQUENCY MEASUREMENTS OF RADAR GROUND CLUTTER AT 42 SITES

J.B. BILLINGSLEY
Group 45
J.F. LARRABEE
Loral Aerospace

TECHNICAL REPORT 916
VOLUME 2: APPENDICES A THROUGH D

15 NOVEMBER 1991

LEXINGTON MASSACHUSETTS

APPENDIX A

PHASE ONE SITES, MEASUREMENT EQUIPMENT, CALIBRATION, AND DATA COLLECTION

TABLE OF CONTENTS

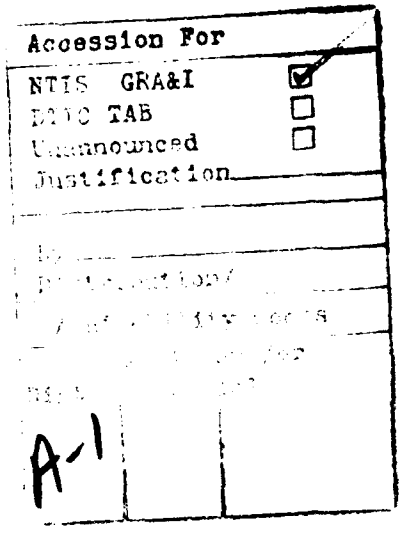

LIST OF ILLUSTRATIONS

LIST OF TABLES

A.1 PHASE ONE SITES

The Phase One multifrequency radar ground clutter measurement equipment was delivered by the contractor, General Electric Company, in October 1981. This equipment was mobile, in a three tractor-trailer configuration. Upon delivery, the equipment was set up on Katahdin Hill at Lincoln Laboratory. Figure A-1 shows the equipment erected at this site. While the equipment was at Katahdin Hill, procedures were developed and exercised for raising and lowering the tower, calibrating the radars, and collecting ground clutter data.

The equipment then undertook a first tour of three clutter sites at Shilo, Neepawa, and Polonia in the western Canadian province of Manitoba during February and March of 1982. The purpose of this first tour was to shake down initial equipment problems and establish smooth operating procedures as well as to make clutter measurements. The equipment was not fully configured during this early shakedown activity: it lacked the S-band transmitter and a dual winching capability that we decided to install to improve safety during tower extension to the full 100 ft.

Problems associated with very cold weather were encountered during this first Canadian tour. Figure A-2 shows the equipment arriving at Shilo. The stowed antenna tower on its tower trailer is pictured in the upper left, upper right, and lower left photos of Figure A-2. The partially erected tower, after it had been tilted vertically off its trailer and its antennas assembled, but before its tower sections had been expanded vertically, is pictured in the lower right photo of Figure A-2. Another photo of the partially erected tower at Shilo is shown in Figure A-3, which provides a relatively clear view of the antennas, their feeds, and the TV camera atop the tower. When this equipment arrived at Shilo, there was a "cold snap" in which daytime temperatures did not exceed -30°F for several weeks. Although the equipment was designed to operate in such cold weather, this early cold period served as an environmental test in which problems like hydraulic fluid failing to pump and shattering of cable sheathing were remedied. Our site selection rationale took us to these northern latitudes. In the end approximately 45 percent of the measurements were made in winter conditions.

Following its first Canadian tour, the clutter measurement equipment returned to Lincoln Laboratory for retrofit to its full equipment configuration. The equipment was then set up at North Truro on Cape Cod in Massachusetts in June and July of 1982 to exercise the new capabilities and to collect sea clutter data as part of our joint measurement program with the Canadian Department of National Defence. Sea states were low while we were at North Truro. Results from this brief sea clutter measurement activity are discussed elsewhere [3]. Figure A-4 shows the equipment erected at North Truro.

The equipment then returned to Alberta in western Canada in August to continue its main series of ground clutter measurements. The complete Phase One schedule of sites is shown in Table A-1, which also includes capsule information summarizing operations at each site. The operations information in Table A-1 includes the length of time spent at each site, whether vertical ascent/descent helicopter propagation tests (P) were performed at the site to help understand the role of the propagation factor F in the clutter strengths $\sigma^{\circ}F^4$ that were being measured, whether this was a repeated visit (n) to a site for seasonal variation, whether external calibrations were performed at the site, and the number of tower sections that were extended in the expandable Phase One antenna tower. Actual antenna heights for a given number of tower sections are provided in Table A-5.

Not indicated in Table A-1 is the fact that, subsequent to the series of measurements summarized there, we continued to operate the equipment at Katahdin Hill on a once-a-week basis well into the next year (until August 1985) for the purpose of providing more depth in our data base with respect to long-term temporal variations associated with wind, weather, and season at a given site. We refer to this subsequent series of once-a-week measurements as Katahdin Hill (3). The measurements from the Katahdin Hill (3) activity are reported elsewhere [1].

Besides measuring backscatter from terrain, considerable attention was devoted to characterizing and describing the terrain at each site, a necessary requirement in the development of ground clutter predictive and modeling capabilities. Our main approach in terrain characterization was careful classification of large kilometer-sized clutter patches through interpretation of large-scale topographic maps and existing stereo aerial photography. High-level information describing site height, location, and terrain type at each Phase One site is provided in Table A-2. The land cover and landform classes shown in Table A-2 reflect the overall terrain at the site, not just the terrain in the repeat sector. The class codes for landform and land cover are defined in Tables 4 and 5 in the body of this report. The effective site heights in Table A-2 are the site heights above the mean of all clutter patches within 12-km range; site height above repeat sector midpoint elevation is given in Table 3. Specific repeat sector terrain descriptive information is provided elsewhere in this report, for example, in Table D-1.

An emphasis in the field with Phase One was to maintain a detailed record of wind, weather, and seasonal conditions during the clutter measurements. To this end, on the raw clutter data tapes, in front of each experiment of clutter data, a terrain descriptive ground truth file was maintained. This file consists of 60 parameters, some descriptive and some numerical. These parameters are listed in Table A-3. An example of a completed ground truth file for one particular clutter experiment is shown in Table A-4. Values are assigned to descriptive parameters (type 1 or type 2) by numerical selection from established lists; values are assigned to numerical parameters (type 3) by direct input. Date and time of last update are recorded for each parameter. Type 1 parameters allow choice of one descriptive value from a list; type 2 parameters allow choice of a number of descriptive values. This ground truth file is of entirely fixed format to allow subsequent sorting of clutter data for particular wind, weather, season, or other conditions. This file was reviewed and updated as necessary before every clutter measurement. We maintained weather stations (wind strength and direction, temperature, humidity) on site and in the clutter measurement zone (see Figures 42 and E-184) to provide information for the ground truth file. Weather station outputs were displayed on large analog dial gauges at the Phase One operations console. Also displayed and recorded at the console was TV video from the bore-sighted TV camera atop the tower. One member of the Phase One site crew had the responsibility to keep the ground truth file on the data tape current. He also documented extensive and detailed field observations within clutter patches (including many photographs) to complement the aerial photo work and ensure correct and consistent terrain classification.

A.2 PHASE ONE MEASUREMENT EQUIPMENT

The Phase One equipment was transported by three tractors and trailers. A view of this equipment erected at Spruce Home, Saskatchewan, in winter season, is shown in Figure A-5. The white trailer stationed near the base of the tower is the electronics trailer, the flat-bed trailer is the tower trailer, and

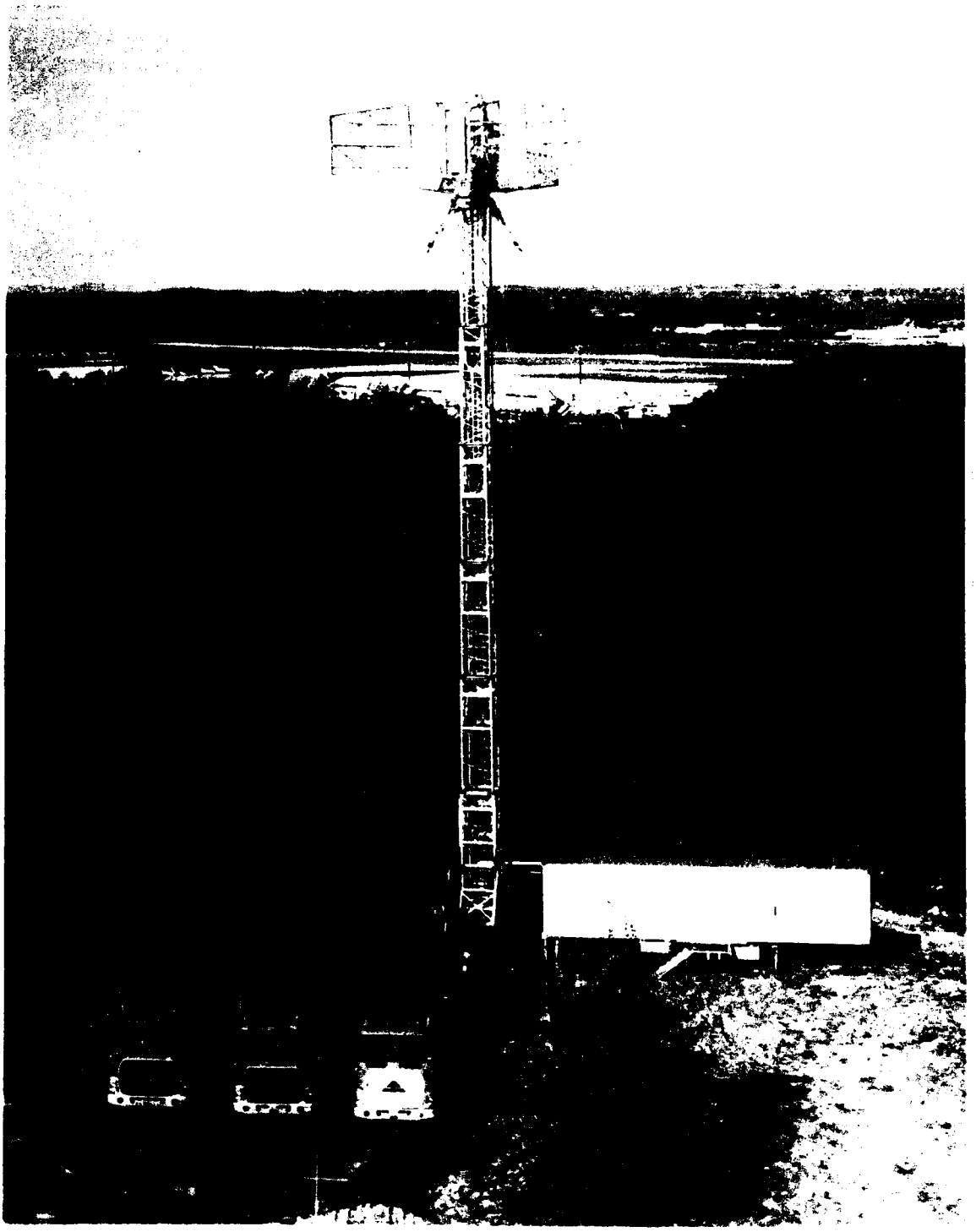

Figure A.1 Phase One equipment at Katahdin Hill. Antenna tower is erected to 100 ft

Figure A-2. Phase One equipment arriving at Shilo.

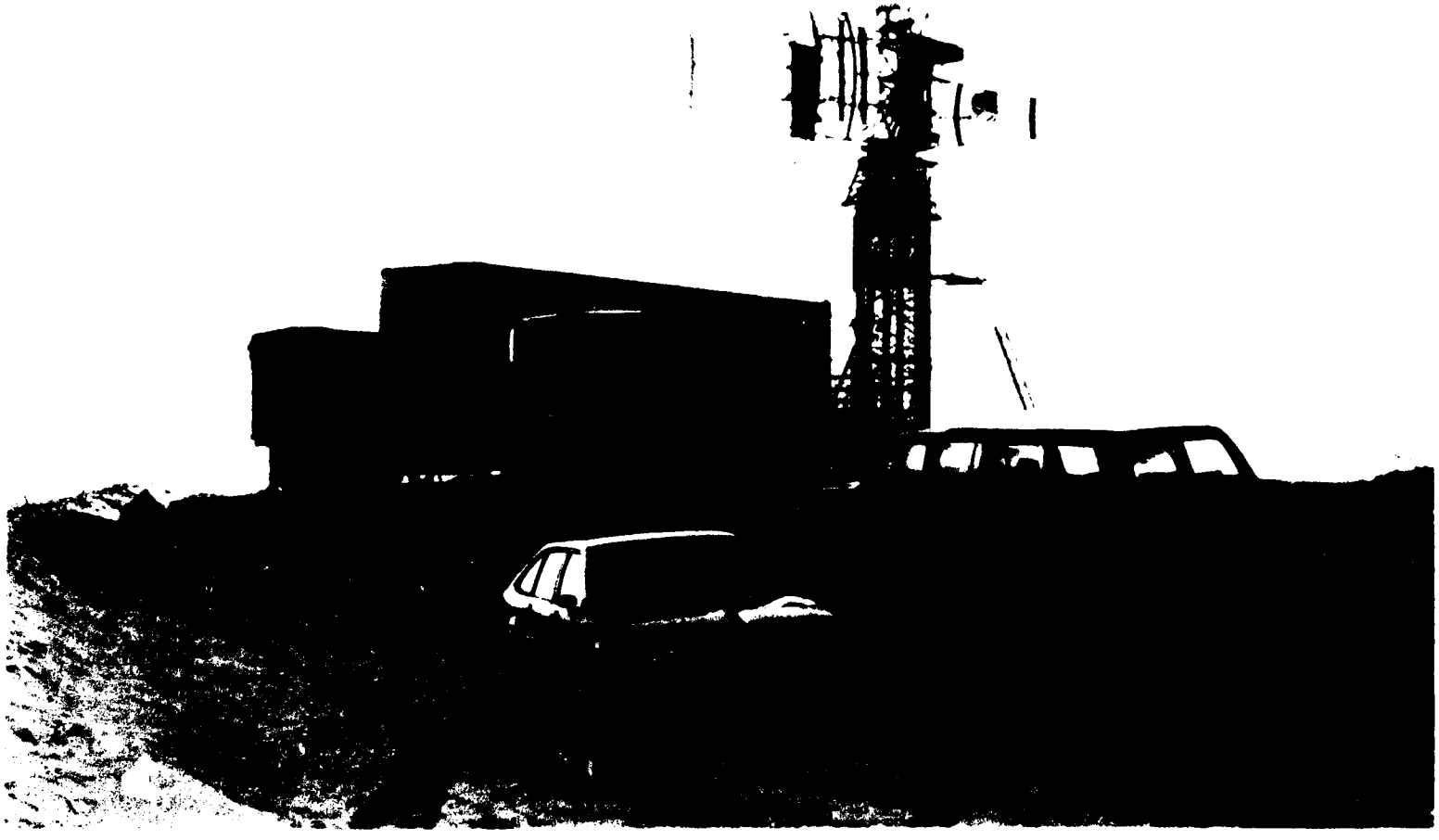

Figure A-3. Phase One tower partially erected at Shilo. February 1982. One tower section.

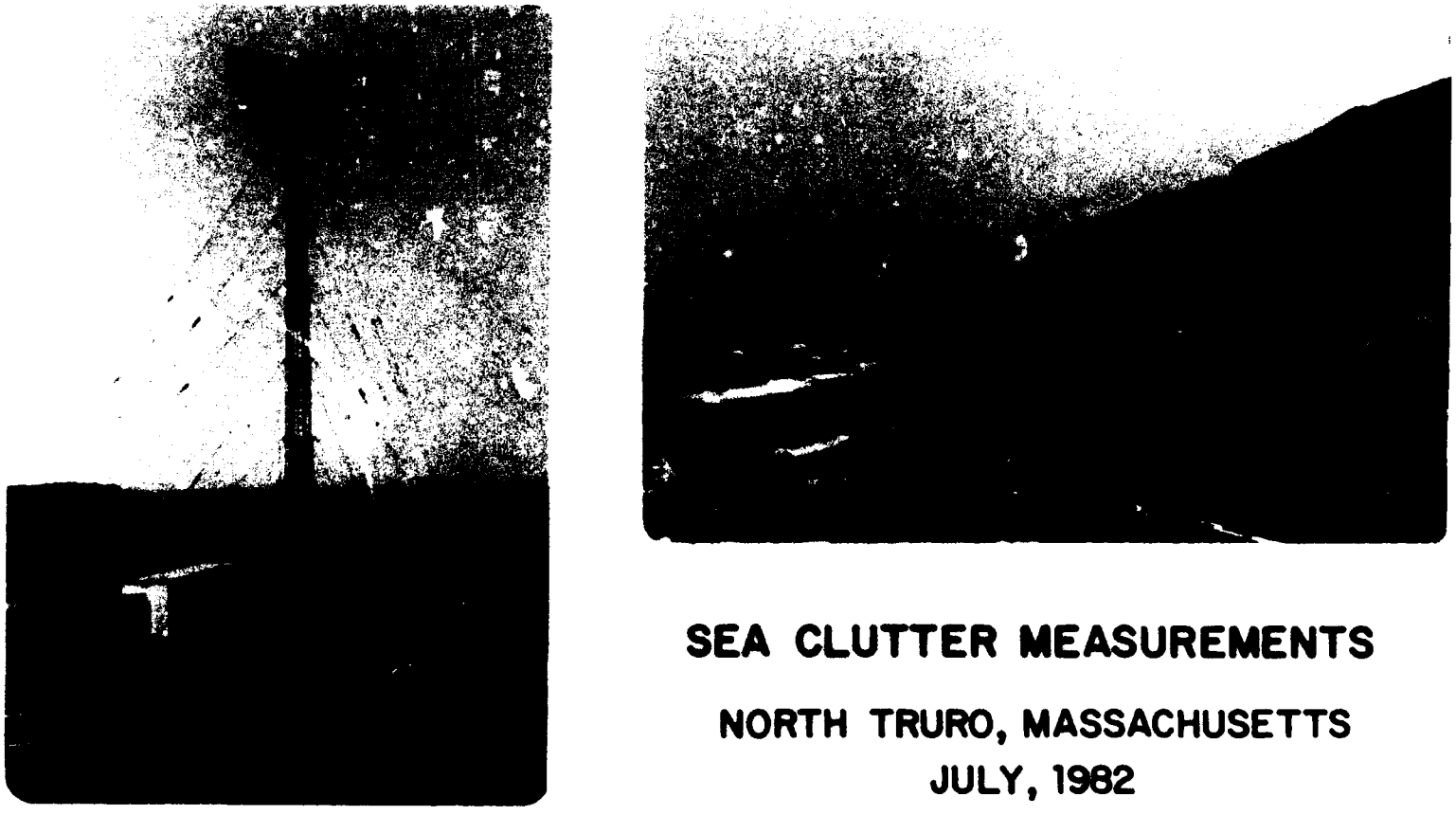

Figure A-4. Phase One equipment at North Truro. Antenna tower is erected to 100 ft.

TABLE A-1
Phase One Site History

Setup Number	Site Name	Number of of Tower Sections	Dates Visited	Time on Site	Ext. Cal.
1.	Katahdin Hill, MA	6	2 Oct-17 Dec 1981	77 Days	●
2.	Shilo, MAN	3, 1	1 Feb-2 March 1982	30 Days	●
3.	Neepawa, MAN	3	3-18 March 1982	16 Days	●
4.	Polonia, MAN	3	19-30 March 1982	12 Days	●
5.	North Truro, MA (P)	6	23 June-21 July 1982	29 Days	●
6.	Cochrane, ALTA	3	11-31 August 1982	21 Days	●
7.	Strathcona, ALTA	3	1-25 Sept 1982	25 Days	●
8.	Penhold II, ALTA	6	27 Sept-16 Oct 1982	20 Days	●
9.	Beiseker, ALTA (P)	3	18 Oct-13 Nov 1982	27 Days	●
10.	Westlock, ALTA	6	15-25 Nov 1982	11 Days	●
11.	Cold Lake, ALTA	6	27 Nov-9 Dec 1982	13 Days	●
12.	Suffield, ALTA	3, 1	11 Dec 1982-21 Jan 1983	42 Days	●
13.	Pakowki Lake, ALTA	3	22 Jan-2 Feb 1983	12 Days	●
14.	Orion, ALTA	3	2-11 Feb 1983	10 Days	●
15.	Beiseker (2), ALTA	3	12-24 Feb 1983	13 Days	●
16.	Cochrane (2), ALTA	3	24 Feb-18 March 1983	23 Days	●
17.	Brazeau, ALTA (P)	6	26 March-13 April 1983	19 Days	●
18.	Lethbridge West, ALTA (P)	3, 1	29 April-17 May 1983	19 Days	●
19.	Magrath, ALTA (P)	3	17 May-6 June 1983	21 Days	●
20.	Waterton, ALTA	3	6-16 June 1983	11 Days	●
21.	Plateau Mountain, ALTA	3	17-24 June 1983	08 Days	—
22.	Picture Butte II, ALTA	3	20 July-6 Aug 1983	18 Days	●
23.	Beiseker (3), ALTA (P)	3	6-24 Aug 1983	19 Days	●
24.	Brazeau(2), ALTA (P)	6	25 Aug-13 Sept 1983	20 Days	●
25.	Puskwaskau, ALTA	6	28 Sept-11 Oct 1983	14 Days	●
26.	Peace River South II, ALTA	6	12 Oct-3 Nov 1983	23 Days	●
27.	Woking, ALTA	3	5-14 Nov 1983	10 Days	—
28.	Beiseker (4), ALTA (P)	3	16-26 Nov 1983	11 Days	●
29.	Wolseley, SASK	3	29 Nov-5 Dec 1983	07 Days	—
30.	Headingley, MAN	3	7-21 Dec 1983	15 Days	●
31.	Altona II, MAN	6	5-31 Jan 1984	27 Days	—
32.	Big Grass Marsh, MAN	3	1-14 Feb 1984	14 Days	●
33.	Gull Lake West, MAN	6	15-25 Feb 1984	11 Days	—
34.	Spruce Home, SASK	3	27 Feb-10 March 1984	13 Days	—
35.	Rosetown Hill, SASK	3	12-21 March 1984	10 Days	●
36.	Wainwright, ALTA	1	23 March-2 April 1984	11 Days	—
37.	Dundurn, SASK	3	3-13 April 1984	11 Days	—
38.	Corinne, SASK	3, 2, 1	13-30 April 1984	18 Days	●
39.	Gull Lake West (2), MAN	6	2-12 May 1984	11 Days	●
40.	Sandridge, MAN	3	12-21 May 1984	10 Days	—
41.	Turtle Mountain, MAN	6	22 May-4 June 1984	14 Days	—
42.	Beulah, ND	3	5-15 June 1984	11 Days	●
43.	Knolls, UT	3	18-25 June 1984	8 Days	—
44.	Booker Mountain, NV	3	17-27 July 1984	11 Days	●
45.	Vananda East, MT	3	30 July-4 August 1984	6 Days	●
46.	Wachusett Mountain, MA	3	15-25 August 1984	11 Days	—
47.	Scranton, PA	3	27 August-11 Sept 1984	16 Days	—
48.	Blue Knob, PA	3	12-22 September 1984	11 Days	●
49.	Katahdin Hill (2), MA	6	25 Sept-19 Oct 1984	25 Days	●

(P): Propagation tests
(n): n^{th} visit (repeated)

TABLE A-2
Location and Description of 42 Phase One Radar Ground Clutter Measurement Sites

Site Name	Province or State	Latitude (°N)	Longitude (°W)	LAND COVER Class Code (Percent Occurrence)	LANDFORM Class Code (Percent Occurrence)	Effective Site Height(m)
Altona II	Man.	49.19	97.66	21(100)	1(100)	-2
Beiseker	Alta.	51.39	113.27	21(100)	3(43),2(36),9(9),7(6),1(4),8(2)	76
Beulah	N.Dak.	47.30	101.74	21(62),31(34),11(4)	2(33),4(23),3(21),1(11),7(11),9(1)	47
Big Grass Marsh	Man.	50.39	98.85	41(31),62(20),31(19), 21(17),33(13)	1(100)	-3
Blue Knob	Pa.	40.29	78.55	43(62),21(31),11(5),70(2)	4(37),7(37),8(17),6(7),5(2)	338
Booker Mt.	Nev.	38.10	117.19	33(46),70(46),12(8)	7(29),8(24),2(18),1(12),4(12),3(5)	336
Brazeau	Alta.	53.04	115.43	43(64),51(13),62(9),21(4), 42(4),61(4),41(1),52(1)	3(31),1(21),4(16),7(14),2(12), 8(5),5(1)	142
Cochrane	Alta.	51.20	114.45	31(52),21(36),41(12)	2(33),7(21),3(17),4(15),5(8),1(4), 6(2)	104
Cold Lake	Alta.	54.43	110.18	21(39),43(39),11(5),52(5),61(5), 12(3),31(2),62(2)	1(40),3(33),2(12),5(9),7(6)	25
Corinne	Sask.	50.05	104.62	21(70),11(15),51(15)	1(60),2(20),3(20)	1
Dundurn	Sask.	51.85	106.57	41(30),21(23),32(23),52(8),11(4), 14(4),31(4),51(4)	3(45),5(35),1(10),2(10)	-3
Gull Lake West	Man.	50.40	96.53	43(49),21(21),33(8),62(8)), 61(6),12(4),52(4)	1(67),3(27)	28
Headingley	Man.	49.88	97.40	21(30),41(22),51(12),14(10), 16(8),11(6),24(6),52(6)	1(69),3(31)	3
Katahdin Hill	Mass.	42.46	71.27	43(55),11(31),12(8),14(5),21(1) 12(5),32(2),62(2),70(2)	5(65),3(22),2(5),4(5),1(3) 7(2)	31
Knolls	Utah	40.74	113.28	70(51),33(49)	1(77),4(9),7(9),5(5)	-1
Lethbridge West	Alta.	49.71	112.93	21(36),31(33),11(13),12(9),	1(30),3(26),9(26),8(10),	25
Magrath	Alta.	49.41	112.97	21(64),31(19),51(11),11(3), 32(3)	2(25),3(20),7(15),9(15), 1(13),4(8),5(2),6(2)	79
Neepawa	Man.	50.33	99.50	21(52),41(46),11(2)	3(35),2(28),7(15),1(13),5(7),9(2)	-30
North Truro	Mass.	42.03	70.05	----	----	--
Orion	Alta.	49.50	110.81	31(56),21(38),62(3),33(1), 51(1),52(1)	2(30),3(21),5(17),7(14),4(10), 9(6),1(2)	41
Pakowki Lake	Alta	49.32	110.85	31(41),21(26),32(21),33(9), 22(3)	1(50),2(19),3(19),5(6),4(3), 7(3)	11
Peace River South II	Alta.	56.20	117.27	41(48),21(40),33(10),51(2)	3(46),7(24),2(18),5(6),1(3),4(3)	12
Pennold II	Alta.	52.18	113.97	21(64),52(11),41(8),43(8), 11(3),12(3),62(3)	1(48),3(28),2(12),7(7)	40
Picture Butte II	Alta.	49.92	112.82	21(83),11(7),14(7),12(3)	3(57),2(31),7(6),9(4),1(2)	54
Plateau Mt.	Alta.	50.21	114.52	42(35),31(29),70(26),41(9), 32(1)	8(91),2(4),3(4),7(1)	279
Polonia	Man.	50.36	99.61	21(63),41(35),11(2)	2(38),3(32),5(15),7(11),1(4)	128
Puskwaskau	Alta.	55.22	117.49	43(56),21(15),62(15),41(7), 52(7)	2(50),1(21),3(21),6(4),7(4)	129
Rosetown Hill	Sask.	51.54	107.93	21(95),11(5)	3(45),1(24),2(14),7(10),5(7)	28
Sandridge	Man.	50.61	97.51	41(52),21(27),33(13),22(5), 14(3)	1(95),3(5)	0
Scranton	Pa.	41.38	75.59	43(56),11(27),12(11),21(6)	4(43),2(32),5(13),7(9),3(3)	262
Shilo	Man.	49.75	99.63	41(44),21(26),31(18),32(6), 11(3),12(3)	1(50),3(36),2(7),5(7)	3
Spruce Home	Sask.	53.45	105.76	43(51),21(42),22(6),11(1)	1(51),3(37),2(12)	25
Strathcona	Alta.	51.03	114.17	11(33),12(20),41(15),31(13), 51(11),21(8)	7(33),3(28),4(19),2(14),1(3), 5(3)	72
Suffield	Alta.	50.27	111.14	31(86),12(7),11(5),52(2)	5(50),3(42),2(8)	20
Turtle Mt.	Man.	49.06	100.18	52(46),43(29),41(25)	5(69),3(31)	8
Vananda East	Mont.	46.45	106.98	33(87),21(10),61(3)	4(41),7(24),2(21),3(12),1(2)	94
Wachusett Mt.	Mass.	42.49	71.89	41(55),21(27),11(9),52(9)	4(59),5(18),7(15),3(8)	333
Wainwright	Alta.	52.82	111.06	41(47),32(27),21(22),52(2), 12(1),51(1)	3(48),7(16),1(14),5(14),2(8)	70
Waterton	Alta.	49.15	113.83	31(27),41(27),33(16),42(14), 70(8),52(5),40(3)	7(33),4(26),8(16),2(10),5(6), 1(3),3(3),6(3)	-88
Westlock	Alta.	54.16	113.70	21(38),41(27),52(14),11(8), 43(8),33(5)	3(59),1(24),2(17)	24
Woking	Alta.	55.55	118.75	41(71),21(29)	2(44),4(26),3(15),7(15)	36
Wolseley	Sask.	50.36	103.15	21(73),41(21),52(4),11(2)	3(47),5(33),1(16),2(4)	17

TABLE A-3
Parameters in Ground Truth File

Par. No.	Parameter Name	Par. Type	Par. No.	Parameter Name	Par. Type
1.	site number and name	1	31	on-site outside relative humidity	3
2.	date of arrival	3	32.	on-site percent cloud cover	3
3.	(north) latitude and (west) longitude of site	3	33.	precipitating on-site	2
4.	universal transverse mercator coords of site	3	34.	raining on-site	2
5.	map reference	3	35.	snowing on-site	1
6.	site magnetic declination	3	36.	raining in measurement zone	1
7.	magnetic bearing of tower trailer	3	37.	snowing in measurement zone	1
8.	number of tower sections extended	3	38.	hailing in measurement zone	1
9.	tower-top height	3	39.	bird activity in measurement zone	1
10.	azimuth alignment by tower trailer	3	40.	insect activity in measurement zone	1
11.	azimuth alignment by antenna wingtips	3	41.	ground vehicle activity in measurement zone	1
12.	azimuth alignment by benchmark	3	42.	aircraft activity in measurement zone	1
13.	azimuth alignment by survey	3	43.	average ground moisture in measurement zone	1
14.	azimuth alignment by other	3	44.	average open-water conditions in measurement zone	1
15.	azimuth servo correction angle	3	45.	average crop conditions in measurement zone	2
16.	operator names and affiliations	3	46.	deciduous foliage conditions in measurement zone	2
17.	landscape overview	2	47.	windborne material in measurement zone	2
18.	season	2	48.	animal activity in measurement zone	2
19.	recent rain	1	49.	type of snow cover in measurement zone	2
20.	recent snow	1	50.	extent of snow cover in measurement zone	1
21.	recent freezing rain	1	51.	snow depth in measurement zone	1
22.	general weather	2	52.	percent soil moisture in measurement zone	3
23.	tower-top mean windspeed	3	53.	percent free water content of snow in meas. zone	3
24.	tower-top maximum windspeed	3	54.	water equivalent of snow in measurement zone	3
25.	tower-top mean wind direction	3	55.	mean windspeed in measurement zone	3
26.	on-site windspeed assessment	1	56.	wind direction in measurement zone	3
27.	on-site wind direction assessment	1	57.	max/min windspeed in measurement zone	3
28.	on-site wind steadiness assessment	1	58.	temperature in measurement zone	3
29.	on-site outside temperature	3	59.	relative humidity in measurement zone	3
30.	on-site outside barometric pressure	3	60.	universal transverse mercator coordinates of remote weather station in measurement zone	3

TABLE A-4
Ground Truth File for a Clutter Experiment at Wachusett Mountain

1-1	SITE	68 WACHUSETT MT	17-AUG-84 10:24:34
2-3	ARRIVAL DATE (DD-MM-YY)	15-AUG-84	17-AUG-84 10:24:56
3-3	N LAT W LONG (D:M:S)	42:29:20.5 71:53:15	23-AUG-84 07:46:33
4-3	UTM	18TYC62670790	23-AUG-84 07:46:37
5-3	MAP REFERENCE	NK 19-4 WACHUSETT MTN	17-AUG-84 10:36:04
6-3	MAG DEC (D:M:S)	15:00 W	17-AUG-84 10:36:36
7-3	TRLR MAG BEARING (D:M:S)		17-AUG-84 10:37:05
8-3	#TOWER SECTIONS EXT	2	17-AUG-84 10:37:13
9-3	TOWER HT (FT)	48	17-AUG-84 10:37:16
10-3	TRAILER ALN (D:M:S)		17-AUG-84 10:37:26
11-3	ANT WINGTIP ALN (D:M:S)		17-AUG-84 10:37:29
12-3	BENCHMARK ALN (D:M:S)		17-AUG-84 10:37:32
13-3	SURVEY ALN (D:M:S)		17-AUG-84 10:37:34
14-3	OTHER ALN (D:M:S)		17-AUG-84 10:37:35
15-3	SERVO ALN CAL (D:M:S)		17-AUG-84 10:37:37
16-3	OPERATOR/AFFILIATION	GE/INTERA/DND	17-AUG-84 10:37:42
17-2	LANDSCAPE OVERVIEW	1 GREEN 4 CROPS UP	17-AUG-84 10:38:35
18-2	SEASON	2 MID 5 SUMMER	17-AUG-84 10:39:02
19-1	RECENT RAIN	1 NONE	24-AUG-84 07:53:28
20-1	RECENT SNOW	1 NONE	24-AUG-84 07:53:30
21-2	RECENT FREEZING RAIN	1 NO	24-AUG-84 07:53:34
22-2	GENERAL WEATHER	1 CLEAR 7 BREEZY 11 HOT 14 HUMID	24-AUG-84 07:54:10
23-3	TT MEAN WINDSPEED (TBD)	17	24-AUG-84 07:54:17
24-3	TT MAX WINDSPEED (TBD)	26	24-AUG-84 07:54:19
25-3	TT WIND DIR (TBD)	335	24-AUG-84 07:54:21
26-3	SITE WINDSPEED (MPH)	6	24-AUG-84 13:50:07
27-3	SITE WIND DIR	300	24-AUG-84 13:50:13
28-3	SITE WIND MAX/MIN (MPH)	9/3	24-AUG-84 13:50:19
29-3	SITE TEMP (DEG-F.)	65	24-AUG-84 13:50:25
30-3	SITE BAR-PRES (TBD)		24-AUG-84 13:50:28
31-3	SITE REL-HUMIDITY (%)	64	24-AUG-84 13:50:37
32-3	SITE % CLOUD COVER (%)	95	24-AUG-84 13:50:47
33-2	SITE PRECIPITION	1 NO	24-AUG-84 13:50:50
34-2	SITE RAIN	1 NO	24-AUG-84 07:56:30
35-1	SITE SNOWFALL	1 NONE	24-AUG-84 07:56:33
36-1	DMZ RAIN	5 NO	24-AUG-84 07:56:41
37-1	DMZ SNOWFALL	5 NO	24-AUG-84 07:56:44
38-1	DMZ HAIL	5 NO	24-AUG-84 07:56:47
39-1	DMZ BIRD ACTIVITY	3 MODERATE	24-AUG-84 07:56:52
40-1	DMZ INSECT ACTIVITY	2 LOW	24-AUG-84 07:57:00
41-1	GND VEHICLE ACTIVITY	3 MEDIUM	24-AUG-84 07:57:09
42-1	AIRCRAFT ACTIVITY	2 LOW	24-AUG-84 07:57:12
43-1	AVE GROUND MOISTURE	3 MODERATE	24-AUG-84 07:57:18
44-1	AVE OPEN WATER COND	2 WAVY	24-AUG-84 07:57:23
45-2	DMZ AVE CROP COND	1 LOW 3 HIGH 6 MATURE GROWTH 7 HARVESTED 8 BARE FIELDS 10 CULTIVATED 14 FLOWERING	24-AUG-84 07:57:31
46-2	DMZ FOLIAGE COND	1 LEAVES ON 5 GREEN LEAVES 9 MATURE LEAVES 18 BLOOM OVER	24-AUG-84 07:57:37
47-2	DMZ WINDBORNE MATERIAL	2 NONE 9 VERY UNLIKELY	24-AUG-84 07:57:50
48-2	DMZ ANIMAL DENSITY	3 LITTLE 6 YES 11 DOMESTIC 12 WILD 13 CATTLE	24-AUG-84 07:57:57
49-2	DMZ SNOW COVER TYPE	12 NON-APPLICABLE	24-AUG-84 07:58:01
50-1	DMZ EXTENT OF SNOW COV	5 NONE	24-AUG-84 07:58:04
51-1	DMZ SNOW DEPTH	5 NA	24-AUG-84 07:58:06
52-3	DMZ SOIL MOISTURE		24-AUG-84 07:58:08
53-3	DMZ SNOW H2O CONTENT (%)		24-AUG-84 07:58:09
54-3	DMZ SNOW H2O EQUIV (%)		24-AUG-84 07:58:10
55-3	DMZ WINDSPEED (MPH)	6	24-AUG-84 07:58:11
56-3	DMZ WIND DIR	280	24-AUG-84 07:58:12
57-3	DMZ WIND MAX/MIN (MPH)	9/1	24-AUG-84 07:58:13
58-3	DMZ TEMP (DEG-F.)	76	24-AUG-84 07:58:14
59-3	DMZ REL-HUMIDITY (%)	66	24-AUG-84 07:58:18
60-3	DMZ WEATHER STA (UTM)	18TYB65829906	24-AUG-84 07:58:19

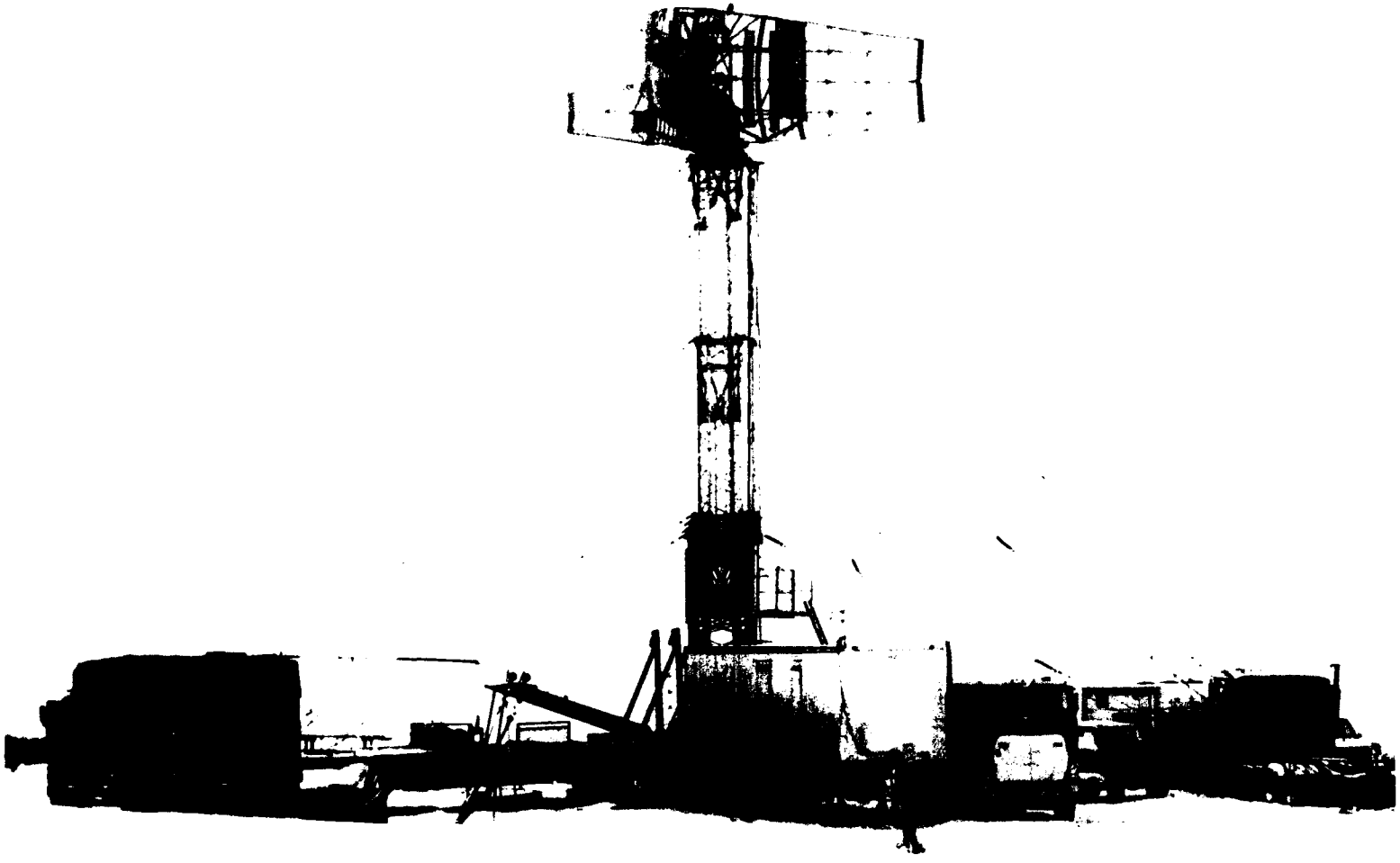

Figure A-5. Phase One equipment at Spruce Home. Antenna tower is elevated to 60 ft. February 1984.

the remaining tarpaulin-covered trailer is the equipment trailer. These three trailers constituted a self-contained transportable five-frequency radar system capable of collecting clutter data at VHF, UHF, L-, S- and X-band. The antennas were mounted on an expandable tower that could be raised to various heights up to 100 ft. At almost all sites, either three tower sections were raised to provide a nominal height of 60 ft or six tower sections were raised to provide a nominal height of 100 ft. Occasionally, some clutter data were acquired with only one or two tower sections raised to provide nominal heights of 30 ft (see Figure A-3) or 45 ft, respectively. The number of tower sections used at each site is shown in Table A-1. Actual antenna heights for one, two, three, and six section tower configurations are given in Table A-5.

TABLE A-5
Phase One Antenna Heights

Frequency Band	Height from Ground Level at Base of Tower to Antenna Feed Point (ft)			
	1 Tower Section Raised	2 Tower Sections Raised	3 Tower Sections Raised	6 Tower Sections Raised
L-, S-	27.5	40.8	54.3	94.3
VHF, UHF	30.3	43.6	57.1	97.0
X-	32.3	45.6	59.1	99.0

The electronics equipment was transported and housed in the white electronics trailer. This trailer contained the five transmitters, receivers, exciter, A/D converters, signal processors, a digital computer, displays, and high-speed data recorders. The tower trailer transported the tower, antenna reflector mid-sections, antenna feeds, and a diesel-operated winch system used to erect the tower. Elements of this winch system, including the hydraulic winches and the platform that first tilted the horizontally stowed tower upright, are visible on the tower trailer bed to the left of the base of the tower in Figure A-5. The equipment trailer to the far left in Figure A-5 transported the 60-kW diesel generator, the waveguide sections, coaxial RF cables, power cables, a lightweight, easily portable 75-ft tower used during system calibration, and portions of the antenna reflectors.

The large reflector was 10 ft high by 30 ft wide and was part of the dual-frequency VHF/UHF antenna system. The crossed-dipole dual-frequency feed of the VHF/UHF antenna is shown in Figure A-6. The smaller open-mesh reflector and feed was the dual-frequency L-/S-band antenna system. The X-band antenna reflector was the solid reflector mounted above the L-/S-band antenna. These two smaller antennas are readily visible in Figure A-3. A close-up view of the L-/S-band radome and the X-band reflector is shown in Figure A-7. The L-/S-band radome housed a crossed-dipole feed at L-band and a feed horn at S-band. Visible above the X-band reflector is a TV camera that provided a boresight video display at the operating console in the electronics trailer. A 360-deg pan of this TV video was recorded at each site. The antenna system and tower were stabilized by 28 guy wires fastened to eight anchors. The guy wires were brought to specified tension, some to 1000 lb, others to 2000 lb. The total rotating dead weight on top of the tower was 3000 lb. The antenna wind load was 8000 lb at the specified survival wind velocity of 75 kn. The anchors, which were emplaced at each site prior to Phase One arrival, had a holding capacity of 20 klb each. A brief Phase One movie is available showing the arrival of equipment on site, the erection of the tower, and some aspects of calibration.

Table A-6 shows gains, beamwidths, and rms side lobe levels of the Phase One antenna beams at a particular selected frequency (most commonly used for Phase One data acquisition) within each band. Note that our initial goal was to provide a VHF antenna gain of about 16 dB. However, the feed arrangement utilizing crossed dipoles at both VHF and UHF situated one-quarter wavelength above a common reflecting feed plane prevented this (see Table A-6). If this reflecting feed plane had been infinite, the phase center of the dipoles and their images would have been in the feed plane at both VHF and UHF, and this common phase center could have been situated at the focal point of the large reflector. However, because the reflecting feed plane was finite, the phase center occurred above the feed plane at different positions for VHF and UHF. These two different phase centers at VHF and UHF could not both be positioned at the focal point of the large reflector. Therefore, the UHF phase center was positioned at the focal point, and the displaced VHF phase center caused about a 3-dB loss in expected gain. The actual gain was used in computations of clutter reflectivity.

The Phase One antennas had elevation beams that were relatively wide, fixed, and boresight-directed at the horizon. For a given azimuth beam position, the terrain at all ranges from one to many kilometers was usually illuminated within the elevation beamwidth as it existed with its boresight fixed to be locally horizontal. No elevation beam control was available. Thus, the backscatter from a clutter patch was measured at some angular position on the fixed elevation antenna pattern. Although this angle was usually small and usually within the one-way 3-dB points on the free-space elevation pattern, it was rigorously zero (i.e., on-boresight) only if the source of clutter backscatter was at the same elevation as the antenna phase center. Because this was seldom rigorously true, we correct our computations of clutter strength for elevation gain variations. To do this requires knowledge of the relative difference in terrain elevation between the radar and the clutter patch (i.e., conversion from a raw measurement of clutter signal strength to an absolute measure of clutter reflectivity cannot be performed on the basis of the radar instrumentation parameters only). We use this relative difference in mean height above sea level between the radar position and the clutter patch, as well as antenna mast height, range to the clutter patch, and the decrease in the effective elevation of the clutter patch due to a 4/3 radius spherical earth, to compute the off-axis angle on the elevation pattern at which the clutter measurement was made. The two-way gain adjustment due to this nonzero off-axis angle is accounted for in computation of absolute clutter reflectivity, even when the angle is within the one-way 3-dB elevation beamwidth. Because this elevation gain correction requires terrain elevation information specific to each site and measurement, it was often not known in advance and was not automatically included in the calibration algorithms by which our raw measurement data were converted to calibrated clutter files. To have included it would have required correlation of clutter measurement data with digital terrain elevation data at calibration time, a rather large undertaking for what was usually a small correction. Rather, this correction is made subsequently in our application programs that access the calibrated clutter files.

The computation of off-axis angle described above assumes a horizontal elevation beam. At X-band, however, there was a contributing boresight (i.e., axis) alignment error. Up to and including the 16th site [Cochrane (2)], the Phase One X-band beam was pointed incorrectly up toward the sky 0.56 deg. Between the 16th and 17th sites, this problem was partially corrected, but the boresight was left pointing up 0.2 deg. Therefore, prior to the 17th site [Brazeau (1)], the X-band boresight error is 0.56 deg; from Brazeau (1) on this boresight error is 0.2 deg. These boresight angular errors are included in the computation of off-axis angle before any X-band off-axis elevation gain correction is determined.

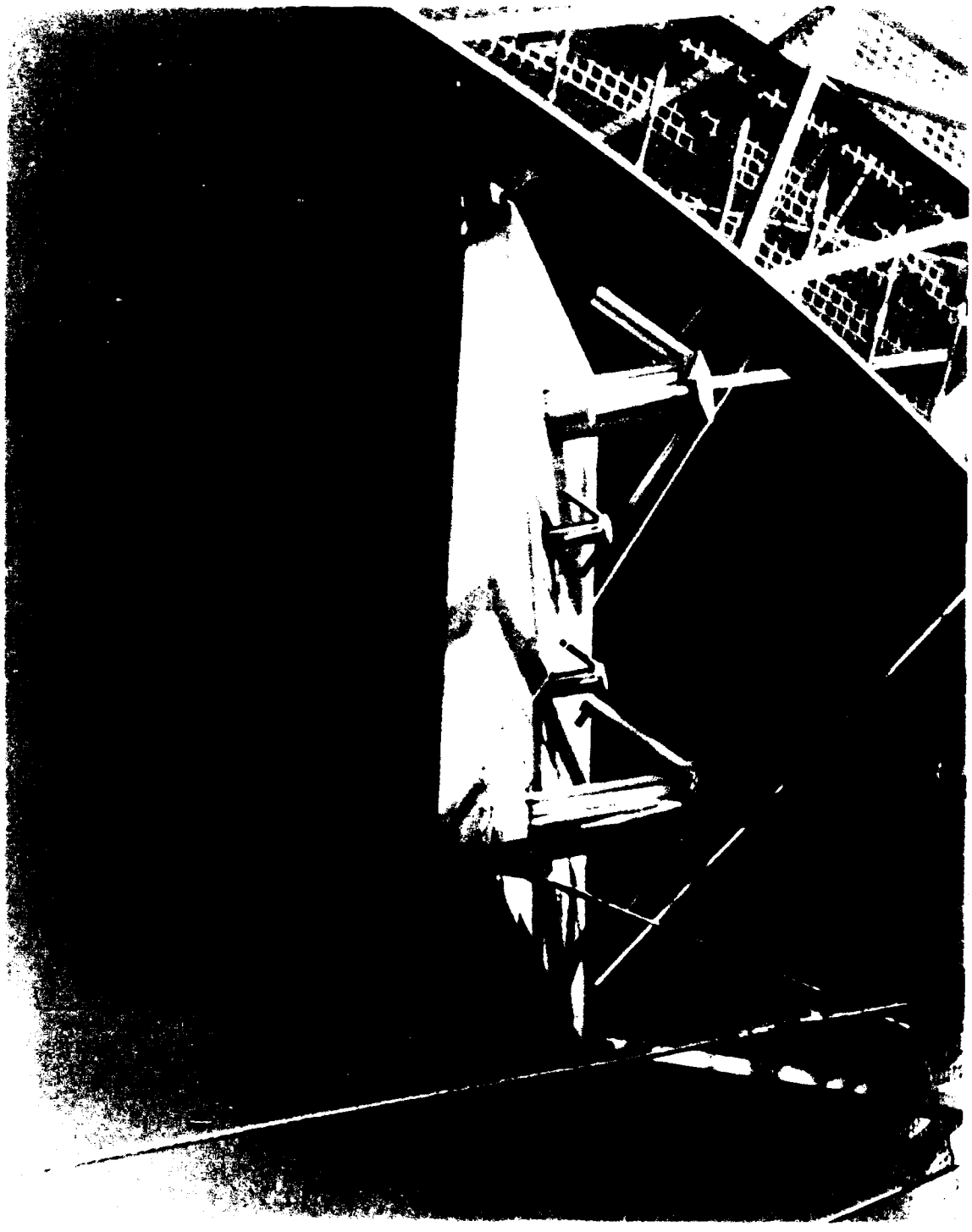

Figure A-6. Crossed dipole feeds of the Phase One VHF-UHF reflector

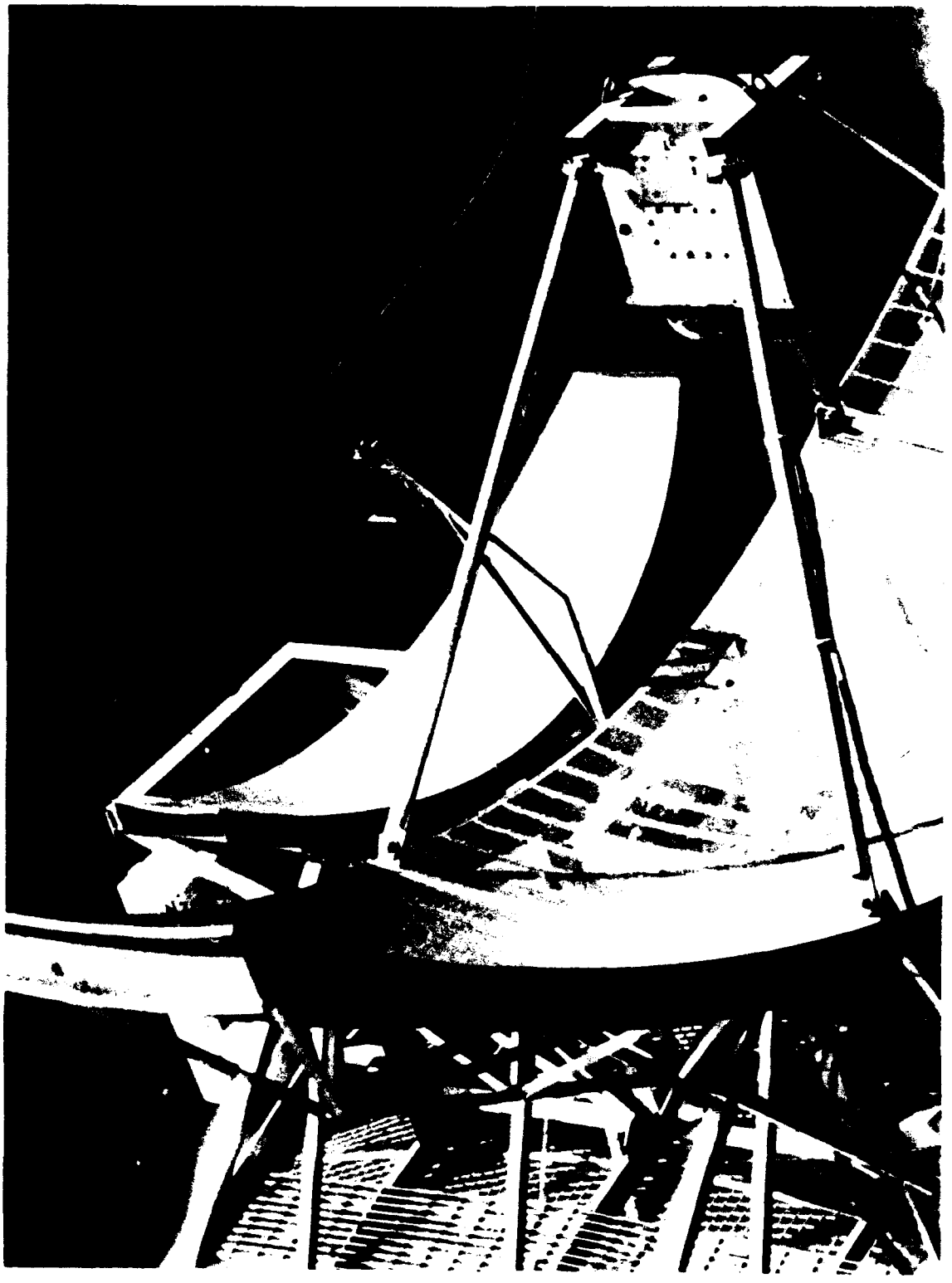

Figure A-7. L- and S-band feed radome, X-band antenna, and tower-top TV camera.

TABLE A-6
Phase One Antenna Pattern Parameters at Selected Frequencies*

Parameters	VHF	UHF	L-Band	S-Band	X-Band
Frequency (MHz)	167	435	1230	3240	9200
One-way Gain (dBi)					
Vertical Polarization	13.60	26.17	28.66	35.06	38.39
Horizontal Polarization	12.55	24.45	28.46	36.02	38.73
Azimuth 3 dB One-way Beamwidth (deg)					
Vertical Polarization	12.55	4.43	3.44	1.27	1.09
Horizontal Polarization	13.95	5.42	3.53	1.20	1.02
Elevation 3 dB One-way Beamwidth (deg)					
Vertical Polarization	42.73	15.59	10.77	4.45	3.40
Horizontal Polarization	41.00	15.67	10.09	4.37	3.27
RMS Side Lobes (dB)	-25	-25	-30	-30	-30

* The selected frequencies within each band are those most commonly used during Phase One data collection.

The overall radar system block diagram is shown in Figure A-8. The system exciter supplied all transmit and receive local oscillator (LO) frequencies and provided the basic timing reference for the system. The basic frequency reference for the exciter was a HP8662A synthesizer signal generator, which had sufficient stability to support an overall system clutter improvement factor of 60 dB.

There were five transmitters in the system. The two higher frequency transmitters (S- and X-bands) had traveling wave tubes (TWTs) as the final high-power output stage. The intermediate and final stages of the three low band transmitters (VHF, UHF, and L-band) used the Eimac type Y-739F planar triodes with Eimac CV-8030 series resonant cavities. A single low band transmitter power supply was used for intermediate and final stages of the three low band transmitters. The cavities could be manually tuned over a few megahertz bands in each of the three low band transmitters. This process required approximately 2 min. The signals from each of the five high-power transmitters were fed through their respective circulators to transmission lines. The S- and X-band signals were transmitted to their antennas in separate waveguides. The two waveguide runs consisted of 12-ft sections that were connected together during tower erection. A single 7/8-in coaxial line was used to carry the VHF, UHF, and L-band signals to their antennas. The appropriate low band signal was switched into the coaxial line by two three-way band select switches; one switch was located near the top of the tower, and the other was located inside the electronics van.

The signals received from the antennas were fed to a separate preamplifier for each frequency band. The first intermediate frequency (IF) for all frequency bands was 740 MHz. The first IF entered into a common receiver used for all frequencies.

The diagram of the receiver and signal processor is shown in Figure A-9. The receiver IF gain could be varied dynamically according to an R^3 or R^4 sensitivity time control (STC) function. R^3 gain variation provides a constant signal output level for a given uniform level of clutter reflectivity. The R^4 function provides constant signal output level for a constant level of clutter RCS. Both STC functions provided 40-dB attenuation at 1 km. In addition, the preamplifiers (shown in Figure A-8) could be bypassed, and fixed attenuation could be switched into the system to avoid system saturation by large target returns.

The 740-MHz IF signal was mixed to 150 MHz where the matched filtering was accomplished. Additional IF amplification was also provided. The 150-MHz IF signal was converted to in-phase and quadrature (I and Q) signals at baseband where the analog-to-digital (A/D) conversion was performed. The Data Collection Unit provided real-time buffering of the I and Q data and routed the clutter data to the PDP-11 computer or tape recorder. The Radar Data Processor (RDP) performed envelope detection or the I and Q samples were fed to a digital-to-analog (D/A) converter, which drove the A-scope as shown. In addition, the RDP performed real-time noncoherent integration of 128 pulse returns. The integrated data were saved by the computer, which, in nonreal-time, could generate a range/azimuth display. The Radar Control Unit consisted of timing and data control logic that accepted commands from the computer and converted them to radar control signals.

Data collection was controlled automatically by the computer. The system operator input parameters via keyboard or floppy disk, which established the range and azimuth limits, frequency, scan rate, waveform, sampling rate, and polarization to be used for each experiment (see Table A-18). Experiment parameter lists on floppy disks were routinely prepared ahead of time at Lincoln Laboratory, although they often required field editing for optimization to the actual conditions being experienced on site. The system software checked the experiment parameters to verify consistency with system capabilities and directed the instrumentation for clutter data collection.

The Phase One system performance parameters are listed in Table A-7. The system was capable of operating within a 5 percent band at each of the five RF frequencies. However, the frequency assignment received from the U.S. Government was a smaller subset of these 5 percent bands. We were generally restricted to a single frequency within each band for the Canadian sites, although more frequencies could have been obtained if required. The system was capable of transmitting and receiving vertical or horizontal polarization. The azimuth and elevation beamwidths are as measured at the 3-dB one-way points (6-dB two-way). The system stability and dynamic range are commensurate with a clutter improvement factor of 60 dB at VHF, UHF, and L-band and 55 dB at S- and X-bands for a two-pulse cancellation technique (i.e., if the complex returns from two consecutive pulses are subtracted, then the differences must be 0.1 percent of the amplitude of the unsubtracted returns). These specified clutter improvement factor levels assume that antenna-motion-induced pulse-to-pulse variations in transmitter amplitude and phase (quantities that were measured in real time and stored on tape in the calibration block of the clutter data record) are corrected within the Lincoln calibration computer programs. In practice, such corrections were usually not required in these subsequent calibrations. Experimental tests showed that antenna motion was minimal (see Section 2.1) and that 60-dB clutter improvement performance was achieved in winds up to 20 kn.

There were two waveforms available at each frequency, a low resolution (150 m) and a high resolution (15 m or 36 m, depending upon frequency) waveform. The waveforms were short uncoded pulses of 1-μs duration for low resolution and of 0.1- or 0.25-μs duration for high resolution. We col-

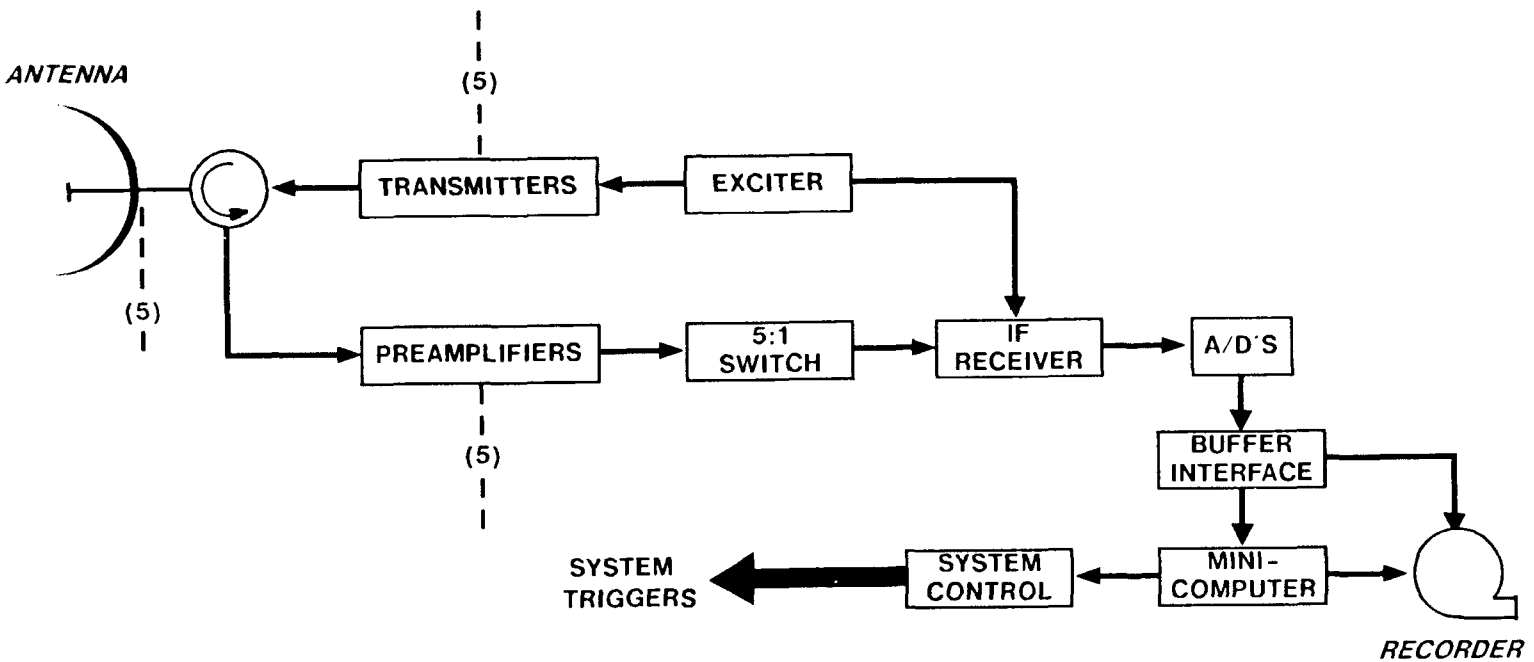

Figure A-8. Phase One instrument block diagram.

loquially refer to the low resolution waveform as "fat" (F) and the high resolution waveform as "thin" (T). The minimum range of 1 km is the closest range from the radar at which clutter data could be collected.

The RCS accuracy performance of 2 dB rms resulted mostly from the ability to calibrate the system to that accuracy (see Section A.3). The instantaneous dynamic range is the amplitude range of clutter reflectivity or target RCS that could be collected with a S/N ratio of 12 dB or greater without saturating or exceeding the linear range of the receiver and A/D converter. The center of the 60-dB instantaneous range could be adjusted in 1-dB steps from 0 to 40 dB. For instance, the total dynamic range could be expanded to 100 dB by first collecting data with 40 dB of attenuation over a particular area and then repeating the data collection over the same area with no attenuation. Data from the first pass is used in combination with the data from the second pass at those locations where the system saturated. Additional control of dynamic range could be effected through bypassing the preamp. The clutter data were recorded in in-phase (I) and quadrature (Q) format at the A/D converter outputs. The maximum A/D converter sampling rate was 10^7 I and Q samples per second with 13 bits each. The A/D data were then buffered for the recorders that had a maximum recording rate of about 625 Kbytes per second.

The system sensitivities shown in Table A-7 apply to the 150-m waveform. The sensitivity to clutter for the 15-m waveform was 20 dB lower (10 dB for the reduction in pulse energy and 10 dB in area illuminated).

There were three basic data collection modes available: the beam scan mode, the parked beam mode, and the beam step mode. During the beam scan mode, data were collected as the antenna beam scanned from one azimuth limit to the next. In the parked beam mode, data were collected while the beam was held at a fixed azimuth. We collected our time-hop (long time dwell) data with a parked beam. For the beam step mode, the beam was stepped through the measurement sector, beam position by beam position, with the beam held fixed at each step while data were recorded. Approximately 15 s were required for antenna stabilization at each step during step beam data collection. Largely because of this antenna stabilization wait time in step mode, we recorded most of our 360-deg survey data in scan mode to keep data volume and data acquisition time reasonable. However, many of our repeat sector measurements were conducted in step mode. The antenna scan was limited to 330 deg due to cable wrap.

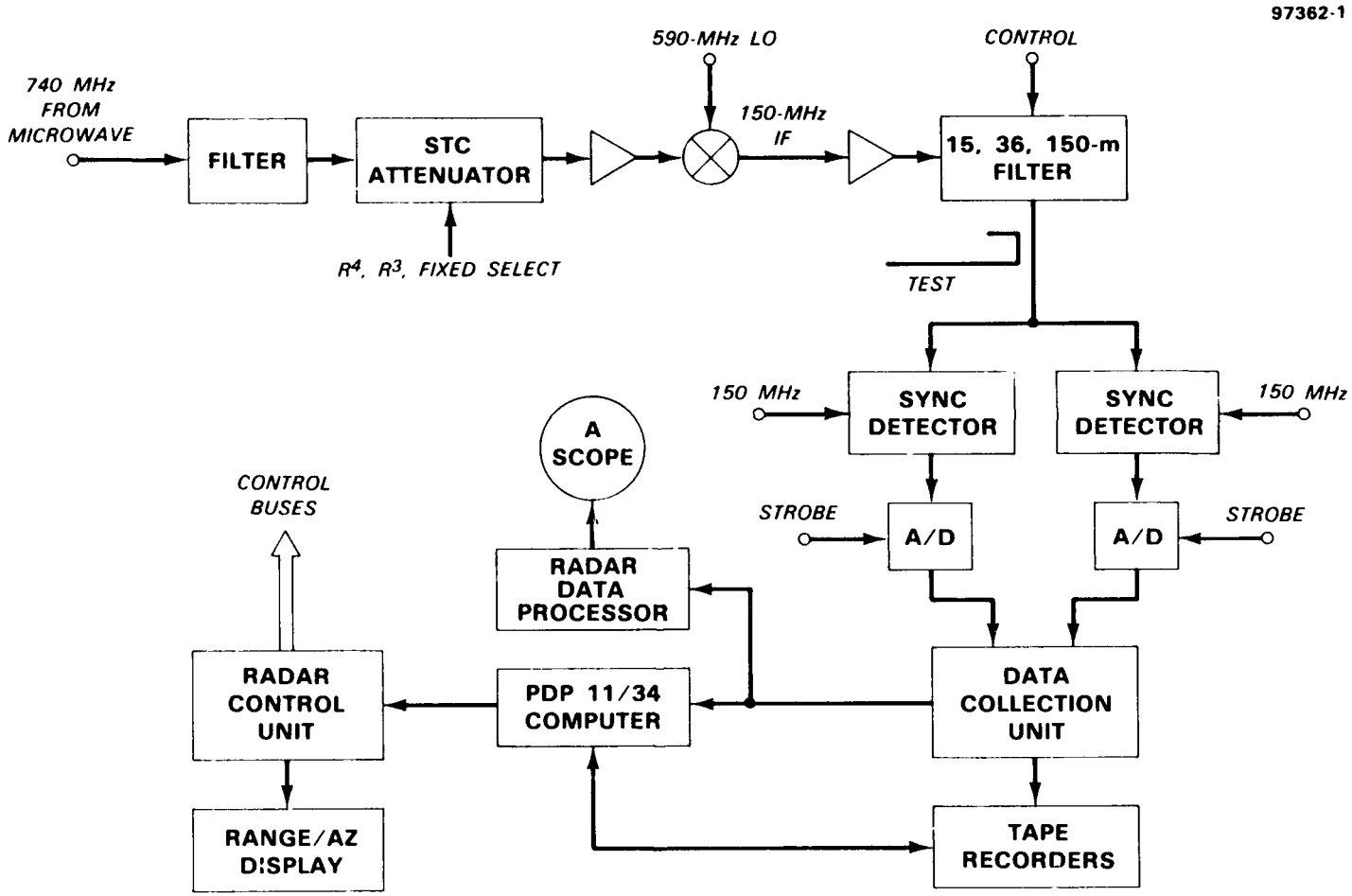

Figure A-9. Phase One receiver and signal processor.

TABLE A-7
Phase One System Capabilities

Frequencies	
VHF	162 MHz to 173 MHz
UHF	420 MHz to 450 MHz
L-Band	1220 MHz to 1280 MHz
S-Band	3220 MHz to 3380 MHz
X-Band	8900 MHz to 9300 MHz
Polarization	HH or VV
Beamwidth (nominal; see Table A.6)	Azimuth/Elevation
VHF	13 deg/42 deg
UHF	5 deg/15 deg
L-Band	3 deg/10 deg
S-Band	1 deg/4 deg
X-Band	1 deg/3 deg
Clutter Improvement Factor	60 dB (55 dB at S- and X-bands)
Range Resolution	
L-, S-, X-Bands	15 or 150 m
VHF, UHF	36 or 150 m
RCS Accuracy (nominal; see Table A-11)	2 dB rms
Minimum Range	1 km
Dynamic Range	
Instantaneous	60 dB
Attenuator Controlled	40 dB
A/D Sampling Rate	1, 2, 5, or 10 MHz
A/D Number of Bits	13
Data Recording Rate	625 Kbytes/sec
Output Data	pulse-by-pulse I & Q
System Sensitivity	
Signal-to-Noise dB (single pulse)	
VHF	9
UHF	14
L-Band	9
S-Band	8
X-Band	12
Clutter Reflectivity	-60 dB
Clutter Range	10 km
Waveform	150 m
Data Collection Modes	Beam Scan
	Parked Beam
	Beam Step
Azimuth Scan Rate	0 to 3 deg/sec

A.3 PHASE ONE CALIBRATION

Clutter measurements with the Phase One radar were accurately calibrated, both in terms of the spatial position in range and azimuth angle of each resolution cell on the ground and in terms of the signal strength that was reflected from each cell. This section provides an overview discussion of what was generally involved in these calibrations. More specific information is available documenting all of the details of calibration for every Phase One measurement site.

Each operating mode of the Phase One radar had associated with it an adjustable system range bias. These range biases were accurately adjusted when the equipment was first set up at Katahdin Hill at Lincoln Laboratory. These initial adjustments were made by measuring radar reflections from known discrete targets in the neighborhood that had previously been very accurately surveyed for other Lincoln projects. Range calibration was checked at every Phase One site, usually by using a prominent discrete object of opportunity (such as a water tower) as a radar target and checking its measured radar range against the value obtained from large-scale maps. This process was aided through use of special calibration software for controlling the radar where the cell containing the largest signal within a specified range and azimuth interval was automatically determined.

Azimuth information was provided in the Phase One system by a precision azimuth encoder in the servo drive mechanism for steering the antennas. Thus, every recorded pulse has associated with it in header information an azimuth position read from this encoder. The quantization interval of the encoder was 0.01 deg, and as such was much less than an antenna beamwidth. Occasionally, even with a supposedly fixed beam position, wind forces could cause very small positional variations which, even though small, were picked up by the encoder and precisely recorded on tape. The raw azimuth encoder data is relative angle information only and must be corrected by an additive offset to provide absolute azimuth with respect to true north. The correction angle varies from site to site, depending on the particular setup geometry realized by the trailer configuration at each site. The same test that checked range calibration at each site using a prominent discrete target as mentioned above, also was used to provide the azimuth servo correction angle (see Table A-3). This correction angle is the necessary angle to make the angular position of the target as provided by the radar agree with that determined from a large-scale map. At many of our western low-relief prairie sites, roads are surveyed to run north/south and east/west at 1-mi intervals. This road network was usually highly visible in the radar PPI display and served to substantiate correct angle alignment, as even small fraction-of-a-degree errors in alignment were easily discernible as slight rotations of this pattern. At occasional wilderness sites where no useful map reference targets were available, an alternate angle alignment procedure was utilized that involved surveying the line from wing tip to wing tip across the large VHF reflector and comparing its raw encoder angle in its surveyed position with survey true north. Thus, raw Phase One recorded clutter data were accurately calibrated in azimuth angle in the field and almost always need no further azimuth angle correction in subsequent data processing at Lincoln Laboratory.

Phase One signal strength calibration involved both internal and external procedures. Every recorded clutter experiment carries with it on the raw data tape both pre- and post-calibration files containing internally measured values of transmitter and receiver parameters. Table A-8 lists the parameters that were internally measured and recorded with each experiment and indicates the frequency at which these measurements were performed. These measurements were (for the most part) automatically performed

and recorded under computer control as part of the operating system of the radar. The internal calibration data were subsequently directly accessed and used in standard data reduction to calibrated clutter tapes in units of absolute clutter reflectivity at Lincoln Laboratory. The amplitude and phase of the transmitted signal were internally and automatically sampled and recorded for every pulse transmitted to allow tracking of minor variations in these data and their subsequent correction in data reduction. The purpose of this procedure was to provide a highly stable transmitted signal and hence a highly coherent reflected signal. However, such correction was generally not required to maintain high coherence in the Phase One calibrated clutter data base.

The automatic internal calibration measurements shown in Table A-8 calibrated the Phase One system up to the transmit and receive couplers. Beyond these couplers, the RF transmission line losses and antenna gains had to be checked by external tests. External calibration tests were conducted at most Phase One sites (see Table A-1). Table A-9 summarizes these external tests. In Table A-9, the boresighting tests refer to range and azimuth calibration using a prominent discrete reflecting object that is also indicated on a map, as discussed previously.

The Phase One antenna beams were not adjustable in elevation but were fixed horizontally aimed at the horizon (i.e., 0-deg depression angle). Thus, these beams always illuminated the ground, and hence, terrain multipath had to be contended with in external tests of signal strength calibration. As a result, these external signal strength tests were usually conducted as system checks to ensure proper operation rather than to provide actual measured calibration constants to be used in data reduction. Then, with proper operation ensured by these checks, standard stored values of transmission line loss and antenna gain, accurately measured at the outset of the program and at occasional, long-term periods through the program, were used in data reduction.

TABLE A-8
Internal Calibration Tests

Test	Frequency
Receiver gain	Each experiment
Transmitter average power	Each experiment
Transmit amplitude and phase	Each pulse
Antenna VSWR	Operator request
Receiver noise figure	Half hour
Synchronous detector balance	Half hour
DC correction loop	Half hour
Fixed attenuator	Each experiment
Sensitivity Time Control (STC)	Each experiment

TABLE A-9
External Calibration Tests

Test	Frequency Bands	Purpose
Standard gain antenna tests (receive and transmit)	VHF, UHF, L-Band	Signal strength calibration
Corner reflector tests	S-Band, X-Band	Signal strength calibration
Boresighting tests	All bands	Range and azimuth calibration
Reference object tests	All bands	Signal strength monitoring

If external test results consistently showed a trend of differing from expected results, they were used to adjust the standard stored values for antenna gains and transmission line losses. The external calibration tests required changes in stored values only twice. The first change occurred near the beginning of the program, when, after measurements at the first few sites, retroactive adjustments in gain at VHF and UHF (e.g., see Section A.2) were implemented in data reduction. That is, the data from the early sites were recalibrated at this point. The second change occurred about halfway through the program when a much longer history of calibration testing was available and allowed additional improvements in calibration accuracy to be made. This second set of improvements is shown in Table A-10. These improvements were not retroactively incorporated in all of the pulse-by-pulse calibrated data generated to that point in time, which would have been a major undertaking. Instead, we leave it to our application software that accesses the pulse-by-pulse calibrated data to make these adjustments on the early pulse-by-pulse data. However, subsequent pulse-by-pulse data and all of our partially integrated calibrated data (discussed later in this section) that were subsequently generated do incorporate these adjustments throughout.

TABLE A-10
Calibration Adjustments (dB) Required in Pulse-by-Pulse Calibrated Clutter Tapes Prior to Peace River South II*

Polarization	VHF	UHF	L-Band	S-Band	X-Band
Vertical	+0.8	−0.6	−1.2	−1.4	−2.6
Horizontal	+0.8	+0.8	+3.4	−2.2	−2.9

* Several early sites require slightly different adjustments than those shown here. These sites are Katahdin Hill (1), Shilo, Neepawa, and Polonia. The calibration adjustments shown are based on multisite external calibration experience up to and including Picture Butte II. Thereafter, the Phase One system tracked remarkably closely, and adjustments computed over the complete Phase One site history differ insignificantly from those shown.

Detailed information documenting the complete Phase One external calibration test history and defining calibration factors at all Phase One sites is available. Beyond the two adjustments mentioned above, the external tests at every site served their checkout function well by uncovering a number of equipment problems that had to be remedied before accurate clutter measurements could continue.

External signal strength calibration checks using standard gain antennas and corner reflectors were conducted before clutter data were taken at each site where external calibration was performed. External calibration tests were conducted as both receive tests and transmit tests at VHF, UHF, and L-band and as corner reflector tests at S- and X-band. The lower band receive tests consisted of radiating a signal from a standard gain antenna (horn at L-band, Yagis at VHF and UHF) located on a tower approximately 100 m from the radar tower. This located the standard gain antenna on the fringe of the near field of all of the low band radar antennas. An HP866A signal generator was used for the RF source. The RF signal was transmitted through a 100-ft coaxial cable to the standard gain antenna on top of the calibration tower, which could be expanded from 37 to 75 ft. By raising or lowering the tower the multipath effects could be accounted for by measuring the maximum and minimum signal level and calculating the free-space signal assuming a relatively constant reflection coefficient. A photograph of calibration with the L-band horn at Magrath is shown in Figure A-10. At the 100-ft radar tower height the multipath was usually less than 2 dB at all of the low band frequencies. At the 60-ft radar tower height the multipath effects remained small at UHF and L-band but were significant at VHF.

The lower band transmit tests were conducted by transmitting at the radar and receiving at the standard gain antenna. The equipment and procedures were identical to the receive tests except that an HP 1/36A power meter was used to measure the power received at the standard gain antenna. The receive test measurements were recorded both manually and on magnetic tape. The manually recorded data were analyzed on site. The tape-recorded data were later checked at Lincoln Laboratory. The results of the transmit tests were manually recorded only and analyzed on site.

The external tests at S- and X-band were conducted using a corner reflector of known RCS. The corner reflector RCS was +36.0 dBsm (i.e., dB with respect to 1 m^2) at X-band (9200 MHz) and +27.5 dBsm at S-band (3240 MHz). The corner reflector was mounted on the calibration tower approximately 3 km from the radar tower and was raised and lowered to account for multipath reflections similarly to the transmit and receive tests. If possible a line of brush or small trees was used to block the terrain multipath. Photographs of calibration with the corner reflector at Vananda East are shown in Figure A-11. The X-band returns seldom varied by more than 2 dB. The S-band returns did more frequently vary by more than 2 dB. However, measurements of the tower without the corner reflector indicated that the tower RCS was approximately 10 dB lower than the corner reflector RCS at S-band. All corner reflector measurements were recorded on tape for off-site processing.

As discussed previously, we did not adjust our calibration constants individually at each site on the basis of the external calibration tests there because the calibration tests were always conducted in a nonfree-space propagation environment and hence had some associated site-specific variation. Instead, we used average results over a multisite history of external tests to set calibration constants. This leaves us with site-to-site variations in our external tests. In other words, we have forced the average values of

Figure A-10. External calibration at Mograth. L-band calibration shown, using standard gain horn on transportable calibration tower.

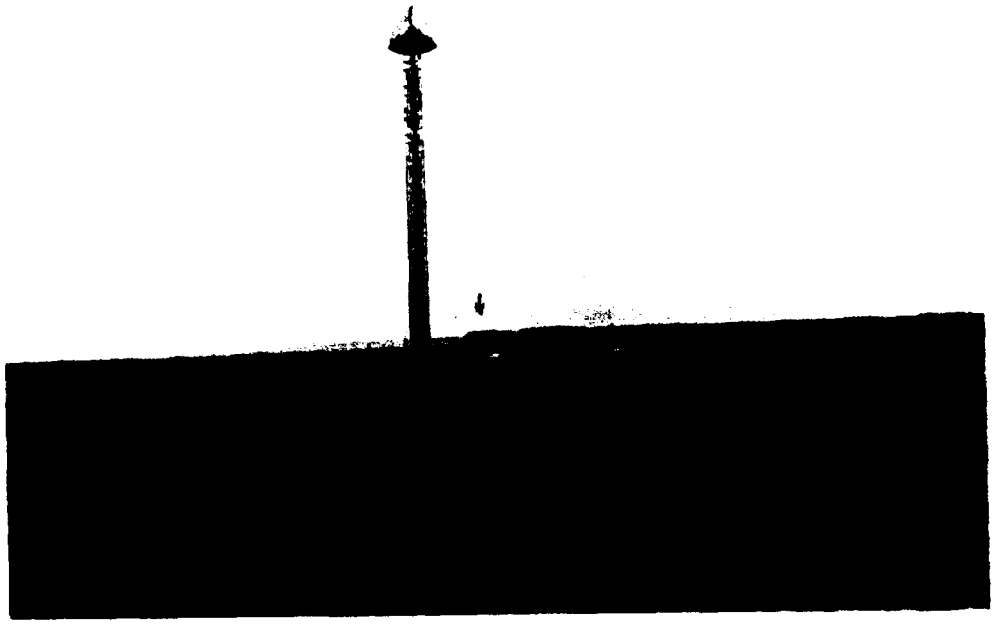

(a)

NW

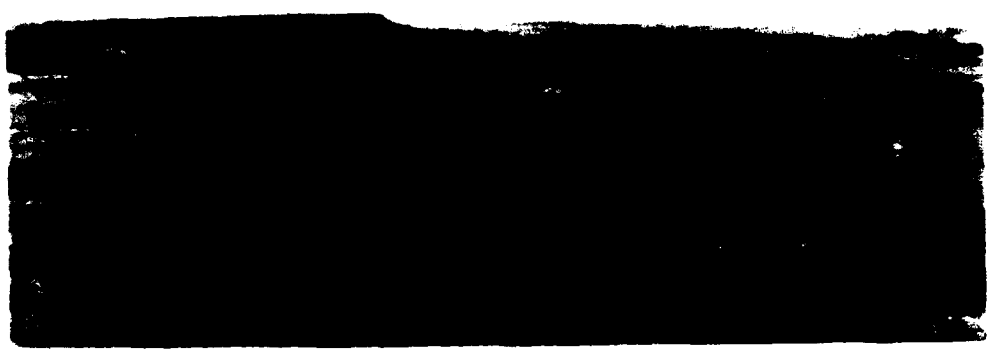

(b)

Figure A-11 External calibration at Vananda East S- and X-band calibration shown using corner reflector in far field. (a) Corner reflector calibration target under illumination from Phase One in background (arrow) and (b) Corner reflector position on protruding bluff (left of center) as seen from Phase One tower top looking NW along edge of escarpment

measured corner reflector RCS (high bands) and measured antenna gain of our standard gain antennas (low bands) equal to their theoretical values as measured over many sites, but there are site-to-site variations in these measurements.

Table A-11 shows the standard deviation by band and polarization in the site-to-site variations in these Phase One external calibration measurements over the history of the program (see Table A-1). Table A-12 shows similar data from a single reference target (see next paragraph) for Phase One's nine-month subsequent setup on Katahdin Hill (3) (see Section A-1). As expected in Tables A-11 and A-12, the variations occurring at a fixed site are less than those occurring across many sites. In totality, we feel that the variations shown in both Tables A-11 and A-12 are satisfactorily small and generally validate our quoted estimate for accuracy of 2 dB rms (see Table A-7).

At all sites, including those at which external signal strength calibration checks using standard gain antennas and corner reflectors were conducted, we attempted to find prior to clutter data collection a discrete reflecting object in the neighborhood suitable for use as a reference target, such as a water tower (it may have been the same object used in range and angle calibration; see Table A-9). Then, prior to and throughout clutter data collection, the return from the reference object was repeatedly measured and recorded to ensure that no changes occurred in system calibration. As a result, a set of measurements of reference target RCS in each band exists for each site. For each site and band we computed the standard deviation across this set of measurements. Table A-13 shows the mean and median values of these standard deviation numbers in each band across all sites. (Table A-13 also shows the standard deviations by site and by band of these standard deviation numbers across all sites.) The data in Table A-13, which summarize many more measurements than Tables A-11 and A-12, also provide satisfactory confirmation of day-to-day calibration repeatability based on measurements from objects such as water towers. This monitoring procedure using a reference target of opportunity also provided occasional indication of system problems requiring subsequent correction.

Finally, we bring into discussion once again the value of our repeated clutter measurements. At each site, a small azimuth repeat sector, usually about 10 or 20 deg wide, was selected for repeated measurements. The purpose of these repeat sector measurements was severalfold. First, they could provide a subsequent basis for revealing problems in equipment and calibration that might have occurred since the last calibration tests. In fact, on one occasion hardware problems were uncovered in subsequent clutter data analysis at Lincoln Laboratory because of unusual trends first observed in repeat sector results. Second, when consistent the measurements would indicate the variability in ground clutter that occurs due to changes in weather and other environmental factors. Third, they allowed the exercise of a broader radar parameter matrix to provide a data base of more depth across a small spatial extent of clutter than would be feasible throughout our overall data collection. Almost all of the Phase One data presented in this report are repeat sector data. Therefore, these data may be considered with higher confidence than normal to be free of anomalies and representative of the general weather and environmental conditions prevailing at a site rather than representative of unusual or extraordinary conditions.

TABLE A-11
Standard Deviations (dB) of External Calibration Measurements for Phase One over the Radar's Three-Year History*

Polarization	Frequency Band				
	VHF	UHF	L-Band	S-Band	X-Band
Vertical	1.5	1.3	1.2	2.3	1.5
Horizontal	2.0	1.6	1.4	2.4	1.6

* External calibrations were performed at 36 Phase One sites. Far-field measurements on a corner reflector were made at X- and S-bands. Near-field receive and transmit calibration tests were conducted at L-band, UHF, and VHF, using standard gain antennas. The standard deviations are of differences between expected and measured results. Calibration constants were set such that mean values of these differences over multiple sites (see Table A-10) were zero.

TABLE A-12
Standard Deviations (dB) of Measurements of Reference Target RCS at Katahdin Hill (3) over a Nine-Month Period*

Polarization	Frequency Band				
	VHF†	UHF	L-Band	S-Band	X-Band
Vertical	1.16	0.73	0.71	0.97	0.99
Horizontal	1.69	0.75	0.90	1.25	0.94

* Following Phase One's tour of Canada and the U.S., the radar collected ground clutter and reference target data once a week over a nine-month period at the Katahdin Hill site [1]. At Katahdin Hill, the reference target was a 120-ft tall, 40-ft diameter cylindrical water tank adjacent (60-ft distant) to a 150-ft tall, triangular-shaped radio tower, located east-northeast of the site at an azimuth of 68.6 deg and a range of 6.46 km.

† Severe VHF interference frequently occurred at the Katahdin Hill site. Although efforts were made to avoid this interference during data collection, it may have affected the consistency of the VHF measurements.

TABLE A-13
Standard Deviations (dB) of Measurements of Reference Target RCS at 33 Sites*

	Frequency Band				
	VHF	UHF	L-Band	S-Band	X-Band
Mean	0.59	0.51	0.69	1.15	1.81
Standard Deviation	0.31	0.26	0.40	0.72	1.22
Median	0.58	0.44	0.62	1.00	1.38

* Daily reference target data were collected at 33 Phase One sites over the radar's three-year history. At each of these sites, a strong discrete reference target of opportunity, such as a nearby water tower, was selected to check day-to-day system repeatability. At nine sites, typically northern wilderness sites, useful reference targets were not found.

Final data reduction of the Phase One clutter tapes containing raw counts of A/D power to calibrated clutter tapes in units of absolute reflectivity took place in a dedicated Phase One data reduction facility at Lincoln Laboratory. In data reduction, clutter reflectivity was calculated from the following equation.

$$\sigma F^4 = \sigma^\circ F^4 \cdot [R \cdot \Delta R \cdot \Delta\theta] = \frac{(4\pi)^3 R^4 P_r L_t L_r L_{STC}}{P_t G_t G_r G_{rec} \lambda^2}$$

where

σF^4 = clutter radar cross section (m^2)

$\sigma^\circ F^4$ = clutter strength or clutter reflectivity (m^2/m^2)

F = propagation factor

ΔR = range resolution (m), see Table A-7

$\Delta\theta$ = azimuth one-way beamwidth (radians), see Table A-6

P_t = peak transmit power (W), see Tables 2 and A-8

G_t = transmit antenna gain including antenna losses

G_r = receive antenna gain including antenna losses

L_t = transmit losses from the transmit coupler to the antenna terminals

L_r = receive losses from the receive coupler to the antenna terminals

L_{STC} = STC attenuation versus range

G_{rec} = receiver gain

λ = wavelength (m)

R = calibrated range (m)

P_r = received power at A/D input (W)

The transmit and receive losses (the convention used here assumes L > 1) represent the losses from the points at which the transmitter power or the receiver gain was measured, respectively, to the antenna terminals. As discussed previously, these losses were measured directly only a few times over the life of the system but were regularly checked along with the antenna gain by the external calibration tests. Also as discussed previously, the transmitter power output, receiver gain, STC attenuation as a function of range, and the fixed attenuation were measured before and immediately after recording each clutter experiment. Because P_r is calculated the same way for signal return as for the receiver gain measurement, all measurements were referenced to the RF signal level coupled into the receiver front end, which was accurately measured with a power meter.

The Phase One data reduction facility at Lincoln Laboratory was situated remotely from the Lincoln Laboratory main computer center. Raw clutter tapes were shipped from site to the data reduction facility where they were processed to generate pulse-by-pulse calibrated clutter tapes that were then moved to the main computer center for subsequent clutter analysis studies. The Phase One data reduction facility was configured around two Digital Equipment Corporation PDP-11/34 minicomputers, which were the same model and thus compatible with the field computer that controlled the radar and recorded the measurements. The dual PDP-11/34s in the data reduction facility shared peripheral devices, and together provided high-density and fast data conversion and recording and high-resolution graphics.

Support personnel for the data reduction facility included a production supervisor, a calibration engineer, two software analysts, and two operators. For a typical measurement site, the raw data might comprise 240 clutter experiments on 20 high density (i.e., 6250 bpi) tapes with 6500 stored records per tape. This set of raw data would be converted to calibrated data in about 12-1/2 days in the data reduction facility, or less than the nominally two-week site turnaround time of the measurement equipment. The 12-1/2 days is broken down as follows. The data reduction facility utilized its dual PDP-11/34s in three eight-hour single machine shifts per day (i.e., 24 computer hours per day). Calibration throughput was about 433 records per hour or 15 hours per raw tape, which expanded to 300 computer hours or 12-1/2 days for all 20 tapes. A tape volume expansion factor of about 2-1/2 occurs in converting raw data to calibrated data, largely because integer numbers (A/D converter counts) are stored on the raw tapes, but real numbers (clutter reflectivity) are stored on the calibrated tapes.

Besides production calibration of the raw clutter tapes, other work carried out at the Phase One data reduction facility included preparation of the radar directive files for clutter experiments at upcoming measurement sites and analysis of all the external calibration experiments for each site as they returned in the raw data package for each site. As the raw data tapes from each site arrived at the data reduction facility, all of their raw headers were stripped onto a single auxiliary tape, which was delivered to the Lincoln Laboratory main computer center. This tape was used to extend the Master File of the data base management system resident on the Amdahl 470 central computer to cover that site. Later, as the cali-

brated clutter tapes in IBM format arrived for use in the main computer center, they were also incorporated within the Master File, which provided general access to the calibrated clutter experiments and to the header information involving measurement equipment and environmental parameters. Our final Master File providing access to all of the voluminous Phase One data is reported on in other documentation.

Altogether, this conversion from raw to calibrated clutter data on a pulse-by-pulse basis resulted in generating 3601 calibrated data tapes. An additional process has been completed, which partially integrates our pulse-by-pulse clutter data over a number of pulses per resolution cell to make an alternative, more manageable data base of reduced tape volume. The number of pulses integrated was often 16 or 32, in any event, less than or equal to one-quarter beamwidth in scan mode and/or much less than a temporal correlation period in scan or step mode. The overall volume reduction factor was about 15. The integrated data continues to be organized on a per experiment basis but also contain a system noise file and saturation file for each experiment in order that the window of dynamic measurement range that existed for each experiment be easily available. Final uniform calibration exists across our complete set of partially integrated data.

A.4 PHASE ONE DATA COLLECTION

A.4.1 Scope

Low-angle radar ground clutter is a complex phenomenon. Nevertheless, as a random process, all of its descriptive attributes must fall somewhere within the list shown in Table A-14. First, we can consider variation that occurs from point to point in space. If we are interested in how strong the clutter is across an ensemble of spatial points, we can answer the question statistically in terms of a histogram of clutter amplitudes, one from each spatial point. The other pertinent question concerning spatial variation is, how far must the sampling point move for the clutter amplitude to change significantly. This question is answered statistically in terms of correlation distance in the random process. Second, we can consider variation that occurs at any given point with passing time. As with spatial variation, we answer the question of temporal variation of clutter strength in terms of a statistical histogram of clutter amplitudes measured consecutively in time at a given point. With temporal variation, the remaining question is, how long does it take for the clutter amplitude to change significantly, and we answer the question statistically in terms of correlation time. It is well known that the spatial information contained in correlation distance and the temporal information contained in correlation time are equivalent to the spectral information in the random process in space and time, respectively, because the Fourier transform of the autocorrelation function is the power spectrum.

How can such a simple overall descriptive scheme as is illustrated in Table A-14 become so complicated when applied to the real phenomenon of low-angle ground clutter? Much of the answer has to do with scale. Clutter is spatially nonhomogeneous. That is, it varies spatially in a complex way. As a result it presents many different observable attributes depending on the scale at which it is observed. For example, consider a woodlot adjacent to an open agricultural field. No one would argue that, at microscale, the clutter statistics within the wooded area constitute an entirely different process and should be investigated separately from those applicable to the open field. By the prefix "micro-," we imply resolution-

cell-sized areas. But what about the clutter statistics from the important boundary region between woodlot and agricultural field? It turns out that the strong clutter returns from such boundary regions, and other features of vertical discontinuity that exist pervasively over almost all landscapes, dominate in low-angle clutter. In this regard the field of low-angle clutter is akin to such modern fields of investigation as digitized map processing, SAR image data compression, pattern recognition, artificial intelligence, and other fields where spatial feature is important. In all of these areas of investigation there is much importance in edges of features and in defining, storing, and recognizing such edges.

TABLE A-14
Radar Ground Clutter Statistics

Spatial Variations
Amplitude Statistics
Correlation Distances
Temporal Variations
Amplitude Statistics
Correlation Times/Spectra

Thus, we are led from microscale to macroscale, where by the prefix "macro-" we imply kilometer-sized regions encompassing hundreds or thousands of spatial resolution cells and many vertical features. The correct empirical approach in dealing with all of these edges of features is to collect meaningful numbers of them together within macropatches and let the terrain classification system carry the burden of statistically describing the attributes of the discontinuous clutter sources within macropatches at a gross overall level of description. In Tables A-15 and A-16 we attempt to summarize briefly such distinctions in scale for spatial and temporal variation in clutter statistics, respectively, and illustrate our principal focuses of interest. Thus, in Table A-15, our main interest in spatial amplitude statistics is their prediction as they occur for ground-based radar over macropatches of visibility. Such spatial patches are, in gross measure, predictable geometrically from digital terrain elevation data. The subsequent problem of predicting clutter strengths within such patches is where we felt we had most to learn and is what took us to many different sites and patches to build up an appropriate supportive statistical data base. With lesser emphasis, we have gone on to statistical issues of patch length and separation and how the occurrence of clutter generally decreases or rolls off with increasing range. We have only done a little work, in terms of a set of individual examples, showing correlation distance at microscale within homogeneous patches. Such microspatial correlation is important, for example, in the detailed processing algorithms of CFAR radars (an important subject but by no means of major emphasis to date in our program).

TABLE A-15
Spatial Variations

Scale	Focus of Interest
Macrospatial Scale = many sites, many square km	Amplitude Statistics Major analysis effort Visibility and Shadow Patch length and separation Range roll-off
Microspatial Scale = resolution cell	Correlation Distance CFAR algorithms

Proceeding on to Table A-16, issues of temporal variation of low-angle ground clutter have generally been of somewhat lesser concern to us compared to our more stressing problem of modeling macrospatial amplitude statistics. But the subjects overlap somewhat in the sense of how our general spatial amplitude statistics vary with long-term macroscale temporal variation associated with weather and season. This report statistically quantifies such long-term variation (see Section 7). Furthermore, for short-term microscale temporal variation, we have generated some information describing the relative frequency of occurrence of temporal amplitude statistics between cells with Rayleigh (i.e., wind-blown foliage) and Ricean (i.e., fixed discretes) statistics and have generated a substantial amount of information on spectral extent and correlation time of L-band radar reflections from wind-blown trees [1].

TABLE A-16
Temporal Variations

Scale	Focus of Interest
Long-Term Scale = seasonal	Amplitude Statistics Monitor trends
Short-Term Scale = ms	Amplitude Statistics Rayleigh vs Ricean Spectra/Correlation Time Wind-blown foliage

A.4.2 Operating Modes

Table A-17 shows the three main operating modes of the computer-controlled Phase One five-frequency radar system. When the Phase One equipment was first set up at a site, prior to actual clutter data collection, the overall nature of the clutter at that site was assessed using a quick-look software module for radar control called Site Assessment Control (SAC). The SAC module allowed a digital PPI clutter plot to be displayed, which showed the spatial extent of the clutter at that site simply by showing where the received signal was above the radar noise level. Examples of Site Assessment digital PPI clutter plots for all five frequency bands at Cochrane are shown in Figure A-12. These PPIs were generated under scan mode. Due to scan constraint (i.e., cable wrap) limitations, it was not possible to generate a complete 360-deg PPI with one scan (about 330 deg were possible). Thus, the complete PPIs shown in Figure A-12 have been assembled from two, nominally 180-deg scans. For the PPIs of Figure A-12, the maximum range is set at 101 km. The basic spatial nature of the clutter in Figure A-12 is seen to be relatively frequency independent, at least to the extent that it can be discerned through the decreasing azimuth resolution (i.e., increasing azimuth beamwidth) as frequency reduces from X- and S-band (beamwidth = 1 deg) through L-band (beamwidth = 3 deg) to UHF (beamwidth = 5 deg) and VHF (beamwidth = 13 deg). Some evidence of interference is observed in the VHF PPI clutter plot. VHF interference was a continuing problem in Phase One data acquisition. Such interference was usually removed in the coherent processing of our calibrated data. Most VHF data were acquired at late night or early morning hours to minimize interference.

TABLE A-17
Phase One Operating Modes

Mode	Purpose
Site Assessment Control (SAC)	Initial checkout of site and system
Clutter Data Collection (CDC)	Mainline data acquisition
Mission Analysis Module (MAM)	Final checkout of recorded data

The main display products available on-board from the raw CDC clutter tapes after data collection (referred to as Clutter Data Collection or CDC in Phase One operations, see Table A-17) were obtained from software collected together in a Mission Analysis Module (MAM). B-scope plots were available in MAM, which showed stepped levels of clutter reflectivity on range (abscissa) and azimuth (ordinate) axes. Examples of MAM B-scope plots for all five frequency bands at Cochrane are shown in Figure A-13. In comparing these plots with the digital PPI plots of Figure A-12, note that the B-scope plot covers an angle interval to the southwest from 190 to 260 deg and a range interval from 1 to 48.4 km. In contrast

to the SAC PPI plots that simply show signal strength above noise, the MAM B-scope plots are roughly calibrated to show absolute reflectivity (i.e., $\sigma^{\circ}F^4$). Calibration of absolute clutter reflectivity within MAM uses nominal design parameters only. In Figure A-13, reflectivity is thresholded to lie between 0 and -60 dB. An exception to this in Figure A-13 is the S-band plot, where the data are uncalibrated due to excess loss introduced by a faulty limiter. Even though the resultant S-band B-scope display is weaker, it is evident that the spatial nature of the clutter is very similar to that at X-band. Also, in Figure A-13, the X- and S-band data within the first 2 or 3 km are stronger than indicated because they were measured at high depression angles well beyond the 3-dB points on the elevation patterns, and these elevation pattern effects are not included in the relatively crude MAM calibration algorithms (note that terrain elevations must be known to correct for elevation pattern effects). It is evident in Figure A-13 that the X- and S-band data were collected under scan mode; whereas, the L-band, UHF, and VHF data were collected under step mode.

Clutter histograms could also be generated in MAM. Histograms of A/D clutter power are shown in Figure A-14 for the same angular sector at Cochrane as was illustrated in the B-scope displays of Figure A-13. An exception is the S-band histogram in Figure A-14, where better calibrated (but still uncertain) data from a narrower (but included) sector is presented. Note that in these A/D clutter power histograms, generally the first few bits are evident at the far left end of the histogram (i.e., 6 dB between first and second bits, 3 dB between second and third bits), followed by roughly Gaussian-distributed noise, and then a tail of high clutter values. The distinction between noise and clutter is less evident at UHF and VHF. MAM histograms of clutter reflectivity (i.e., $\sigma^{\circ}F^4$) corresponding to the A/D clutter power histograms of Figure A-14 and the B-scope displays of Figure A-13 are shown in Figure A-15. Although the MAM calibration algorithm attempts to remove radar noise samples from these reflectivity histograms, the MAM estimate of radar noise level is uncertain, and the lower (or far left) ends of these histograms are likely to be noise contaminated. However, the upper (or far right) ends, even though only roughly calibrated, definitely contain valid, strong clutter samples, and it is these strong samples that primarily determine mean level and other important statistics. Note that the top tail reaches up to about $\sigma^{\circ}F^4 = -7.5$ dB at all frequencies in Figure A-15 (except S-band, where calibration is uncertain).

The quick-look, on-board data displays available under SAC and MAM from the CDC tapes containing raw A/D counts should not be confused with our mainline analysis efforts based either on the pulse-by-pulse Calibrated Clutter Tapes (CCTs) or Integrated Clutter Tapes (ICTs, see Section A-3), both in absolute units of reflectivity. We include this brief discussion of SAC and MAM here partly for completeness and historical interest and partly to emphasize that, in any large-scale measurement program like this, acquisition of raw data is only half the battle. Such programs require major calibration and analysis elements well beyond the sort of quick-look SAC and MAM efforts illustrated here.

A.4.3 CDC Experiment Types

The basic entity in which we recorded Phase One data was as a Clutter Data Collection (CDC) experiment. In each experiment, clutter returns were measured pulse by pulse from every resolution cell on the ground over some area defined by beginning and ending limits on both range and azimuth for a given antenna mode and for a fixed set of radar parameters. Each experiment is defined by a Radar Directive File (RDF). The RDF controlled the Phase One measurement system during acquisition of the

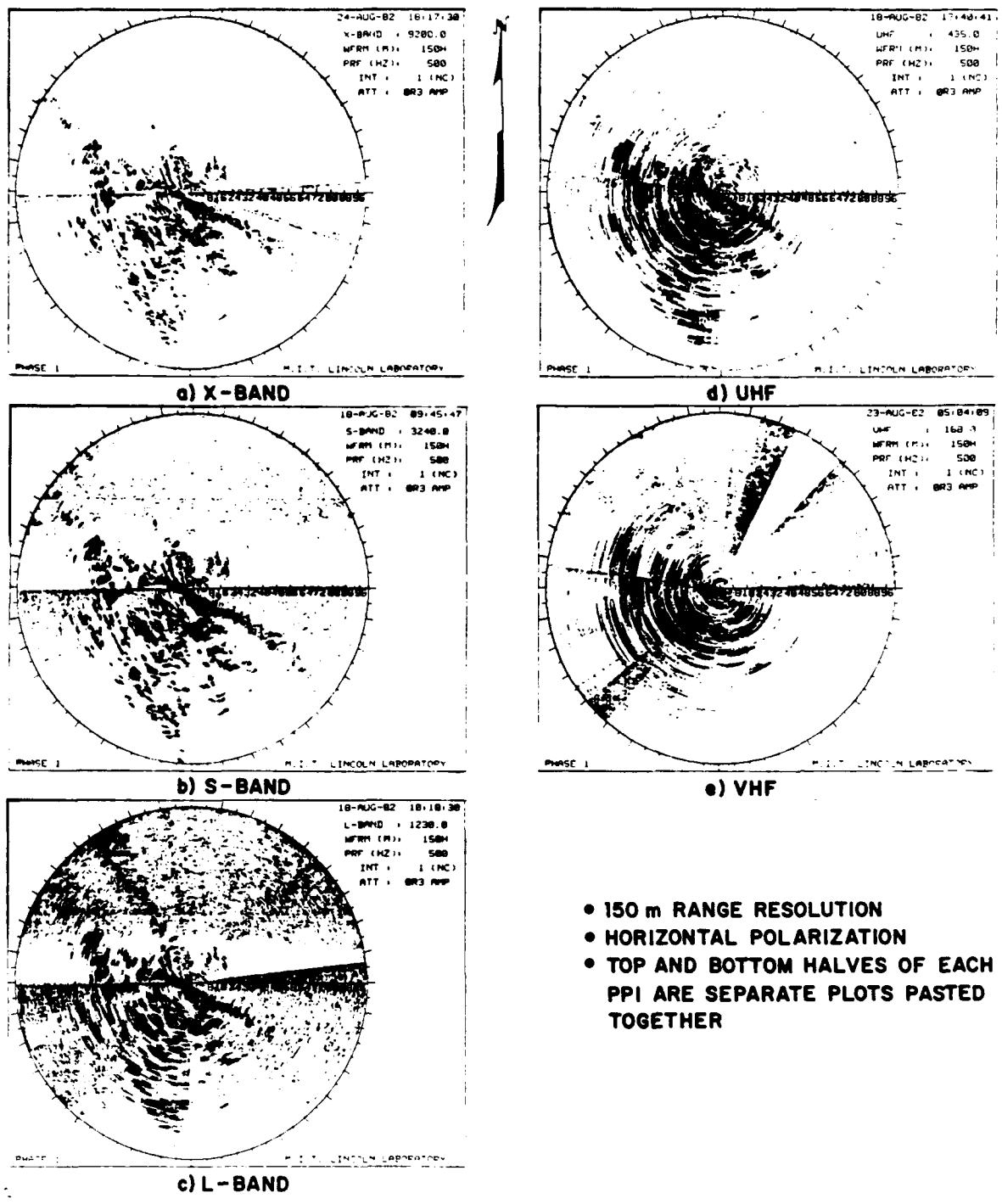

Figure A-12. Phase One site assessment digital PPI clutter plots for Cochrane. Clutter shown to 101-km range for all five frequency bands.

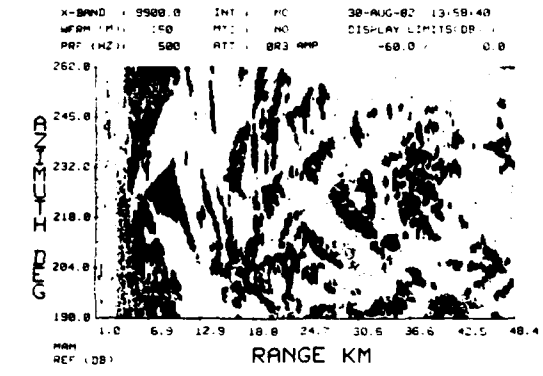

a) X-BAND

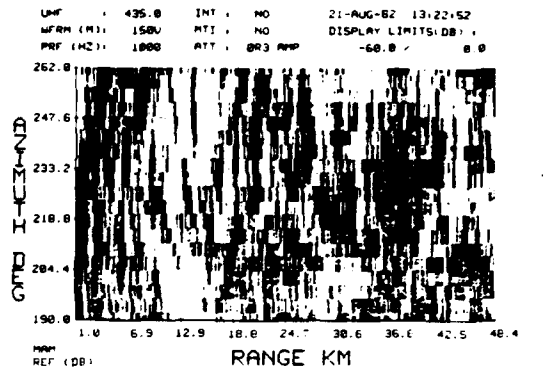

d) UHF

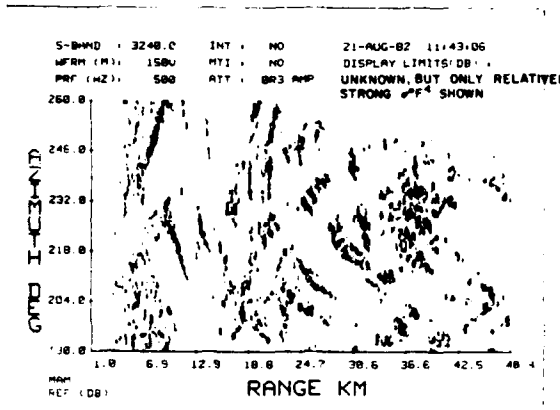

b) S-BAND (uncalibrated)

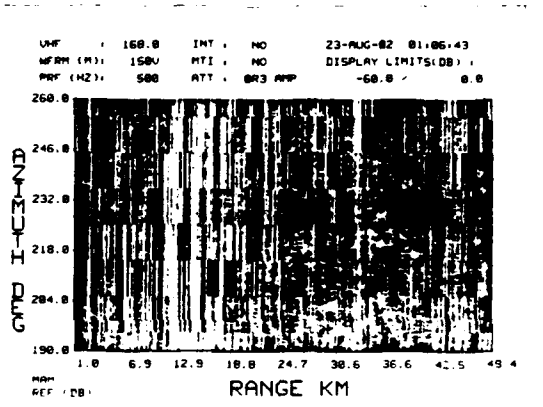

e) VHF

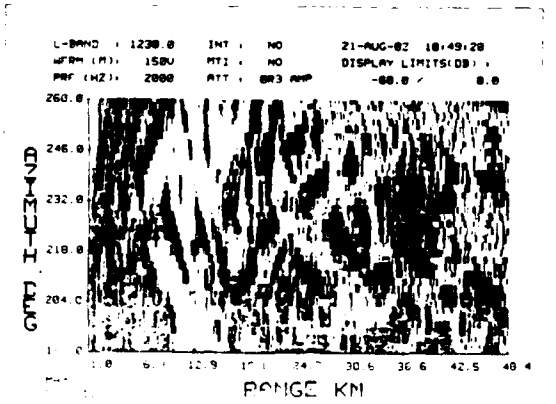

c) L-BAND

- 150 m RANGE RESOLUTION
- VERTICAL POLARIZATION
- $-60\ dB \leq \sigma^{\circ}F^{4} \leq 0\ dB$
- TRUE NORTH = 0 DEGREES AZIMUTH

Figure A-13. Phase One mission analysis $\sigma^{\circ}F^{4}$ range/azimuth B-scope plots for a southwest sector at Cochrane. All five frequency bands.

clutter data within each experiment. The RDF parameters requiring specification for each CDC experiment are shown in Table A-18. Our mainline clutter data were obtained as either "survey," "repeat," or long time dwell or "hop" data. Our reasoning for distinguishing our experiments in these three categories is summarized in Table A-19 and expanded upon in Tables A-20, A-21, and A-22. This threefold distinction serves only as an indication of what our intent was for taking each type of data. The RDF contains all of the actual defining information for all CDC experiments.

Elsewhere in this report long time dwell experiments were mentioned, where, within the repeat sector, we collected long time dwells, often comprising 30,720 pulses, from selected resolution cells. Historically, we came to refer to these long time dwell experiments as "hop" experiments because we often repeated these experiments five times, one right after another, with 3-min wait periods between 1.024 min data-recording intervals at 500 Hz PRF while the computer re-cycled.* In this manner we extended the overall duration of our standard five-hop record of temporal data to 17.12 min. Although survey data and repeat sector experiments were recorded at all sites, in the interest of speeding up data collection operations time-hop experiments were not recorded for a sequence of 12 sites, Westlock (setup number 10) through Plateau Mountain (setup number 21).

TABLE A-18
Radar Directive File Parameters for Clutter Data Collection Experiments

Measurement Sector	**Radar Parameters**	
Range (km): (a) START (b) EXTENT	Frequency:	VHF, UHF, L-, S-, X-Band
Azimuth (deg): (a) START (b) STOP	Polarization:	VV or HH
Antenna Mode	Resolution (m):	15, 36, 150
(1) Step: (a) Azimuth increment (deg); (b) Number of recorded pulses ≤ 30,720	Range Sampling Rate (MHz):	1, 2, 5, 10
	PRF (Hz):	500, 1000, 1500, ... 4000
or	Record 1 out of N Pulses:	N = 1, 2, 4, 8, 16
(2) Scan: (a) Scan velocity ≤ 3 deg/s	Attenuation:	
	Fixed:	1, 2, 3, ... 40 dB
	STC:	R^3 or R^4; 40 dB at 1 km

* Such sequences of repeated experiments were automated in our software control of the radar under a "burst mode" of data collection. See Table A-24, fields 100 and 102.

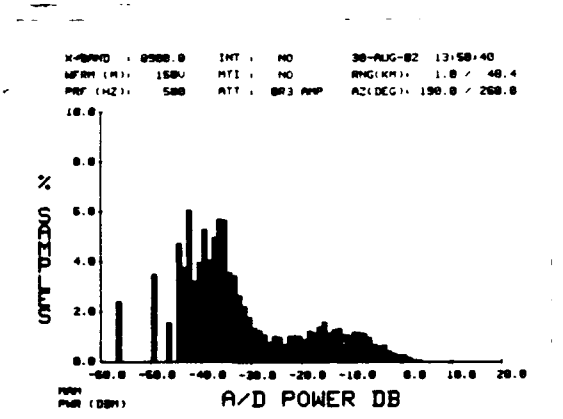

a) X-BAND

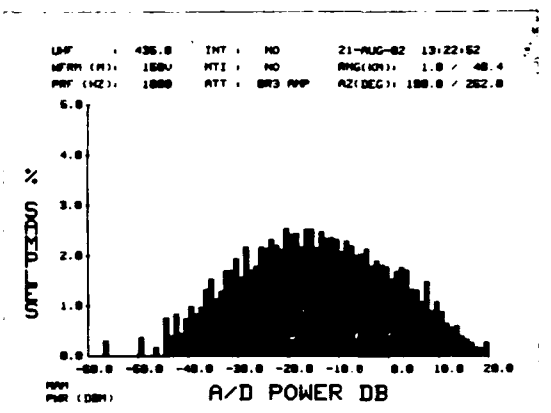

d) UHF

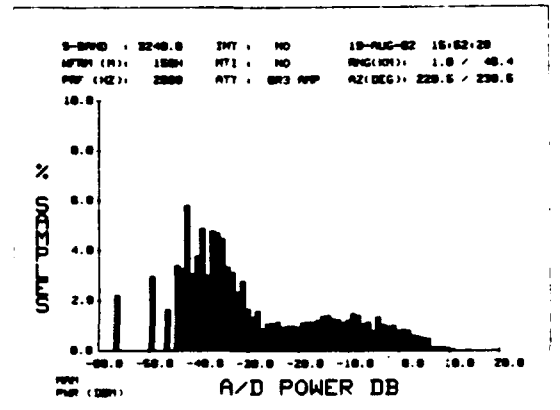

b) S-BAND (calibration uncertain)

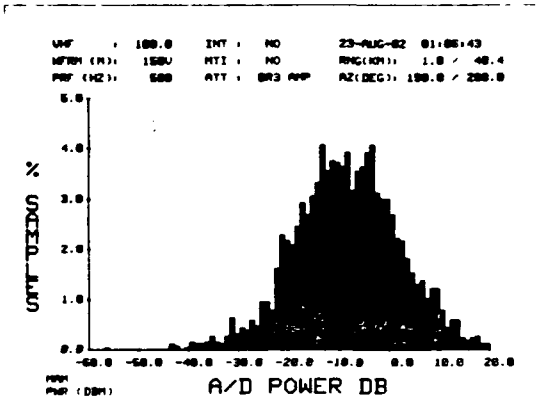

e) VHF

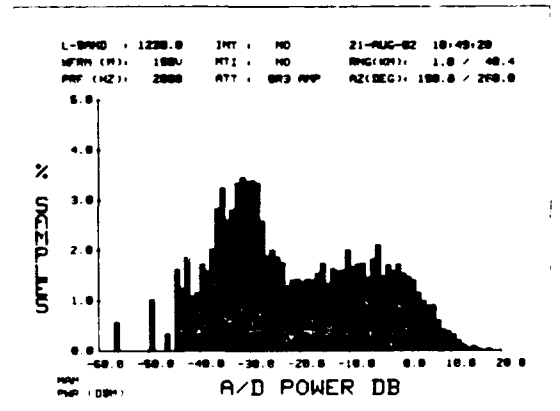

c) L-BAND

- 150 m RANGE RESOLUTION
- VERTICAL POLARIZATION (EXCEPT HORIZONTAL POLARIZATION AT S-BAND)

Figure A-14. Phase One mission analysis A/D power histograms for a southwest sector at Cochrane. All five frequency bands.

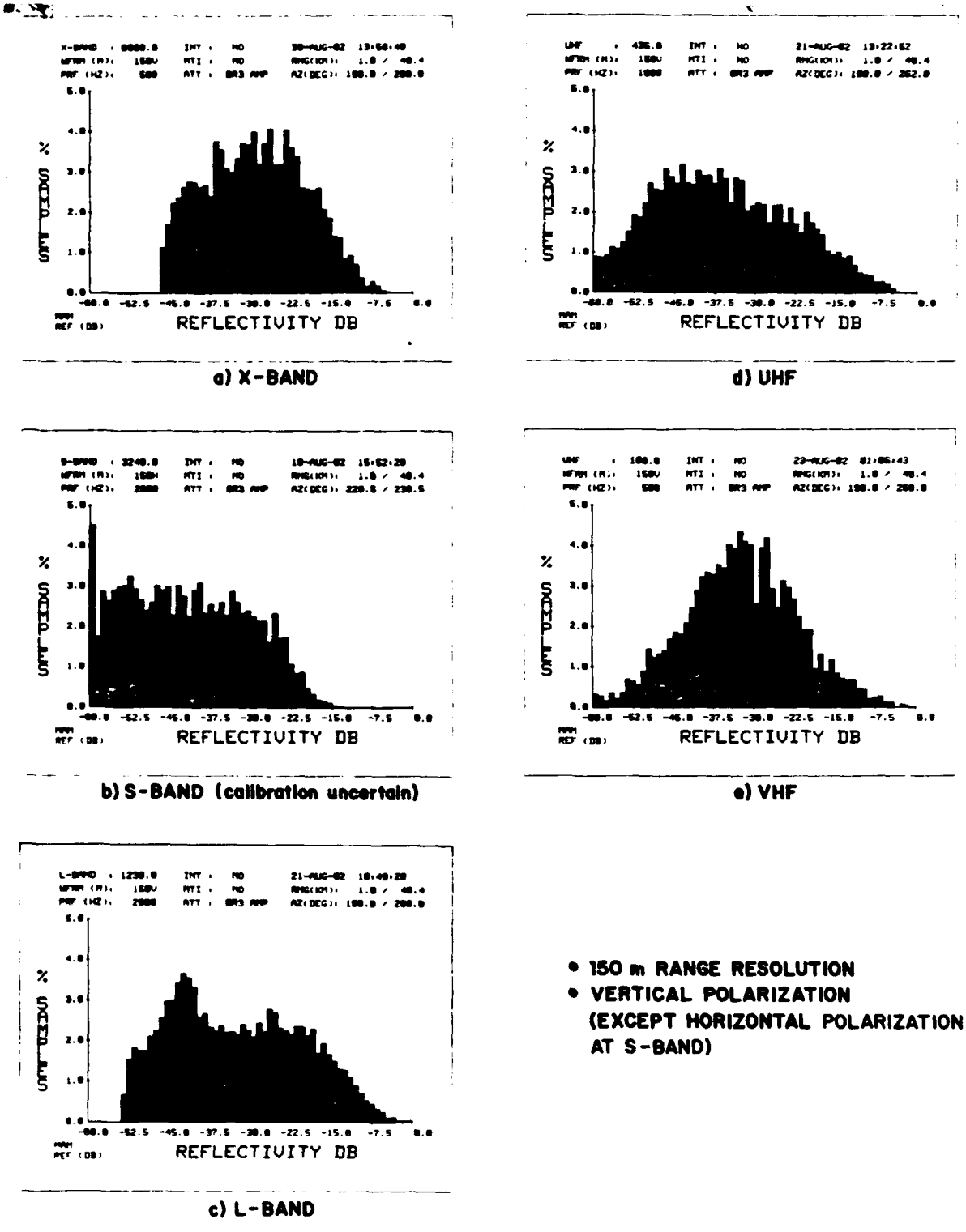

Figure A-15. Phase One mission analysis $\sigma^{\circ}F^{4}$ histograms for a southwest sector at Cochrane. All five frequency bands.

TABLE A-19
Nomenclature for Clutter Data Collection Experiments

Survey
Measure all clutter within field-of-view
Repeat
Several repeated measurements of a selected narrow sector
Hop
Measure long time histories on a few selected cells

TABLE A-20
Survey Experiments in Clutter Data Collection

Purpose
Macrospatial amplitude statistics
Long-term temporal variations
Method
Record all discernible clutter
Use fast scan (e.g., 2°/s), low sampling frequency (e.g., 125 Hz) to keep data volume down
Leads to:
(1) Few samples per cell (e.g., 125)
(2) Short temporal records (e.g., <1 or 2 correlation periods)
(3) Little temporal averaging
Data
49 setups
2073 calibrated clutter tapes

TABLE A-21
Repeat Sector Experiments in Clutter Data Collection

Purpose

- Sector of concentration
- Environmental variations
- System monitor

Method

- Narrow sector, 10 or 20 deg
- Experiments repeated several times within time-on-site
- More samples/cell (e.g., 1024)
- High sampling rate (e.g., 2000 Hz) for integration gain
- Low sampling rate (e.g., 31 Hz) for time averaging
- Step versus scan
- Occasional radar parameter variations (e.g., tower height)

Data

- 49 setups
- 1137 calibrated clutter tapes

TABLE A-22
Long Time Dwell or Hop Experiments in Clutter Data Collection

Purpose

- Short-term temporal variations
- Correlation periods
- Doppler spectra

Method

- Parked beam
- Few selected range gates (e.g., 16)
- Record time history over many correlation periods (e.g., 5 successive 60-s bursts, 2-ms sampling period, successive bursts separated by 3 min)

Data

- 37 setups (12 sites omitted, Westlock through Plateau Mountain)
- 391 calibrated clutter tapes

A.4.4 Master File

In Table A-23 a printout is provided of the Lincoln Laboratory Master Directory File listing some of the CDC ground clutter experiments recorded at the Altona II measurement site. The Master File provides enough high-level descriptive information for each measured Phase One data file to serve as the point of entry into our Phase One measurements. The complete Phase One Master File is provided elsewhere.

The Altona II Master File printout of Table A-23 is organized in two parts. Part (a) shows all of the X-band experiments collected. In the interest of saving space, part (b) shows only the high range resolution, vertical polarization (i.e., thin vertical or TV) experiments collected in all five bands. Each line in the Master File represents one clutter data collection experiment (see Table A-17). Each experiment is defined by its Radar Directive File (see Table A-18). The fourth entry on each line of the Master File is the RDF name for that experiment. The RDF name is simply an arbitrary sequence of up to eight alphanumeric characters intended as a high-level scratch pad indicator of the purpose of that experiment. Our general scheme for naming many of our RDFs was as follows.

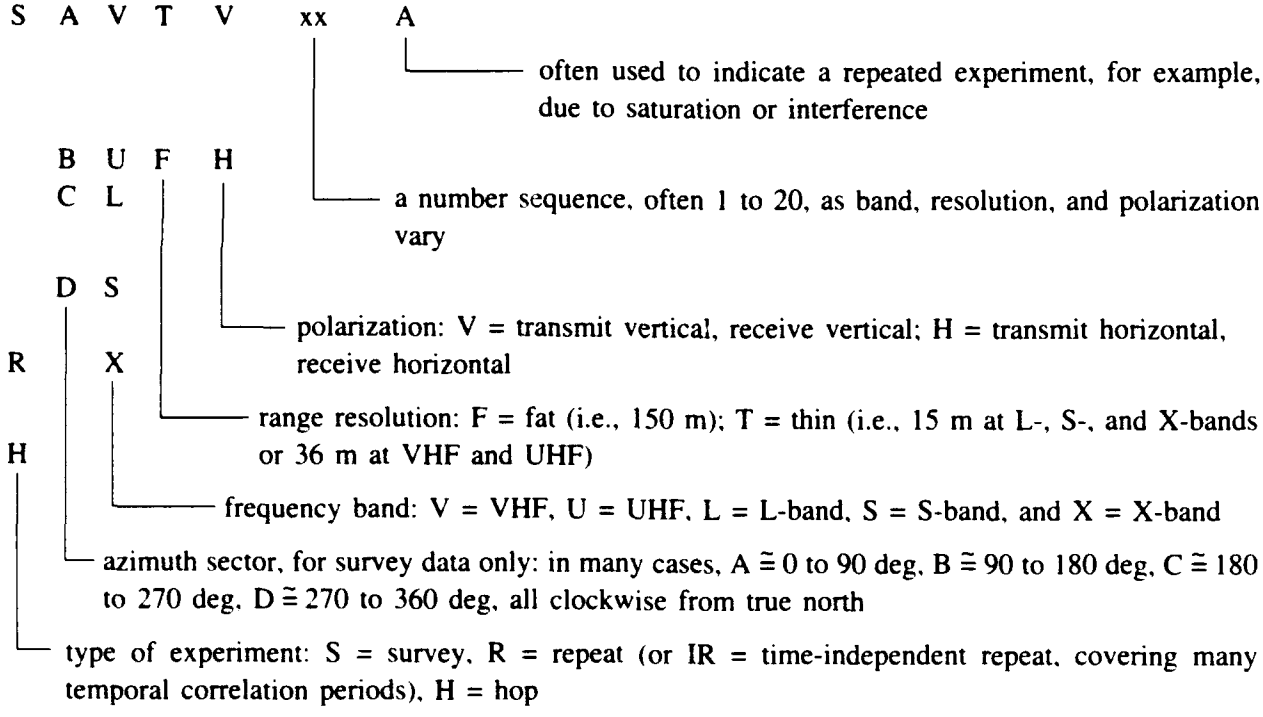

Thus, a considerable amount of information describing the intended purpose of an experiment and the radar parameters of that experiment is often directly available in the RDF name. In both parts of Table A-23, survey experiments are listed first, followed in turn by repeat sector experiments, hop experiments, and then all other experiments. Beyond this high-level organization, experiments are ordered in increasing alphabetical or numerical order by character position in the RDF name, with the far right character

TABLE A-23 (a)
Phase One Master File for Altona II.
X-band experiments only.

```
0000000001111111111222222222233333333334444444444555555555566666666667777777777888888888899999999990000000001111111111222222222233
 4 31 6 SAXFH20   17  3  1.0 47.4  92.0 357.0  38  2  1.0 47.4  92.0 357.0 1  4   3 16 0  0 4 1 1 0 0 -2.000  2 1  1 0 270184 40212
 4 31 6 SAXFV19   17  1  1.0 47.4  92.0 357.0  38  1  1.0 47.4  92.0 357.0 1  4   2 16 0  0 4 1 1 0 0 -2.000  2 1  1 0 270184 40211
 4 31 6 SAXTH18   17  2  1.0 19.0  92.0 357.0  39  1  1.0 18.9  92.0 357.0 1  4   6 16 0  0 0 1 1 0 0 -2.000  2 1 10 0 270184 40262
 4 31 6 SAXTV17   16  4  1.0 19.0  92.0 357.0  37  1  1.0 18.9  92.0 357.0 1  4   1 16 0  0 0 1 1 0 0 -2.000  2 1 10 0 270184 40261
 4 31 6 SBXFH20   15  3  1.0 47.4 187.0  88.0  36  2  1.0 47.4 187.0  88.0 1  3  16 16 0  0 4 1 1 0 0 -2.000  2 1  1 1 270184 402 8
 4 31 6 SBXFV19   15  2  1.0 47.4  88.0 187.0  36  1  1.0 47.4  88.0 187.0 1  3  15 16 0  0 4 1 1 0 0  2.000  2 1  1 0 270184 40210
 4 31 6 SBXTH18   15  1  1.0 19.0 187.0  88.0  33  1  1.0 18.9 187.0  88.0 1  3  10 16 0  0 0 1 1 0 0 -2.000  2 1 10 0 270184 40227
 4 31 6 SBXTV17   14 12  1.0 19.0  88.0 187.0  32  1  1.0 18.9  88.0 187.0 1  3   9 16 0  0 0 1 1 0 0  2.000  2 1 10 0 270184 40213
 4 31 6 SCXFH20   16  2  1.0 47.4 272.0 183.0  36  3  1.0 47.4 272.0 183.0 1  3  17 16 0  0 4 1 1 0 0 -2.000  2 1  1 1 270184 402 9
 4 31 6 SCXFV19   16  3  1.0 47.4 183.0 272.0  36  4  1.0 47.4 183.0 272.0 1  3  18 16 0  0 4 1 1 0 0  2.000  2 1  1 0 270184 402 8
 4 31 6 SCXTH18   16  1  1.0 19.0 272.0 183.0  35  2  1.0 18.9 272.0 183.0 1  3  14 16 0  0 0 1 1 0 0 -2.000  2 1 10 0 270184 40226
 4 31 6 SCXTV17   15  4  1.0 19.0 183.0 272.0  34  2  1.0 18.9 183.0 272.0 1  3  12 16 0  0 0 1 1 0 0  2.000  2 1 10 0 270184 40241
 4 31 6 SDXFH20   17  4  1.0 47.4 268.0   1.0  38  3  1.0 47.4 268.0   1.0 1  4   4 16 0  0 4 1 1 0 0  2.000  2 1  1 1 270184 40226
 4 31 6 SDXFV19   17  5  1.0 47.4 268.0   1.0  38  4  1.0 47.4 268.0   1.0 1  4   5 16 0  0 4 1 1 0 0  2.000  2 1  1 0 270184 40216
 4 31 6 SDXTH18   18  2  1.0 19.0 268.0   1.0  41  1  1.0 18.9 268.0   1.0 1  4   8 16 0  0 0 1 1 0 0  2.000  2 1 10 0 270184 40253
 4 31 6 SDXTV17   18  1  1.0 19.0 268.0   1.0  40  1  1.0 18.9 268.0   1.0 1  4   7 16 0  0 0 1 1 0 0  2.000  2 1 10 0 270184 40246
 4 31 6 RXFH20    12  4  1.0 45.6 271.5 262.5  27  2  1.0 45.6 271.5 262.5 1  2  62 32 0  0 0 0 1 1 0   1024  1 4  1 0 260184 40214
 4 31 6 RXFH20    12  4  1.0 45.6 271.5 262.5  27  2  1.0 45.6 271.5 262.5 1  3  43 32 1  0 0 0 1 1 0   1024  1 4  1 0 260184 40214
 4 31 6 RXFH20    18  3  1.0 45.6 271.5 262.5  42  1  1.0 45.6 271.5 262.5 1  0   0  0 0  0 0 0 0 1 0   1024  0 4  0 0 270184 402 0
 4 31 6 RXFH20    24  7  1.0 45.6 271.5 262.5  56  2  1.0 45.6 271.5 262.5 1  6  22 32 0  0 0 0 1 1 0   1024  1 4  1 0 280184 40214
 4 31 6 RXFH20A   12  5  1.0 45.6 262.5 271.5  27  3  1.0 45.6 262.5 271.5 1  2  63 32 0  0 3 0 1 1 0   1024  1 4  1 1 260184 40217
 4 31 6 RXFH20A   12  5  1.0 45.6 262.5 271.5  27  3  1.0 45.6 262.5 271.5 1  3  44 32 1  0 3 0 1 1 0   1024  1 4  1 1 260184 40217
 4 31 6 RXFH20B   12  6  1.0 45.6 271.5 262.5  27  4  1.0 45.6 271.5 262.5 1  2  64 32 0  0 4 0 1 1 0   1024  1 4  1 1 260184 40218
 4 31 6 RXFH20B   12  6  1.0 45.6 271.5 262.5  27  4  1.0 45.6 271.5 262.5 1  3  45 32 1  0 4 0 1 1 0   1024  1 4  1 1 260184 40218
 4 31 6 RXFV19    12  2  1.0 45.6 271.5 262.5  27  1  1.0 45.6 271.5 262.5 1  2  61 32 0  0 0 0 1 1 0   1024  1 4  1 0 260184 402 8
 4 31 6 RXFV19    12  2  1.0 45.6 271.5 262.5  27  1  1.0 45.6 271.5 262.5 1  3  42 32 1  0 0 0 1 1 0   1024  1 4  1 0 260184 402 8
 4 31 6 RXFV19    18  4  1.0 45.6 271.5 262.5  43  1  1.0 45.6 271.5 262.5 1  4  10 32 0  0 0 0 1 1 0   1024  1 4  1 0 270184 40220
 4 31 6 RXFV19    18  4  1.0 45.6 271.5 262.5  43  1  1.0 45.6 271.5 262.5 1  6  13 32 1  0 0 0 1 1 0   1024  1 4  1 0 270184 40220
 4 31 6 RXFV19    24  5  1.0 45.6 271.5 262.5  54  3  1.0 45.6 271.5 262.5 1  4  57 32 0  0 0 0 1 1 0   1024  1 4  1 0 280184 40220
 4 31 6 RXFV19    24  5  1.0 45.6 271.5 262.5  54  3  1.0 45.6 271.5 262.5 1  6  17 32 1  0 0 0 1 1 0   1024  1 4  1 0 280184 40220
 4 31 6 RXTH18    12  3  1.0  9.1 262.5 271.5  26  3  1.0  9.1 262.5 271.5 1  2  59 32 0  0 0 0 1 1 0   1024  1 4 10 0 260184 40237
 4 31 6 RXTH18    12  3  1.0  9.1 262.5 271.5  26  3  1.0  9.1 262.5 271.5 1  3  41 32 1  0 0 0 1 1 0   1024  1 4 10 0 260184 40237
 4 31 6 RXTH18    19  2  1.0  9.1 262.5 271.5  42  3  1.0  9.1 262.5 271.5 1  0   0  0 0  0 0 0 0 1 0   1024  0 4  0 0 270184 402 0
 4 31 6 RXTH18    24  6  1.0  9.1 262.5 271.5  56  1  1.0  9.1 262.5 271.5 1  6  25 32 1  0 0 0 1 1 0   1024  1 4 10 0 280184 402 0
 4 31 6 RXTV17    12  1  1.0  9.1 262.5 271.5  26  2  1.0  9.1 262.5 271.5 1  2  58 32 0  0 0 0 1 1 0   1024  1 4 10 0 260184 40237
 4 31 6 RXTV17    12  1  1.0  9.1 262.5 271.5  26  2  1.0  9.1 262.5 271.5 1  3  40 32 1  0 0 0 1 1 0   1024  1 4 10 0 260184 40237
 4 31 6 RXTV17    19  1  1.0  9.1 262.5 271.5  42  2  1.0  9.1 262.5 271.5 1  4   9 32 0  0 0 0 1 1 0   1024  1 4 10 0 270184 40231
 4 31 6 RXTV17    19  1  1.0  9.1 262.5 271.5  42  2  1.0  9.1 262.5 271.5 1  6  12 32 1  0 0 0 1 1 0   1024  1 4 10 0 270184 40231
 4 31 6 RXTV17    24  4  1.0  9.1 262.5 271.5  55  2  1.0  9.1 262.5 271.5 1  4  61 32 0  0 0 0 1 1 0   1024  1 4 10 0 280184 40234
 4 31 6 RXTV17    24  4  1.0  9.1 262.5 271.5  55  2  1.0  9.1 262.5 271.5 1  6  20 32 1  0 0 0 1 1 0   1024  1 4 10 0 280184 40234
 4 31 6 IRXFH20   14  4  1.0 47.4 271.5 262.5  35  1  1.0 47.4 271.5 262.5 1  3  13  2 0  0 0 0 1 0 0 -0.125 16 1  1 0 270184 402 7
 4 31 6 IRXFH20   14  4  1.0 47.4 271.5 262.5  35  1  1.0 47.4 271.5 262.5 1  6  11  2 1  0 0 0 1 0 0 -0.125 16 1  1 0 270184 402 7
 4 31 6 IRXFH40   14  7  1.0 47.4 271.5 262.5  31  2  1.0 47.4 271.5 262.5 1  3   5  2 0  0 0 0 1 1 0   256 16 1  1 0 270184 40220
 4 31 6 IRXFH40   14  7  1.0 47.4 271.5 262.5  31  2  1.0 47.4 271.5 262.5 1  6   8  2 1  0 0 0 1 1 0   256 16 1  1 0 270184 40220
 4 31 6 IRXFV19   14  2  1.0 47.4 262.5 271.5  34  1  1.0 47.4 262.5 271.5 1  3  11  2 0  0 0 0 1 0 0 0.125 16 1  1 0 270184 40215
 4 31 6 IRXFV19   14  2  1.0 47.4 262.5 271.5  34  1  1.0 47.4 262.5 271.5 1  6  10  2 1  0 0 0 1 0 0 0.125 16 1  1 0 270184 40215
 4 31 6 IRXFV39   14  6  1.0 47.4 271.5 262.5  26  4  1.0 47.4 271.5 262.5 1  2  60  2 0  0 0 0 1 1 0   256 16 1  1 0 270184 40210
 4 31 6 IRXTH18   14  3  1.0  9.5 271.5 262.5  30  3  1.0  9.5 271.5 262.5 1  3   3  2 0  0 0 0 1 0 0 -0.125 16 1 10 0 270184 40223
 4 31 6 IRXTH18   14  3  1.0  9.5 271.5 262.5  30  3  1.0  9.5 271.5 262.5 1  6   6  2 1  0 0 0 1 0 0 -0.125 16 1 10 0 270184 40223
 4 31 6 IRXTH38   14  8  1.0 23.7 262.5 271.5  31  3  1.0 23.7 262.5 271.5 1  6   9  2 1  0 0 0 1 1 0   256 16 1 10 0 270184 40237
 4 31 6 IRXTV17   14  1  1.0  9.5 262.5 271.5  29  3  1.0  9.5 262.5 271.5 1  6   3  2 1  0 0 0 1 0 0 0.125 16 1 10 0 270184 40211
 4 31 6 IRXTV37   14  5  1.0 23.7 262.5 271.5  31  1  1.0 23.7 262.5 271.5 1  3   4  2 0  0 0 0 1 1 0   256 16 1 10 0 270184 40236
 4 31 6 IRXTV37   14  5  1.0 23.7 262.5 271.5  31  1  1.0 23.7 262.5 271.5 1  6   7  2 1  0 0 0 1 1 0   256 16 1 10 0 270184 40236
 4 31 6 HXFH20    13  6  5.5  2.4 267.0 267.0  30  2  5.5  2.4 267.0 267.0 1  3   2 32 0  0 0 0 1 5 3 30720  1 1  1 0 260184 402 1
 4 31 6 HXFH20    13  6  5.5  2.4 267.0 267.0  30  2  5.5  2.4 267.0 267.0 1  6   5 32 1  0 0 0 1 5 3 30720  1 1  1 0 260184 402 1
 4 31 6 HXFV19    13  4  5.5  2.4 267.0 267.0  29  2  5.5  2.4 267.0 267.0 1  2  71 32 0  0 0 0 1 5 3 30720  1 1  1 0 260184 402 1
 4 31 6 HXFV19    13  4  5.5  2.4 267.0 267.0  29  2  5.5  2.4 267.0 267.0 1  6   2 32 1  0 0 0 1 5 3 30720  1 1  1 0 260184 402 1
 4 31 6 HXTH18    13  5  6.5  1.1 267.0 267.0  30  1  6.5  1.1 267.0 267.0 1  3   1 32 0  0 0 0 1 5 3 30720  1 1 10 0 260184 402 5
 4 31 6 HXTH18    13  5  6.5  1.1 267.0 267.0  30  1  6.5  1.1 267.0 267.0 1  6   4 32 1  0 0 0 1 5 3 30720  1 1 10 0 260184 402 5
 4 31 6 HXTV17    13  3  6.5  1.1 267.0 267.0  29  1  6.5  1.1 267.0 267.0 1  2  70 32 0  0 0 0 1 5 3 30720  1 1 10 0 260184 402 7
 4 31 6 HXTV17    13  3  6.5  1.1 267.0 267.0  29  1  6.5  1.1 267.0 267.0 1  6   1 32 1  0 0 0 1 5 3 30720  1 1 10 0 260184 402 7
 4 31 6 MXFV      14  9  1.0 47.4 260.0 280.0  31  4  1.0 47.4 260.0 280.0 1  3   6 32 0  0 0 1 1 1 0   512  1 1  1 0 270184 40268
 4 31 6 MXFV2     14 10  1.0  9.5 280.0 260.0  31  5  1.0  9.5 280.0 260.0 1  3   7 32 0  0 0 1 1 1 0   512  1 1  5 0 270184 40299
 4 31 6 MXFV3     14 11  1.0 47.4  80.0 100.0  31  6  1.0 47.4  80.0 100.0 1  3   8 32 0  0 0 1 1 1 0   512  1 1  1 0 270184 40239
 4 31 6 XNOISF     3 10  1.0 47.4   0.0   0.0   5  8  1.0 47.4   0.0   0.0 1  1  25 32 0  0 0 1 0 1 0  1024  1 1  1 0 130184 40220
```

TABLE A-23 (b)
Phase One Master File for Altona II.
Thin vertical (TV) experiments only.

```
0000000001111111111222222222233333333334444444444555555555566666666667777777778888888889999999990000000001111111112222222223333
 4 31 6 SALTV09   21  2  1.0 19.0  92.0 357.0  46  2  1.0 18.9  92.0 357.0 1  4  27 16 0  0 0 1 1 0 0 -2.000  4 1 10 0 280184 40237
 4 31 6 SASTV13    2  3  1.0 19.0  92.0   3.0   4  2  1.0 18.9  92.0   3.0 1  1  17 32 0  0 0 1 1 0 0 -2.000  2 1 10 0 130184 40229
 4 31 6 SASTV13    3 11  1.0 19.0  92.0 357.0   7  1  1.0 18.9  92.0 357.0 1  1  31 32 0  0 0 1 1 0 0 -2.000  2 1 10 0 140184 40228
 4 31 6 SAUTV05   10  1  1.0 19.0   3.0  92.0  21 13  1.0 18.9   3.0  92.0 1  2  27  8 0  0 4 1 1 0 0  2.000  8 1  5 0 160184 40245
 4 31 6 SAVTV01    9  2  1.0 19.0   3.0  92.0  19 10  1.0 18.9   3.0  92.0 1  2   5  4 0  0 0 1 1 0 0  2.000 16 1  5 0 150184 40230
 4 31 6 SAXTV17   16  4  1.0 19.0  92.0 357.0  37  1  1.0 18.9  92.0 357.0 1  4   1 16 0  0 0 1 1 0 0 -2.000  2 1 10 0 270184 40261
 4 31 6 SBLTV09   20  6  1.0 19.0  88.0 187.0  47  1  1.0 18.9  88.0 187.0 1  4  32 16 0  0 0 1 1 0 0  2.000  4 1 10 0 280184 40236
 4 31 6 SBSTV13    5  1  1.0 19.0  88.0 187.0  10  1  1.0 18.9  88.0 187.0 1  1  34 32 0  0 0 1 1 0 0  2.000  2 1 10 0 140184 40233
 4 31 6 SBUTV05   10  5  1.0 19.0  88.0 181.0  22  3  1.0 18.9  88.0 181.0 1  2  32  8 0  0 4 1 1 0 0  2.000  8 1  5 0 160184 40255
 4 31 6 SBVTV01    9  6  1.0 19.0  88.0 181.0  19 14  1.0 18.9  88.0 181.0 1  2   9  4 0  0 0 1 1 0 0  2.000 16 1  5 0 150184 40220
 4 31 6 SBXTV17   14 12  1.0 19.0  88.0 187.0  32  1  1.0 18.9  88.0 187.0 1  3   9 16 0  0 0 1 1 0 0  2.000  2 1 10 0 270184 40213
 4 31 6 SCLTV09   19  3  1.0 19.0 183.0 272.0  43  2  1.0 18.9 183.0 272.0 1  4  11 16 0  0 0 1 1 0 0  2.000  4 1 10 0 280184 40231
 4 31 6 SCSTV13    5  2  1.0 19.0 183.0 272.0  12  1  1.0 18.9 183.0 272.0 1  1  39 32 0  0 0 1 1 0 0  2.000  2 1 10 0 140184 40232
 4 31 6 SCUTV05   11  6  1.0 19.0 272.0 177.0  25  3  1.0 18.9 272.0 177.0 1  2  54  8 0  0 0 1 1 0 0 -2.000  8 1  5 0 180184 40275
 4 31 6 SCVTV01    9 10  1.0 19.0 272.0 177.0  20  5  1.0 18.9 272.0 177.0 1  2  14  4 0  0 0 1 1 0 0 -2.000 16 1  5 0 150184 40219
 4 31 6 SCXTV17   15  4  1.0 19.0 183.0 272.0  34  2  1.0 18.9 183.0 272.0 1  3  12 16 0  0 0 1 1 0 0  2.000  2 1 10 0 270184 40241
 4 31 6 SDLTV09   20  2  1.0 19.0 268.0   1.0  45  1  1.0 18.9 268.0   1.0 1  4  21 16 0  0 0 1 1 0 0  2.000  4 1 10 0 280184 40216
 4 31 6 SDSTV13    7  1  1.0 19.0 268.0   1.0  15  1  1.0 18.9 268.0   1.0 1  6  21 32 0  0 0 1 1 0 0  2.000  2 1 10 0 140184 40212
 4 31 6 SDUTV05   19  9  1.0 19.0 268.0   7.0  44  3  1.0 18.9 268.0   7.0 1  4  17  8 0  0 0 1 1 0 0  2.000  8 1  5 0 280184 40221
 4 31 6 SDVTV01    9 14  1.0 19.0 268.0   7.0  21  3  1.0 18.9 268.0   7.0 1  2  17  4 0  0 0 1 1 0 0  2.000 16 1  5 0 150184 40218
 4 31 6 SDXTV17   18  1  1.0 19.0 268.0   1.0  40  1  1.0 18.9 268.0   1.0 1  4   7 16 0  0 0 1 1 0 0  2.000  2 1 10 0 270184 40246
 4 31 6 RLTV09     7  6  1.0  9.1 263.0 271.0  16  4  1.0  9.1 263.0 271.0 1  1  47 32 0  0 4 1 1 1 0  1024  1 4 10 0 140184 40235
 4 31 6 RLTV09    10 13  1.0  9.1 263.0 271.0  22 11  1.0  9.1 263.0 271.0 1  2  40 32 0  0 4 1 1 1 0  1024  1 4 10 0 170184 40237
 4 31 6 RLTV09    11  8  1.0  9.1 263.0 271.0  24  4  1.0  9.1 263.0 271.0 1  2  50 32 0  0 4 1 1 1 0  1024  1 4 10 0 260184 40241
 4 31 6 RLTV09    11  8  1.0  9.1 263.0 271.0  24  4  1.0  9.1 263.0 271.0 1  3  36 32 1  0 4 1 1 1 0  1024  1 4 10 0 260184 40241
 4 31 6 RLTV09    23  8  1.0  9.1 263.0 271.0  51  2  1.0  9.1 263.0 271.0 1  4  48 32 0  0 4 1 1 1 0  1024  1 4 10 0 280184 40244
 4 31 6 RSTV13     1  1  2.5  5.9 262.5 271.5   1  1  2.5  5.9 262.5 271.5 1  1   1 32 0  0 0 0 1 1 0  1024  1 6 10 0 120184 40217
 4 31 6 RSTV13     1  1  2.5  5.9 262.5 271.5   1  1  2.5  5.9 262.5 271.5 1  3  19 32 1  0 0 0 1 1 0  1024  1 6 10 0 120184 40217
 4 31 6 RSTV13    10 17  2.5  5.9 262.5 271.5  23  4  2.5  5.9 262.5 271.5 1  2  44 32 0  0 0 0 1 1 0  1024  1 6 10 0 170184 40221
 4 31 6 RSTV13    10 17  2.5  5.9 262.5 271.5  23  4  2.5  5.9 262.5 271.5 1  3  32 32 1  0 0 0 1 1 0  1024  1 6 10 0 170184 40221
 4 31 6 RSTV13    12  7  2.5  5.9 262.5 271.5  28  1  2.5  5.9 262.5 271.5 1  2  66 32 0  0 0 0 1 1 0  1024  1 6 10 0 260184 40227
 4 31 6 RSTV13    12  7  2.5  5.9 262.5 271.5  28  1  2.5  5.9 262.5 271.5 1  3  47 32 1  0 0 0 1 1 0  1024  1 6 10 0 260184 40227
 4 31 6 RSTV13    12  8  2.5  5.9 262.5 271.5  28  2  2.5  5.9 262.5 271.5 1  2  67 32 0  0 0 0 1 1 0  1024  1 6 10 0 260184 40223
 4 31 6 RSTV13    12  8  2.5  5.9 262.5 271.5  28  2  2.5  5.9 262.5 271.5 1  3  48 32 1  0 0 0 1 1 0  1024  1 6 10 0 260184 40223
 4 31 6 RSTV13    23 12  2.5  5.9 262.5 271.5  54  5  2.5  5.9 262.5 271.5 1  4  59 32 0  0 0 0 1 1 0  1024  1 6 10 0 280184 40223
 4 31 6 RSTV13    23 12  2.5  5.9 262.5 271.5  54  5  2.5  5.9 262.5 271.5 1  6  19 32 1  0 0 0 1 1 0  1024  1 6 10 0 280184 40223
 4 31 6 RSTV13A   11  2  2.5  5.9 262.5 271.5  25  1  2.5  5.9 262.5 271.5 1  2  52 32 0  0 0 1 1 1 0  1024  1 6 10 0 170184 40225
 4 31 6 RSTV13A   11  2  2.5  5.9 262.5 271.5  25  1  2.5  5.9 262.5 271.5 1  3  38 32 1  0 0 1 1 1 0  1024  1 6 10 0 170184 40225
 4 31 6 RUTV05     7  2  1.0 23.4 265.0 269.0  16  2  1.0 23.4 265.0 269.0 1  1  45 32 0  0 0 1 1 1 0  1024  1 2  5 0 140184 40299
 4 31 6 RUTV05     7  2  1.0 23.4 265.0 269.0  16  2  1.0 23.4 265.0 269.0 1  1  70 32 0  0 0 1 1 1 0  1024    2  5 0 140184 40299
 4 31 6 RUTV05    10  9  1.0 23.4 265.0 269.0  22  7  1.0 23.4 265.0 269.0 1  2  36 32 0  0 4 1 1 1 0  1024    2  5 0 170184 40299
 4 31 6 RUTV05    23  6  1.0 23.4 265.0 269.0  53  2  1.0 23.4 265.0 269.0 1  4  52 32 0  0 4 1 1 1 0  1024    2  5 0 280184 40299
 4 31 6 RVTV01     8  4  1.0 28.4 267.0 267.0  18  5  1.0 28.4 267.0 267.0 1  1  62 32 0  0 0 1 1 1 0  1024  1 1  5 0 150184 40299
 4 31 6 RVTV01     9 21  1.0 28.4 267.0 267.0  21 10  1.0 28.4 267.0 267.0 1  2  24 32 0  0 0 1 1 1 0  1024  1 1  5 0 150184 40299
 4 31 6 RXTV17    12  1  1.0  9.1 262.5 271.5  26  2  1.0  9.1 262.5 271.5 1  2  58 32 0  0 0 0 1 1 0  1024  1 4 10 0 260184 40237
 4 31 6 RXTV17    12  1  1.0  9.1 262.5 271.5  26  2  1.0  9.1 262.5 271.5 1  3  40 32 1  0 0 0 1 1 0  1024  1 4 10 0 260184 40237
 4 31 6 RXTV17    19  1  1.0  9.1 262.5 271.5  42  2  1.0  9.1 262.5 271.5 1  4   9 32 0  0 0 0 1 1 0  1024  1 4 10 0 270184 40231
 4 31 6 RXTV17    19  1  1.0  9.1 262.5 271.5  42  2  1.0  9.1 262.5 271.5 1  6  12 32 1  0 0 0 1 1 0  1024  1 4 10 0 270184 40231
 4 31 6 RXTV17    24  4  1.0  9.1 262.5 271.5  55  2  1.0  9.1 262.5 271.5 1  4  61 32 0  0 0 0 1 1 0  1024  1 4 10 0 280184 40234
 4 31 6 RXTV17    24  4  1.0  9.1 262.5 271.5  55  2  1.0  9.1 262.5 271.5 1  6  20 32 1  0 0 0 1 1 0  1024  1 4 10 0 280184 40234
```

TABLE A-23 (b) (Continued)
Phase One Master File for Altona II.
Thin vertical (TV) experiments only.

```
000000000011111111112222222222333333333344444444445555555555666666666677777777778888888888999999999900000000001111111111222222222233
 4 31 6 IRLTV09    7 10  1.0  9.5 263.0 271.0  17  2  1.0  9.5 263.0 271.0 1  1  51  4 0  0 4 1 1 0 0  0.125 16 1 10 0 140184 40222
 4 31 6 IRLTV29    7 14  1.0 23.7 263.0 271.0  17  6  1.0 23.7 263.0 271.0 1  1  55  4 0  0 4 1 1 1 0    512 16 1 10 0 140184 40238
 4 31 6 IRSTV13    1  7  1.0  9.5 262.5 271.5   2  2  1.0  9.5 262.5 271.5 1  1   7  4 0  0 0 0 1 0 0  0.125 16 1 10 0 120184 40219
 4 31 6 IRSTV13    1  7  1.0  9.5 262.5 271.5   2  2  1.0  9.5 262.5 271.5 1  3  23  4 1  0 0 0 1 0 0  0.125 16 1 10 0 120184 40219
 4 31 6 IRSTV33    1  9  1.0 23.7 262.5 271.5   2  4  1.0 23.7 262.5 271.5 1  1   9  4 0  0 0 0 1 1 0    256 16 1 10 0 130184 40237
 4 31 6 IRSTV33    1  9  1.0 23.7 262.5 271.5   2  4  1.0 23.7 262.5 271.5 1  3  25  4 1  0 0 0 1 1 0    256 16 1 10 0 130184 40237
 4 31 6 IRUTV05   22  9  1.0 19.0 264.0 270.0  49  4  1.0 18.9 264.0 270.0 1  4  40  4 0  0 0 1 1 0 0  0.125 16 1  5 0 280184 40299
 4 31 6 IRUTV25   22  3  1.0 28.4 265.0 269.0  48  3  1.0 28.4 265.0 269.0 1  4  34  4 0  0 4 1 1 1 0   1024 16 1  5 0 280184 40299
 4 31 6 IRVTV01    8  8  1.0 19.0 265.0 269.0  18  2  1.0 18.9 265.0 269.0 1  1  60  4 0  0 0 1 1 0 0  0.125 16 1  5 0 150184 40284
 4 31 6 IRVTV21    8 12  1.0 28.4 267.0 267.0  19  4  1.0 28.4 267.0 267.0 1  1  67  4 0  0 0 1 1 1 0   1920 16 1  5 0 150184 40240
 4 31 6 IRXTV17   14  1  1.0  9.5 262.5 271.5  29  3  1.0  9.5 262.5 271.5 1  6   3  2 1  0 0 0 1 0 0  0.125 16 1 10 0 270184 40211
 4 31 6 IRXTV37   14  5  1.0 23.7 262.5 271.5  31  1  1.0 23.7 262.5 271.5 1  3   4  2 0  0 0 0 1 1 0    256 16 1 10 0 270184 40236
 4 31 6 IRXTV37   14  5  1.0 23.7 262.5 271.5  31  1  1.0 23.7 262.5 271.5 1  6   7  2 1  0 0 0 1 1 0    256 16 1 10 0 270184 40236
 4 31 6 HLTV09    21  6  6.5  1.1 267.0 267.0  50  1  6.5  1.1 267.0 267.0 1  4  44 32 0  3 0 1 1 5 3  30720  1 1 10 0 280184 402 5
 4 31 6 HSTV13     2  2  6.5  1.1 267.0 267.0   5  1  6.5  1.1 267.0 267.0 1  1  18 32 0 10 0 1 1 5 3  30720  1 1 10 0 130184 402 7
 4 31 6 HUTV05    22 11  5.5  2.3 267.0 267.0  52  1  5.5  2.3 267.0 267.0 1  4  49 32 0  7 0 1 1 5 3  30720  1 1  5 0 280184 402 5
 4 31 6 HVTV01     9  1  6.0  2.3 267.0 267.0  20  1  6.0  2.3 267.0 267.0 1  2  10 32 0  0 0 1 1 5 3  30720  1 1  5 0 150184 402 6
 4 31 6 HXTV17    13  3  6.5  1.1 267.0 267.0  29  1  6.5  1.1 267.0 267.0 1  2  70 32 0  0 0 0 1 5 3  30720  1 1 10 0 260184 402 7
 4 31 6 HXTV17    13  3  6.5  1.1 267.0 267.0  29  1  6.5  1.1 267.0 267.0 1  6   1 32 1  0 0 0 1 5 3  30720  1 1 10 0 260184 402 7
 4 31 6 LNOIST     3  5  1.0 19.0   0.0   0.0   5  5  1.0 18.9   0.0   0.0 1  1  22 32 0  0 0 1 0 1 0   1024  1 1 10 0 130184 40279
 4 31 6 SNOIST     3  7  1.0 19.0   0.0   0.0   6  1  1.0 18.9   0.0   0.0 1  1  26 32 0  0 0 1 0 1 0   1024  1 1 10 0 130184 40275
 4 31 6 UNOIST     3  3  1.0 19.0   0.0   0.0   5  3  1.0 18.9   0.0   0.0 1  1  20 32 0  0 0 1 0 1 0   1024  1 1  5 0 130184 40237
 4 31 6 VNOIST     3  1  1.0 19.0   0.0   0.0   4  1  1.0 18.9   0.0   0.0 1  1  16 32 0  0 0 1 0 1 0   1024  1 1  5 0 130184 40232
 4 31 6 XNOIST     3  9  1.0 19.0   0.0   0.0   6  2  1.0 18.9   0.0   0.0 1  1  27 32 0  0 0 1 0 1 0   1024  1 1 10 0 130184 40269
```

varying fastest. Detailed and comprehensive information for decoding all of the specific variations of RDF names used over the history of the Phase One program is available.

Table A-24 provides information describing the entries on each line of the Master File. On the raw CDC tape, clutter returns are uncalibrated and are given in terms of A/D counts. On the calibrated tape, however, for each pulse emitted, the coherent clutter return from each range gate is calibrated in absolute units of (radar cross section)$^{1/2}$ in both in-phase and quadrature channels. As our program evolved, we made two changes in our calibration algorithms (see Section A.3). When the second change occurred, we did not go back and retroactively adjust all of our existing pulse-by-pulse calibrated clutter files, but instead we left that task to our application and analysis software. The complete definition of the details of these changes is available. Our partially integrated data base, generated subsequently, does incorporate all calibration adjustments and is thus uniformly calibrated across all calibration eras according to our best calibration constants.

Another qualification concerning absolute calibration of our measurements is with respect to elevation angle gain correction. We discussed this matter in Section A.2, but we raise it again here for completeness in this discussion of our calibrated data. Thus, to repeat, the Phase One equipment provided no control on elevation angle. That is, the beams were fixed at 0-deg elevation (i.e., boresights pointed at the horizon), under the assumption that in this configuration most ground clutter returns would be received close to the peak of the elevation pattern. Calibration of the raw data proceeded under this assumption because accurate computation of elevation angle gain variation would have required accurate knowledge of the terrain elevation in every clutter resolution cell, and this was not available a priori at calibration time. Thus, these elevation angle gain corrections to our calibrated clutter files also are made by our application software, which does have terrain elevation information available.

TABLE A-24
Master File Format

Item	Field		
Site ID Number	1	3	See Table A-25
Setup Number	5	6	See Table A-25
Number of Tower Sections	8	8	1, 2, 3, or 6 (see Table A-1)
RDF Name	10	18	See page A-53
CDC Tape	19	21	Raw Tape Number
CDC Experiment	23	24	Raw Experiment Number
Raw Range Start	26	29	km
Raw Range Extent	30	34	km
Raw Azimuth Start	36	40	deg
Raw Azimuth Stop	42	46	deg

TABLE A-24 (Continued)
Master File Format

Item	Field		
CCT I-Tape Number	48	50	Cal Tape Number (pulse by pulse)
CCT Experiment	52	53	Cal Exp Number (pulse by pulse)
Cal Range Start	55	58	km
Cal Range Extent	59	63	km
Cal Azimuth Start	65	69	deg
Cal Azimuth Stop	71	75	deg
Cal = Raw?	77	77	1 = yes, Same R & Az
ICT N-Tape Number or H-Tape Number	79	80	Integ Tape Number
ICT Experiment Number	82	84	Integ Exp Number
Integration Factor	86	87	Number of pulses integrated
Filter Flag	89	89	1 = filtered for A/D spikes
Fixed Attenuation	91	92	dB
STC	94	94	0 = None, 3 = R^3, 4 = R^4
RF Amplifier	96	96	1 = enabled 0 = bypassed
XMT Enable	98	98	1 = on
Antenna Mode or Burst Count	100	100	0 = Scan; 1 = Step; Burst Count if BSTCNT > 1
Burst Delay	102	102	Burst Delay (min)
Scan Velocity or PRI Dwell	104	109	If Ant Mode = 0, Scan Velocity (deg/sec); If Ant Mode ≥ 1, Number of Pulses/Step Recorded
N	111	112	One out of N Pulses Recorded
PRF	114	114	PRF/500
Sampling Rate	116	117	1, 2, 5, or 10 MHz
LVSWR Flag	119	119	If VSWR Loss > 3 dB, Flag = 1 If VSWR Loss ≤ 3 dB, Flag = 0
Date	121	126	Day, Month, Year of Measurement
CAL Version	128	129	Version of CAL Program
CAL Period	130	130	Calibration Period
Noise Drops	131	132	If > 99, Drops = 99

We mention here another matter affecting the quality of our Phase One data. At many sites, there were occasional spurious high-level responses of the A/D converter at relatively low probability of occurrence (e.g., $\approx 10^{-5}$). These occasional A/D spikes always occurred on isolated pulses. Hence, we were able to devise an accurate "error detect and correct" filtering algorithm based on the average level of neighboring pulses in our pulse-by-pulse data. However, this filter was expensive (i.e., highly consuming of CPU time) to run in production processing across all of our data. In fact, the infrequent A/D spikes were almost always insignificant in studies involving amplitude statistics. The spikes did become deleterious in amplitude studies when data were recorded relatively low in the dynamic range of the A/D converter. Thus, we implemented a procedure where during our "integration processing" (but in the pulse-by-pulse data prior to actual integration of these data) we filtered experiments in which 10 dB or more of fixed attenuation were used and/or where data were recorded with the RF preamplifier bypassed. We also filtered some arbitrarily selected experiments not constrained by these criteria. In addition, we filtered all time-hop experiments because isolated spikes have a major deleterious effect in spectral analysis. We kept nonfiltered versions of all filtered experiments in our partially integrated data base for all but three sites* for purposes of further study. Filtered experiments are indicated in field 89 in our Master File (see Table A-24). Filtered experiments thus only exist in our partially integrated data base (N-tapes) and our final time-hop data base (H-tapes); filtered experiments do not exist in our original pulse-by-pulse data (I-tapes); see Section A.4.5.

For each experiment in the Master File, clutter data are provided at the sampling rate of the radar, beam position by beam position, pulse by pulse, and range cell by range cell, on the raw CDC tapes and on the calibrated CCT tapes. The final set of partially integrated calibrated ICT tapes integrate a number of pulses (often 16 or 32, see columns 86, 87 in Master File, Table A-24) per resolution cell to have available data of reduced tape volume. Locations of raw data (A/D counts), calibrated pulse-by-pulse data [$(RCS)^{1/2}$, units = meters], and partially integrated data [$(RCS)^{1/2}$, units = meters] are indicated on each line.

Behind the high-level parameters contained in the Master File shown in Table A-23 lie all of the additional system and site parameters residing on all of the headers of the raw measurement tapes. These additional parameters constitute a severalfold increase in number over those directly contained in the Master File. Some of them have been absorbed in calibrating the raw data into absolute RCS units and are thus not of particular direct interest in themselves. However, supporting software is available such that, for any requested experiment in the Master File, these background header files of detailed information can be provided. Included among them is the ground truth file discussed in Section A.1.

Our partially integrated data base continues to be organized on a per experiment basis and contains a noise file and a saturation file for each experiment to keep the available window of dynamic measurement range defined for each experiment in the integrated data. Figures A-16 and A-17 show the noise

* For these three sites, namely, Woking, Blue Knob, and Wachusett Mountain, all integrated experiments were first filtered, of which only about 25 experiments at each site are also available unfiltered in the partially integrated data.

file for two experiments. The noise file provides the Phase One system noise level in each range gate of the experiment. The noise floor units shown in Figures A-16 and A-17 are normalized to equivalent units of RCS in m^2. Hence, ideally, these plots of noise floor in equivalent units of RCS would increase as R^4, where R is range. A least-mean-squares R^4 approximation to the actual noise floor data is also included in Figures A-16 and A-17 as a dashed line. The parameters defining this approximation are also included in our recorded noise files.

This noise level in each range gate of a clutter experiment is determined from the actual clutter data comprising that experiment. This is done by means of a relatively complicated algorithm based on 128-point FFT processing in each range gate. Nonzero Doppler cells must pass criteria for proper Rayleigh-like noise behavior. They are then combined to establish an average system noise level in that gate. If the first group of 128 pulses fails to provide acceptable nonzero Doppler noise behavior, the algorithm proceeds to the next group of 128 pulses. This process is not continued very far because it quickly becomes expensive in CPU time. As a result, the algorithm can fail to provide a noise level in occasional range gates. The number of such failures is indicated as "noise drops" in the Master File.

The Phase One system noise floor does not always show a well-behaved R^4 characteristic. Obviously, an R^4 noise floor characteristic does not result when STC dynamic attenuation is utilized in recording the data. Furthermore, use of STC attenuation can result in loss of coherency in the data due to dc biases on the low-level bits of the A/D converters resulting from contaminants from the STC attenuation circuit in experiments where STC was used. Figure A-17 shows the noise floor from an experiment where STC was used; whereas, Figure A-16 shows the noise floor for an experiment where STC was not used.

A.4.5 Data Base Summary

Altogether, the Master File contains 12,726 lines (or records or experiments). The original pulse-by-pulse calibrated clutter data (denoted I-tapes, i.e., reel numbers begin with I*) forming this data base reside on 3601 tapes (6250 bpi), of which 2073 tapes contain survey data, 1137 tapes contain repeat data, and 391 tapes contain hop data. These original pulse-by-pulse data were further processed in a subsequent production cycle that we refer to as "integration." During integration, besides partially integrating the pulse-by-pulse data, we filtered some experiments for occasional spurious A/D spikes (see Section A.4.4), brought all experiments into final uniform calibration by adjusting for minor offsets in different calibration eras, and added noise files and saturation files. This required 1500 lines of software code and about a year of processing to accomplish. The product of integration was two separate data bases, a time-hop data base (denoted H-tapes, i.e., reel numbers begin with H) suitable for temporal studies and a partially integrated data base (denoted N-tapes, i.e., reel numbers begin with N) of much reduced volume suitable for spatial studies.

First, this final time-hop data base (H-tapes) will be described. In the original pulse-by-pulse calibrated data the time-hop or long time dwell experiments were intermixed on the same tapes with repeat

* For IBM format, in contrast to the raw CDC tapes that were in Digital Equipment Corporation PDP-11 format.

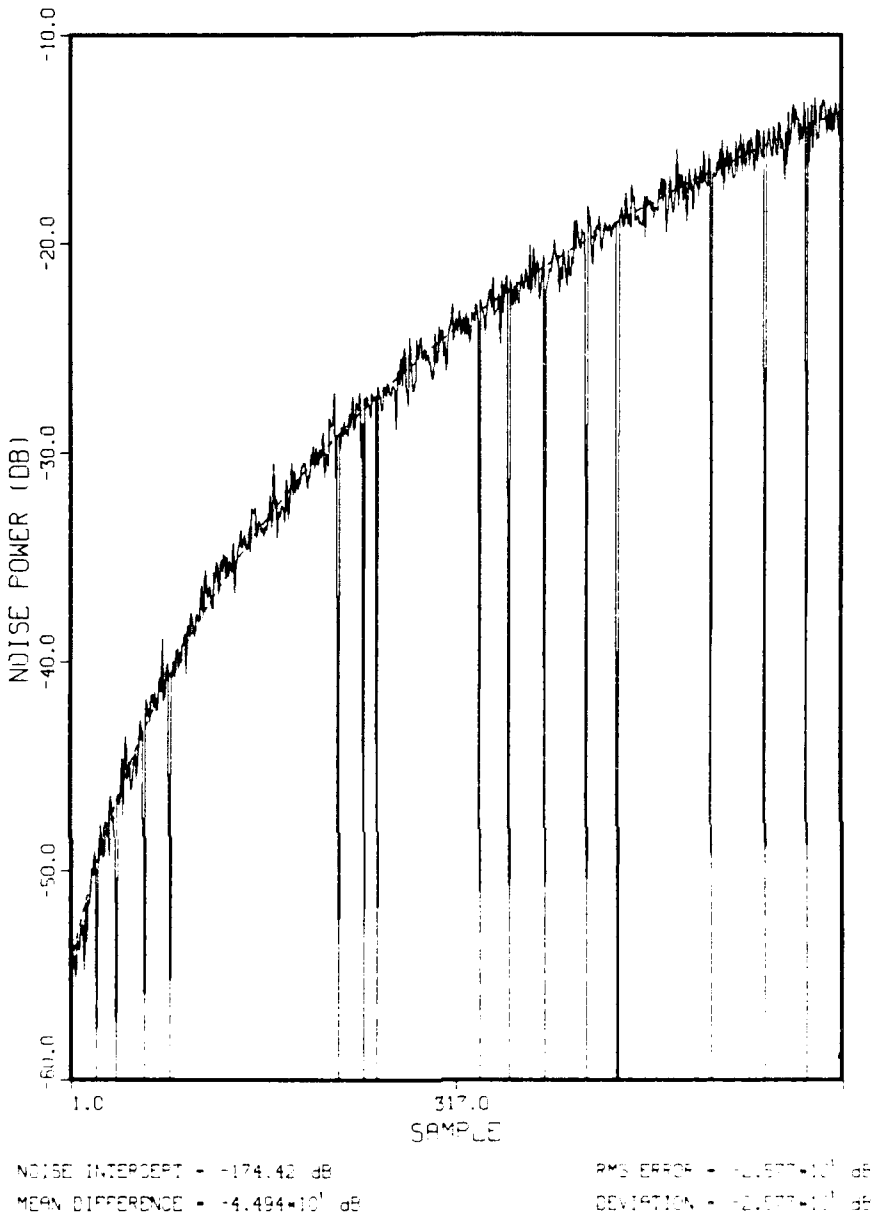

Figure A-16. Phase One system noise level for an experiment without STC attenuation. Turtle Mountain, tape 1, experiment 16. Number of noise dropouts = 16.

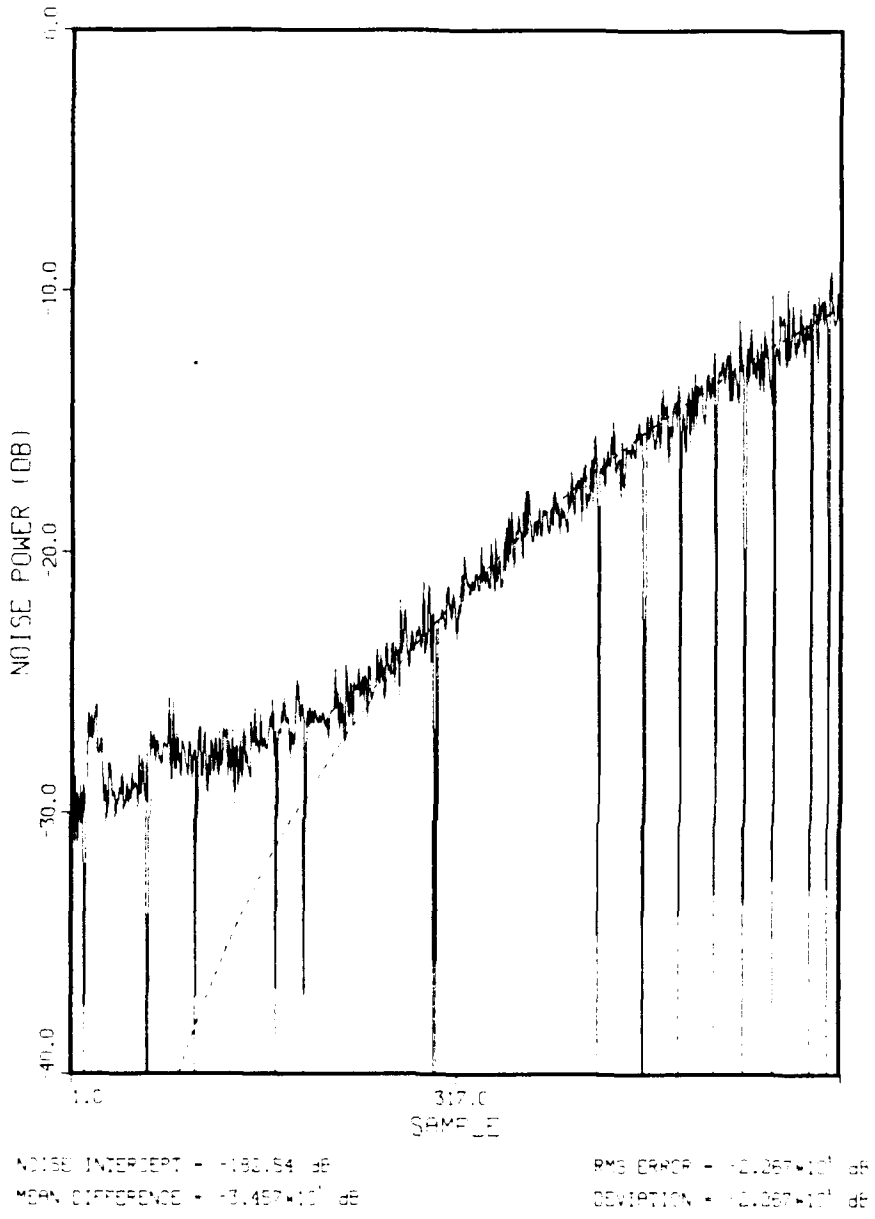

Figure A-17. Phase One system noise level for an experiment with STC attenuation. Turtle Mountain, tape 1, experiment 82. Number of noise dropouts = 17.

and survey data over all 3601 tapes. During integration, we stripped these temporal experiments from their original tapes, filtered all of these experiments for occasional spurious A/D spikes, adjusted calibration and added noise files and saturation files as in the partially integrated data, and stored these experiments back on a new dedicated set of 391 separate temporal tapes (denoted H-tapes). Although the entire process was accomplished using integration production software, during processing the integration factor was set to one, which means the data were not actually integrated but retained in pulse-by-pulse format. This final time-hop data set constitutes the only subset of Phase One data that is kept immediately available in original pulse-by-pulse format. These data are used for analysis of spectral and correlative properties of ground clutter temporal signals. These time-hop data (H-tapes) also include so-called discrete experiments, which were long time dwell experiments on the reference target (e.g., a water tower) in each band at each site.*

Next, the partially integrated data base (N-tapes) will be discussed. All of the experiments were partially integrated, including the time-hop and discrete experiments in the time-hop data base.† These data were processed during integration similarly to the time-hop data base, except that only occasional experiments were filtered for A/D spikes (see Section A.4.4), and an integration factor ≤ 32 but greater than unity was used throughout (see columns 86 and 87 in the Master File). That is, these data continue to exist in pulse group-by-pulse group format where the number of pulses that have been coherently integrated within each pulse group ≤ 32. These partially integrated N-tape data completely preserve the spatial characteristics of the Phase One data and are thus suitable for generating PPI clutter maps, amplitude versus range sector displays, and spatial histograms and cumulative distributions. However, these data in total now occupy only 228 tapes and hence are all immediately available, which was not the case for the original pulse-by-pulse data. These partially integrated data have been further integrated and reduced to spatial cell-by-cell clutter map format at DREO/Ottawa.

Besides these basic Phase One data bases being maintained in I and Q format at or near the original sampling rate of the radar, files are maintained of Phase One clutter statistics reduced, for example, as spatial amplitude distributions or as temporal autocorrelation functions and power spectra. Concerning spatial amplitude distributions, there are two main files of reduced data: a file of 4465 repeat sector patch histograms stored on three tapes, and a file of 99,466 survey patch histograms stored in special packed format on five tapes (one tape per RF frequency band). Each of these stored histograms of clutter amplitude statistics comes from a particular spatial macroregion or patch of terrain, either a repeat sector patch (one patch per site) or one of the 3440 macropatches defined in the 360-deg survey data (i.e., approximately 80 patches per site). Each stored histogram has associated with it terrain descriptors of the applicable patch and is corrected for elevation gain at the depression angle at which the patch was illuminated.

---

* An example of an RDF name of a discrete experiment is DSFV, meaning discrete experiment, S-band, low resolution (i.e., fat), and vertical polarization. Often, discrete experiments were repeated multiple times at each site. They are almost always low resolution, vertical polarization.

† Except for a very few experiments (less than 0.5 percent) that failed to "integrate."

Concerning temporal autocorrelation functions and power spectra, there are also two main files of reduced data, both based on the long time dwell or time-hop experiments. The first file encompasses 17 of the 37 sites at which Phase One made long time dwell measurements with a stationary beam (viz., five urban sites, seven forested sites, and five farmland or rangeland sites). This study was focused on three frequencies (UHF, L-, and S-band), on horizontal polarization, and on 150-m range resolution. At each site, we selected several range gates in which we processed long time dwell bursts of 30,720 pulses to provide autocorrelation and power spectral characteristics. Altogether in this study we examined and stored on tape 153 pairs of autocorrelation function and power spectrum. The second file also consists of many pairs of autocorrelation function and power spectrum from long time dwell experiments, but this file is based only on our once-a-week Phase One measurements between November 1984 and August 1985 at our own Lincoln Laboratory site of Katahdin Hill (3). This study covered all five frequency bands and both high and low range resolution and vertical and horizontal polarization on the same few resolution cells each week. These two files of pairs of autocorrelation function and power spectrum provide a useful data base descriptive of the temporal properties of ground clutter. However, the large majority of our measured long time dwell sequences is as yet unexamined in this manner.

A.4.6 Data Acquisition Summary

Table A-25 provides a brief data acquisition summary for all of the 49 Phase One site visits. Detailed Master File information is available for each site visit, as illustrated in Section A.4.4. Table A-25 also provides capsule information summarizing equipment difficulties encountered at each site (see footnotes on the second page of the table). With complex equipment comprising five instrumentation radars and a data-recording system undergoing rough transportion conditions, it is not surprising that complete data were not acquired at every site. Table A-25 provides a useful summary overview indicating the site-by-site history of which transmitters operated at which sites and sites where only partial or questionable data were obtained in some bands.

As indicated in Table A-25, S-band was the most troublesome frequency band during Phase One's history. First, the S-band transmitter was not available for the first four sites. Second, all S-band data from a group of ten early Phase One sites [Cochrane (1) through Cold Lake and Pakowki Lake through Cochrane (2)] and 50 percent of the S-band data from an eleventh site (Suffield) were rendered questionable or not collected because of a major hardware problem in the S-band receiver (faulty RF limiter and circulator). The S-band data collected during that period exhibited both low and rapidly fluctuating signal strengths. Third, the S-band clutter signal strengths at eight later Phase One sites (Corinne (partial) and Gull Lake West (2) through Vananda East) were shifted by approximately - 4 dB because of a second hardware problem. A broken shield on the cable from the rotary joint to the S-band antenna feed manifested itself in both the measured calibration shift and abnormally high VSWRs. The calibration software VSWR adjustments, which are automatically applied during the calibration of the raw clutter data, resulted in clutter strengths that were still approximately 4 dB low, according to the corner reflector external calibration measurements made at those sites. Consequently, all affected S-band clutter strengths from those eight sites have been adjusted by + 4 dB in this report.

X-band was also troublesome for Phase One. The X-band transmitter failed three times (at Cochrane (1), Plateau Mountain, and Headingley) . The first two failures led to the loss of data at subsequent sites (two following Cochrane (1) and four following Plateau Mountain). The Headingley failure only led to partial loss of Headingley data. X-band transmitter repairs produced long delays at Beiseker (1) and Peace River South II.

Another Phase One problem experienced during Phase One's three-year history was chronic severe RF interference, particularly at VHF. Most of the VHF data had to be collected between midnight and 6 a.m. in order to avoid excessive levels of RF interference. High range resolution VHF data were more seriously affected by interference and in fact were precluded at three sites [Suffield, Puskwaskau and Gull Lake West (1)] and possibly contaminated at several others. RF interference precluded UHF data collection at North Truro and also may have affected UHF data collected at two other sites (Brazeau (1) and Altona II). RF interference may have affected L-band data at two sites (Brazeau (1) and Suffield).

TABLE A-25
Phase One Data Acquisition Summary*

SETUP #	SITE NAME	DATA COLLECTION					SITE ID
		X	S	L	UHF	VHF	
1.	Katahdin Hill, MA	D	N[1]	D	D	D	067
2.	Shilo, MAN	D	N[1]	D	D	D	006
3.	Neepawa, MAN	D	N[1]	D	D	D	030
4.	Polonia, MAN	D	N[1]	D	D	D	031
5.	North Truro, MA (P)	D	D	D	N[2]	D	105
6.	Cochrane, ALTA	Q[3]	Q[3]	D	D	D[15]	017
7.	Strathcona, ALTA	N[3]	Q[3]	D	D	D	107
8.	Penhold II, ALTA	N[3]	Q[3]	D	D	D	094
9.	Beiseker, ALTA (P)	D	Q[3]	D	D	D	018
10.	Westlock, ALTA	D	Q[3]	D	D	D	013
11.	Cold Lake, ALTA	D	Q[3]	D	D	D	047
12.	Suffield, ALTA	D	D,Q[3]	D,Q[2]	D	D(F)[4]	022
13.	Pakowki Lake, ALTA	D	Q[3]	D	D	D,Q[4]	041
14.	Orion, ALTA	D	N[3]	D	D	D,Q[4]	040
15.	Beiseker (2), ALTA	D	N[3]	D	D	D,Q[4]	018
16.	Cochrane (2), ALTA	D	N[3]	D,Q[6]	D,Q[6]	D,Q[4]	017
17.	Brazeau, ALTA (P)	D	D	D,Q[2]	D,Q[2]	D	060
18.	Lethbridge West, ALTA (P)	D	D	D,Q[13]	D	Q[2,5]	046
19.	Magrath, ALTA (P)	D	D	D	D	D	044
20.	Waterton, ALTA	D	D	D	D	Q[8]	064
21.	Plateau Mountain, ALTA	N[3]	D	D	D	D	020
22.	Picture Butte II, ALTA	N[3]	D	D	D	D	021
23.	Beiseker (3), ALTA (P)	N[3]	D	D	D	D	018
24.	Brazeau(2), ALTA (P)	N[3]	D	D	D	D	060
25.	Puskwaskau, ALTA	N[3]	D	D	D	D(F)[4]	055
26.	Peace River South II, ALTA	D	D	D	D	D	091
27.	Woking, ALTA	D	D	D	D	D	054
28.	Beiseker (4), ALTA (P)	D	D	D	D	D	018
29.	Wolseley, SASK	D	D	D	D	D	007
30.	Headingley, MAN	½D[3]	D(H)[3,9]	D	D	N[2,3,9]	005
31.	Altona II, MAN	D	D	D	Q[2]	D	004
32.	Big Grass Marsh, MAN	D	D,Q[6,7]	D	D	D	029
33.	Gull Lake West, MAN	Q[8]	D	D	D	D(F)[4]	016
34.	Spruce Home, SASK	D	D	½D[10]	D	D	035
35.	Rosetown Hill, SASK	D	D	D	D	D,Q[4]	038
36.	Wainwright, ALTA	D	D	D	D	D	012
37.	Dundurn, SASK	D	D	D	D	D	010
38.	Corinne, SASK	D	DQ[6,7,8,12,14]	D	D	D	032
39.	Gull Lake West (2), MAN	D	Q[6,7,8,12]	D	D	D	016
40.	Sandridge, MAN	D	Q[6,7,8]	D	D	D	028
41.	Turtle Mountain, MAN	D	Q[7,8]	D	D	D	033
42.	Beulah, ND	D	Q[6,7,8,12]	D	D	D	104
43.	Knolls, UT	D	Q[7,8]	D	D	D	099
44.	Booker Mountain, NV	D	Q[6,7,8]	D	D	D,Q[3,7]	106
45.	Vananda East, MT	D	Q[6,7,8,12]	D	D	D	103
46.	Wachusett Mountain, MA	D	D	D	D	D,Q[4]	068
47.	Scranton, PA	D	D	D	D	D,Q[3]	075
48.	Blue Knob, PA	D	D	D	D	D	076
49.	Katahdin Hill (2), MA	D	D	D	D	D,Q[2]	067

* Abbreviations and footnotes on next page.

TABLE A-25 (Continued)
Phase One Data Acquisition Summary

Abbreviations

D: Good data
Q: Questionable data
N: No data or no useful data
D(H): Horizontal polarization data only
D(F): Fat pulse data only
1/2 D: Data collection was ≈50%
(P): Propagation tests
(n): n^{th} visit (repeated)

Footnotes

1. No S-band tube.
2. Excessive interference.
3. Hardware problems.
4. Excessive interference affected high resolution data only.
5. Antenna drive motor interference.
6. High VSWRs observed in calibration and/or reference target data.
7. High VSWRs observed in clutter data.
8. Inconsistent clutter data.
9. Extremely cold weather.
10. 50% L-band data precluded when abort-level VSWRs developed.
11. Hardware and weather problems.
12. Inconsistent calibration and/or reference target data.
13. L-band frequency was changed to 1255 MHz on 16 May, and high VSWRs were observed.
14. S-band VSWRs high at 2 tower sections only.
15. Excessive interference limited data quantity.

APPENDIX B

MULTIPATH PROPAGATION

TABLE OF CONTENTS

LIST OF ILLUSTRATIONS

LIST OF TABLES

B.1 BACKGROUND

In considering the physics of the low-angle clutter phenomenon, there are two important factors. The first is the role of depression angle such that mean strengths of low-angle clutter spatial amplitude distributions increase and their spreads decrease with increasing angle. This important first factor is associated directly with the intrinsic terrain backscattering processes themselves. In contrast, the second factor is associated with the effects of the intervening terrain on the illumination at the backscattering cell. As a result, this second factor is only indirectly (but still, importantly) associated with the intrinsic terrain backscatter.

This important indirect factor associated with illumination will now be more closely considered. As is indicated in Figure B-1, the terrain between the radar and the clutter patch influences the illumination of the clutter patch. For example, multipath reflections can interfere with the direct illumination and cause lobing on the free-space antenna pattern. All terrain propagation effects including reflection and diffraction are included within the propagation factor F, which is defined as the ratio of the incident field that actually exists at the clutter cell being measured to the incident field that would exist there if the clutter cell existed by itself in free space. Ideally, one would wish to separate this effect of illumination from the backscatter measurement. For example, in the classical definition of RCS, the strength of illumination is normalized (i.e., divided) out.

In the real world of ground clutter, however, the actual effects of terrain on illumination cannot be separated out. To do so would require a separate measurement of illumination strength in every clutter cell. As to what this would entail, consider that the illuminating field strength is often a rapid function of elevation near the ground, making it difficult to either measure or predict the actual illuminating field distributions over typical vertical clutter features (e.g., tree, silo). Our Spherical Earth with Knife Edges (SEKE) radar propagation computer code [7], based on Defense Mapping Agency (DMA) digital terrain elevation data (DTED), was developed principally for predicting field strengths at aircraft altitudes. At X-band, this code is useful for providing physical insight on the statistical average over large spatial regions at clutter source heights [2], but is not accurate enough to allow deterministic cell-by-cell computation and separation of F in our measurements. At VHF, however, propagation variation exhibits less scintillation, and we did investigate using SEKE to predict and separate F from our VHF measurements. However, this attempt to separate F at VHF was unsuccessful because the local cell-to-cell variations in clutter strength $\sigma^\circ F^4$ were not well correlated with the SEKE predictions of F. Consequently, the resultant separated distributions of intrinsic σ° became broader instead of narrower than the corresponding distributions of $\sigma^\circ F^4$.

Therefore, what we measure as real-world clutter strength is the product of the clutter coefficient, σ°, defined to be RCS per unit ground area in the resolution cell, and the fourth power of the propagation factor. The propagation factor is raised to the fourth power as it enters into clutter strength because clutter strength (actually clutter intensity) is proportional to power (i.e., the square of the field strength), and a two-way propagation path is involved. Implicit in our definition of clutter strength is the proper assumption of unit plane wave illumination in the definition of RCS, as well as the proper incorporation of the real unknown illumination within the propagation factor. Throughout this report we represent clutter strength by the symbols $\sigma^\circ F^4$ to demonstrate explicitly that clutter strength depends on two important factors, the intrinsic backscatter and the illumination. We do not separate these two factors in our empirical data in this report.

Although we do not separate σ° and F^4 in this report, within our Phase One clutter measurement program we did make measurements of illumination strength and the effects of propagation on illumination at a few

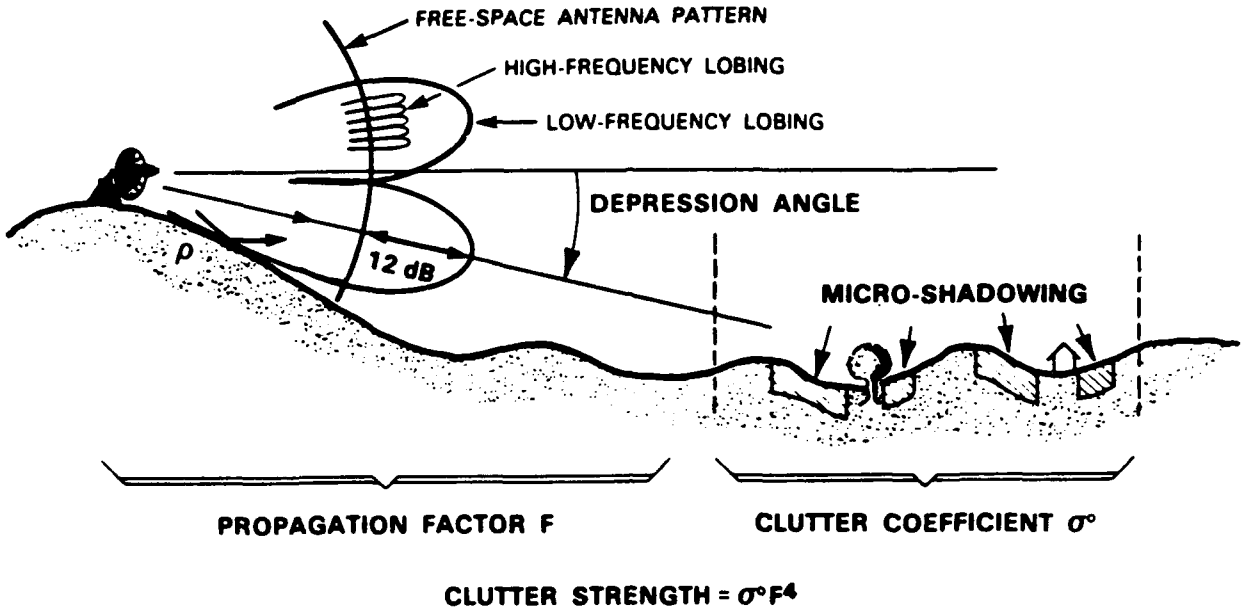

Figure B-1. Clutter physics.

Phase One sites. These propagation measurements were recorded in a helicopter (i.e., Phase One transmits, helicopter receives) flying vertical ascents and descents above selected clutter cells. The eight Phase One sites at which such helicopter propagation measurements were performed are noted in Table A-1 in Appendix A with a "(P)" after the site name. We do not report on these propagation measurements here, but we do incorporate the important findings from them in our interpretation of our clutter data. Information describing these measurements is available.

How terrain effects on illumination affect clutter strength will now be considered. Again, refer to Figure B-1. At X-band, our highest RF frequency band, terrain reflection coefficients are often lower, and hence, multipath effects are diminished from those that can exist at lower radar frequencies. Our propagation measurements definitely revealed, however, that substantial multipath lobing did exist at X-band on typical low-relief prairie landscapes in the Canadian west. When they exist at X-band, propagation lobes are relatively narrow.* High clutter sources such as trees and buildings over much visible terrain often subtend a number of such lobes when they exist. As a result, the effects of propagation are diminished at X-band when compared with lower frequencies.

As RF frequency decreases, especially below L-band to UHF and VHF, influences of terrain on propagation and illumination strength can become dominant. First, at the lower frequencies, terrain reflection coefficients increase so that multipath lobing becomes stronger. Second, for a given antenna height, as RF

* At X-band, height to first maximum on lobing pattern is 14.6 ft at 10-km range (60-ft tower, level reflecting surface).

frequency decreases, the widths of the multipath lobes become broader.* This result may be understood on the basis of the lobing pattern simply being an interference pattern between the actual source of radiation and its image in the reflecting terrain surface. For a given antenna height, as RF frequency decreases, the effective separation of the source point and its image measured in wavelengths decreases, and the angular periodicity (i.e., lobe width) in the interference pattern increases. Even at X-band, clutter strengths on level open terrain may be somewhat reduced because of illumination of low clutter sources from the underside of just the first propagation lobe (see Section 4.1.4.3). In contrast to X-band, however, at lower frequencies the broad multipath lobes can be of dominant influence over typical sources and patches. That is, they can strongly change (either increase or decrease) the effective gain over whole patches and over the complete vertical extents of typical clutter sources within patches. This situation is illustrated in Figure B-1 where a strong low-frequency multipath lobe caused by a terrain reflection coefficient ρ of unity increases effective antenna gain over the whole patch by 12 dB. Such an increase is evident in the Strathcona repeat sector clutter measurements at VHF. The theoretical upper limit to gain increase over free space caused by a single Fresnel multipath reflection is 12 dB, which is the result of both incident and scattered field strengths being doubled by terrain reflection.

Our objective in analyzing our clutter data is to statistically determine important fundamental trends in clutter strength $\sigma^\circ F^4$ as measured from regions of visible terrain. Except at low frequencies on level open terrain, the effects of multipath propagation on clutter strength are usually specific to the particular terrain profile occurring for any given measurement and hence statistically dispersive across a set of nominally similar measurements as the details of the multipath lobing vary from measurement to measurement. Thus, our measurement program requires many sites and patches to average out such specific influences. As noted above, it might be initially supposed that the theoretical high ground would be to separate propagation from backscatter. This becomes even more the case when we consider that illumination strength of a discrete vertical clutter source in the presence of multipath is a function of geometrical factors such as antenna height and range to the clutter source and that a clutter model should explicitly account for such factors and not statistically subsume them. These matters are discussed from time to time in the body of this report. But our practical goal in this report is to move in a statistical fashion past this difficult position of separating propagation to useful new results for predicting low-angle ground clutter strengths as actually experienced in ground-based radar. In the process we are gathering statistics as much on propagation F as on terrain backscatter σ°.

In thus appreciating the significant effects of propagation F in clutter strength $\sigma^\circ F^4$, it is oversimplifying to attribute most of the variability in $\sigma^\circ F^4$ over any given spatial region to propagation. Attempts to model the low-angle clutter phenomenon as constant σ° with a subsequent overlay of propagation computation are not realistic.† The histograms of clutter strength shown in Appendix E illustrate the intrinsic variability of low-angle clutter. Figure E-52 shows 53 dB of cell-by-cell clutter variability at UHF in the Woking forested repeat sector; these multipath-free data illustrate variability in intrinsic σ° (i.e., F=1). Figure E-125 shows 79 dB of cell-by-cell variability at S-band in the Beiseker farmland repeat sector; in attempting to model these data as constant σ° with superimposed multipath variations, consider that single-bounce multipath augmentation of clutter strength over the constant σ° assumed is limited to a maximum of 12 dB.

---

* At VHF, height to first maximum on lobing pattern is 864 ft at 10-km range (60-ft tower, level reflecting surface).

† Of course, attempts to model low-angle clutter as constant σ° without including effects of propagation are even more unrealistic.

In this appendix, two topics associated with propagation effects in our clutter measurements are discussed in more detail. Because most of our repeat sector clutter measurements occur at relatively short ranges, typically of less than 10 or 20 km, the dominant mechanism of propagation entering our measurements is multipath reflection. At many sites, the multipath enters in a manner very specific to the terrain involved. In Section B.2, we show how to get intuitive insight into the multifrequency effects of multipath in our repeat sector measurements by considering multipath from a flat surface local to the Phase One antenna but tilted at the hillside slope where the measurements are taken. Even so simply approximated, this approach shows how multipath effects in clutter strength are often very strongly dependent on precise local terrain slopes near the radar. The local terrain slopes involved can be determined as accurately as necessary from large-scale maps or even surveys. Thus, we are able to understand these effects without recourse to DTED, which is often insufficiently accurate to define the local slopes to the precision necessary.

For quantitative propagation prediction, we utilize our SEKE propagation code. The SEKE code is set up to run using DMA DTED. This code predicts single or multiple forward reflections from Fresnel zones on the spherical earth, diffraction loss over knife edges, and diffraction loss beyond the horizon on the spherical earth. We utilized the SEKE code to estimate propagation at clutter source heights in many of our repeat sectors at VHF, UHF, and L-band. These SEKE estimates were usually within appropriate general propagation regimes; for example, they usually successfully separated strongly multipath-dominated situations from nonmultipath situations. However, from a more specific cell-by-cell point of view, the SEKE estimates were seldom useful in assisting us in quantitatively understanding our clutter measurements. Local variations with frequency and/or range in SEKE propagation estimates in a given repeat sector were not accurately borne out in the clutter measurement data. Multifrequency differences in measured clutter strength were not accurately predicted. A major reason for these disparities was insufficient DTED accuracy. Recall that the DTED data that we have gradually acquired for our clutter measurement sites over the duration of our program were largely generated from 1:250,000 scale topographic maps. At this small scale, the terrain in many of our repeat sectors is relatively grossly represented (e.g., at this scale, a 10-km repeat sector covers only 1-1/2 inches on the original map). Ten-meter elevation errors are common, and much important detail is omitted. In addition, SEKE provides more accurate estimates of propagation at target altitudes above the ground than at clutter source heights at or very near ground level. Thus, in running SEKE over a bare earth DTED terrain profile at very low altitudes into a short-range repeat sector, the answer tends to be highly sensitive to artificial nuances in the terrain profile resulting from extensive interpolation in the original 1:250,000 scale source map. Of course, we are using DTED for a purpose here for which it was not designed. As more accurate digitized terrain elevation data becomes available, for example, from 1:50,000 scale source material, and with improved range-specific estimates of land cover along the bare earth DTED terrain profile, we can expect more accurate SEKE clutter propagation estimates.

We referred above to the fact that because our repeat sector clutter measurements are largely from directly visible terrain at relatively short range, diffraction loss in these measurements is usually not dominant, and most of our interest in propagation effects in these data focuses on multipath. However, in Section B.3 some Phase One measurements are provided of long-range mountain clutter obtained in our survey (as opposed to repeat sector) data acquisition mode. Although visible within line-of-sight, these mountains were observed near grazing incidence at very long ranges of more than 100 km. As a result, associated with their clutter returns is an approximately 12-dB diffraction loss, even though they were visible. One purpose of

showing these long-range mountain clutter data here is to expand the understanding of how propagation effects, not only reflective but also diffractive, can dominate low-angle clutter from visible terrain.

B.2 HILLSIDE MULTIPATH

Phase One often set up to make clutter measurements on a local topographic high in open prairie terrain. In such situations, Phase One initially looked down the side of the hill it was set up on over terrain outwardly inclined at angle α with respect to horizontal and then out to clutter sources distributed over more level terrain at longer range in the repeat sector clutter patch. In the body of this report, we interpreted multifrequency clutter strength results in a number of such measurement situations under the assumption that dominant multipath occurred from the side of the hill at relatively close range. That is, a multipath lobing pattern was assumed to be set up by the presence of a plane reflecting ground surface outwardly inclined at angle α. The effect of the inclination of this plane was to tilt the lobing pattern down by angle α. As a result, clutter sources on level terrain at much longer range were illuminated up on the pattern at positive elevation angle α rather than deep in the horizon plane null as they are when the reflecting surface is level. This rotation of the multipath lobing pattern by the local terrain slope in the direction of the repeat sector was often a dominant influence in the multifrequency clutter strength characteristic of the repeat sector clutter patch measured there, even for what were often relatively small terrain slopes. We now set out to understand this effect more thoroughly and will show how it can be simply quantified using large-scale topographic maps.

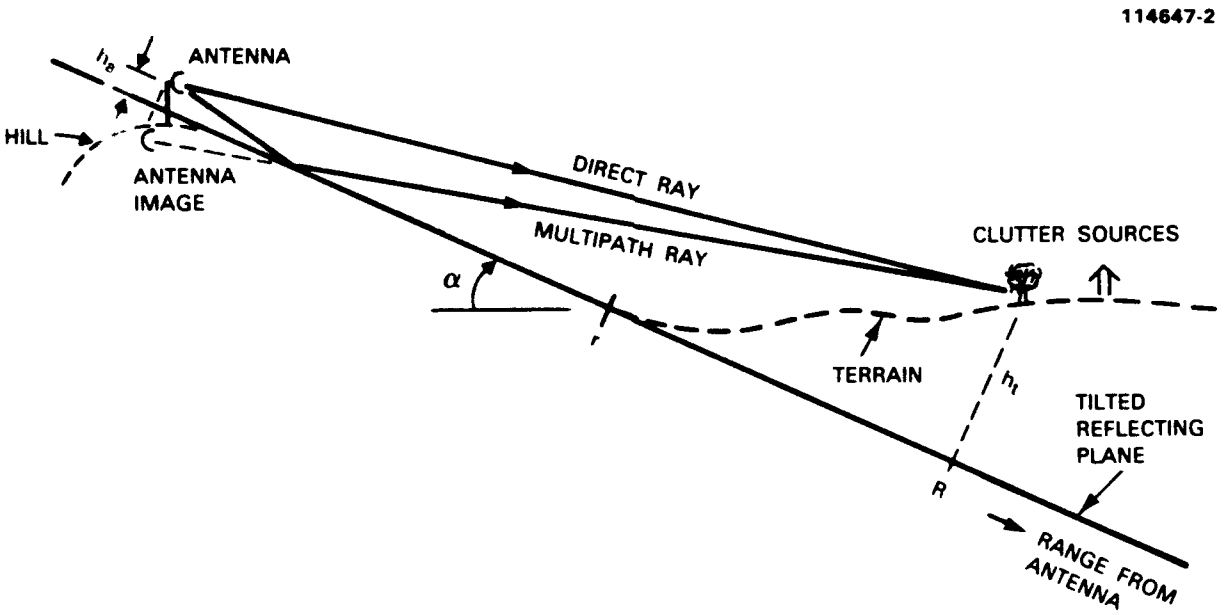

Figure B-2. Multipath from a tilted refelecting plane.

First, assume a situation involving an antenna at h_a above a tilted, perfectly reflecting, infinite planar surface tilted at angle α with respect to horizontal, as depicted in Figure B-2. Also shown dashed in Figure B-2 is the profile of the actual terrain as it deviates from the inclined planar surface, both at the hilltop and into more level terrain far out in the clutter patch. In this simple model, we allow backscatter from clutter sources distributed on this more level terrain but do not allow additional multipath from it (i.e., we allow multipath only from the tilted plane). In Figure B-2, the height of the antenna above the tilted plane is h_a, the height of the clutter source above the tilted plane is h_t, the range along the reflecting plane from the antenna to the clutter source is R, and the range along the reflecting plane from the antenna to the bottom of the hill is r. We wish to know the clutter strength $\sigma^\circ F^4$ from the indicated clutter source, where σ° is the intrinsic reflectivity of the source (i.e., σ° equals the RCS of the clutter source divided by the ground area in the resolution cell), and F is the propagation factor (i.e., the ratio of the field strength at the source in the presence of the tilted reflecting plane divided by the field strength that would exist at the target in free space). Under the conditions that $R>>h_a$, $h_t>>h_a$, and the reflection coefficient equals -1, the factor F^4 is given by

$$F^4 = 16 \sin^4\left(\frac{2\pi}{\lambda} h_a \cdot \theta_h\right) \quad , \tag{B.1}$$

where λ equals RF wavelength, and $\theta_h = h_t/R$.

Note that, in Equation (B.1), θ_h varies with every clutter source position. Thus, so far, we have not made much progress in simplification. That is, we are still in a situation requiring a separate computation of F^4 for every clutter source position. In this respect we are similar to more complicated propagation codes that take the actual terrain profile into account, whereas we are just assuming reflections from a plane. Rather than compute F^4 at every clutter source position in a repeat sector clutter patch, an impracticable undertaking, what we would like is to perform a simple one-time computation to help us understand, at least in gross terms, the effect of multipath in causing large variations in mean clutter strength versus frequency over the whole repeat sector clutter patch.

A first step toward such generality is to assume that R is very large, or, in other words, that the range to the clutter patch R is much greater than the range to the bottom of the hill r. Let x equal the range from the bottom of the hill to the clutter patch, i.e., let $x = R-r$. Then, for large R,

$$\theta_h = \frac{h_t}{R} = \frac{h_t}{x+r} \equiv \frac{h_t}{x} = \alpha \quad . \tag{B.2}$$

Thus, when R is large, we may substitute α for θ_h in Equation (B.1). The quantity α is a fixed quantity, equal to the hillside slope upon which Phase One is set up and down which Phase One looks when looking out to the repeat sector clutter patch at long range. Now we have made substantial progress in simplification because in Equation (B.1) we have replaced θ_h, a quantity that varies with clutter source position, with α, a fixed quantity. When we make this substitution what we are really assuming is that all the clutter sources in the repeat sector clutter patch are at long enough range that they are essentially illuminated by a horizontal direct ray and an interfering horizontal multipath ray reflected from the hillside slope below Phase One. This situation is depicted in Figure B-3.

A number of the Phase One measurement sites are reasonably well modeled by the situation illustrated in Figure B-3 (e.g., Orion, Rosetown Hill, Spruce Home, and Polonia). At a number of other sites,

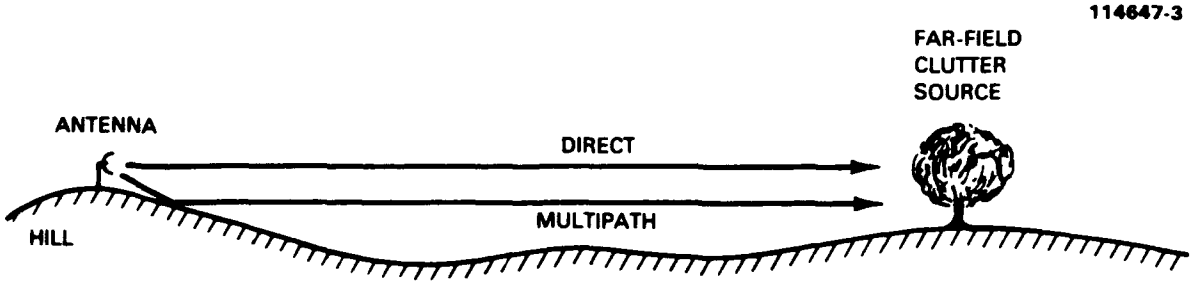

Figure B-3. Far-field interference between a direct ray and a local hillside slope reflected multipath ray.

the terrain is more bowl-shaped and, rather than leveling off beyond the foot of the hill, rises back up to the repeat sector clutter patch so that the assumption of near-horizontal direct and multipath rays illuminating the clutter patch remains a good first approximation (e.g., Beulah, Magrath, and Beiseker). At still other hilltop sites, where horizontal direct and multipath rays do not approximate the conditions of illumination, the clutter patch may be localized enough that a one-time computation of F^4 from Equation (B.1) using a single value of θ_h at the clutter patch centroid position may provide useful insight. However, in these latter circumstances, we are beginning to stray quite far from the simple hilltop above the plain, horizontal illumination situation in which simple multipath insights can often explain singular features in the measured multifrequency mean clutter strength characteristic. Thus, to summarize, in Section 4 in this report, when we interpret multifrequency clutter measurement characteristics on the basis of local terrain slope tilting a multipath lobing pattern down by the amount of the terrain slope, we are assuming multipath only from a tilted plane, and we are assuming clutter sources in the repeat sector clutter patch illuminated at near-zero depression angle, either because they are on nominally level terrain at long range or because a bowl-shaped terrain profile raises the clutter sources back up.

Figures B-4 and B-5 show F^4 versus θ_h as given by Equation (B.1) for the Phase One VHF, UHF, and L-band antennas, for three tower sections expanded in Figure B-4 and for six tower sections expanded in Figure B-5. (See Table A-5 for antenna mast heights.) When Phase One is set up in a situation where the above model as depicted in Figure B-3 works, all we need do is estimate α, the slope of the hill we are on in the direction of the clutter patch, and read multipath loss (or gain) F^4 at VHF, UHF, and L-band at $\theta_h = \alpha$ in Figures B-4 or B-5, depending on antenna height.* In these prairie farmland situations, intrinsic σ° is roughly frequency independent (see Section 4), so a frequency band that provides a considerably different value of mean clutter strength than the other bands, either higher or lower, can often be satisfactorily explained on the basis of its being at a peak or null in the lobing pattern.

* That is, in these circumstances, Figures B-4 and B-5 give multipath loss versus hillside slope angle θ_h.

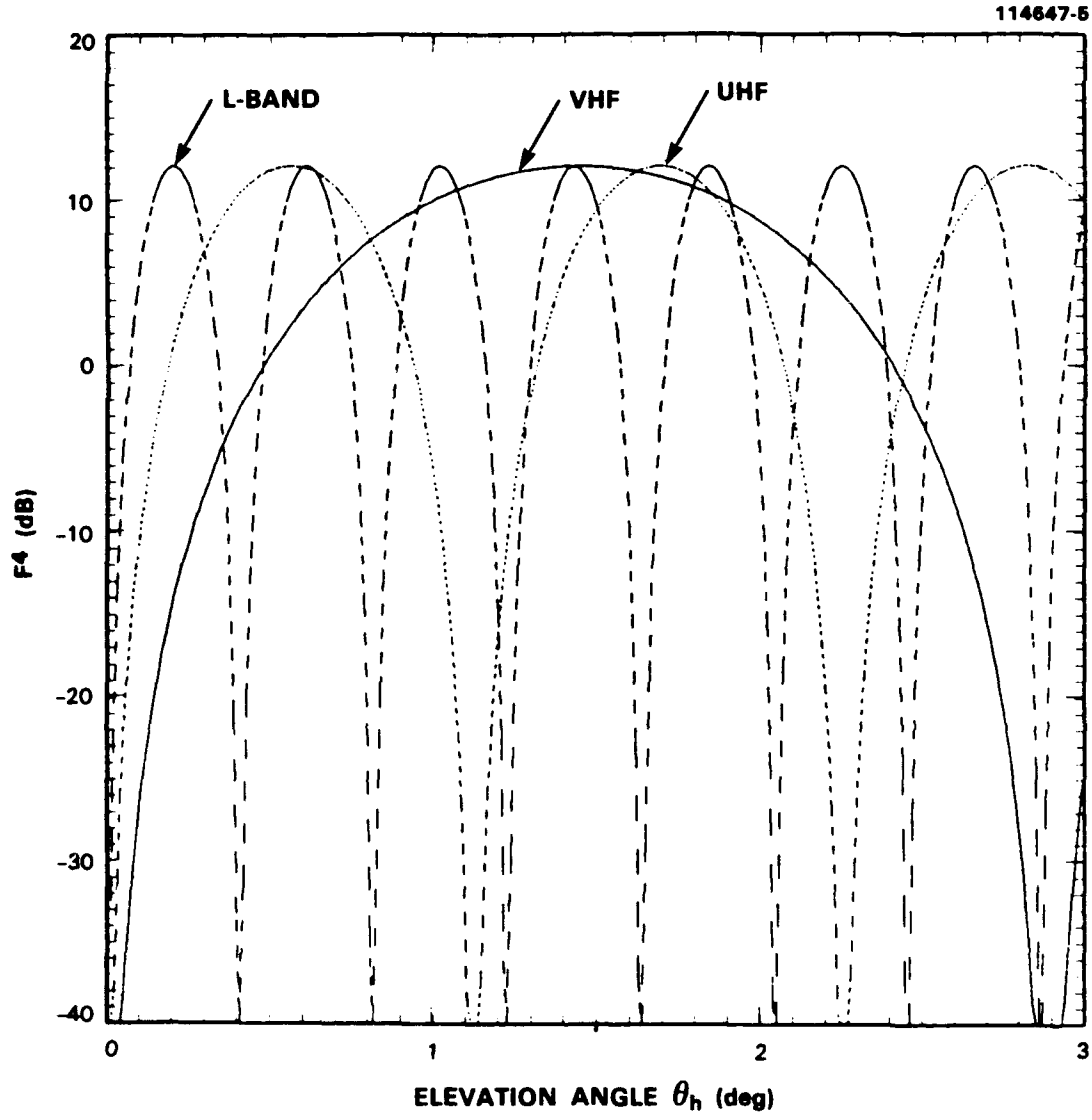

Figure B-4. Two-way multipath propagation loss F^4 versus hillside slope angle θ_h for the Phase One antennas with three tower sections extended. Computed by Equation (B.1), h_a = 17.4 m, 17.4 m, and 16.6 m for VHF, UHF, and L-band, respectively; see Table A-5.

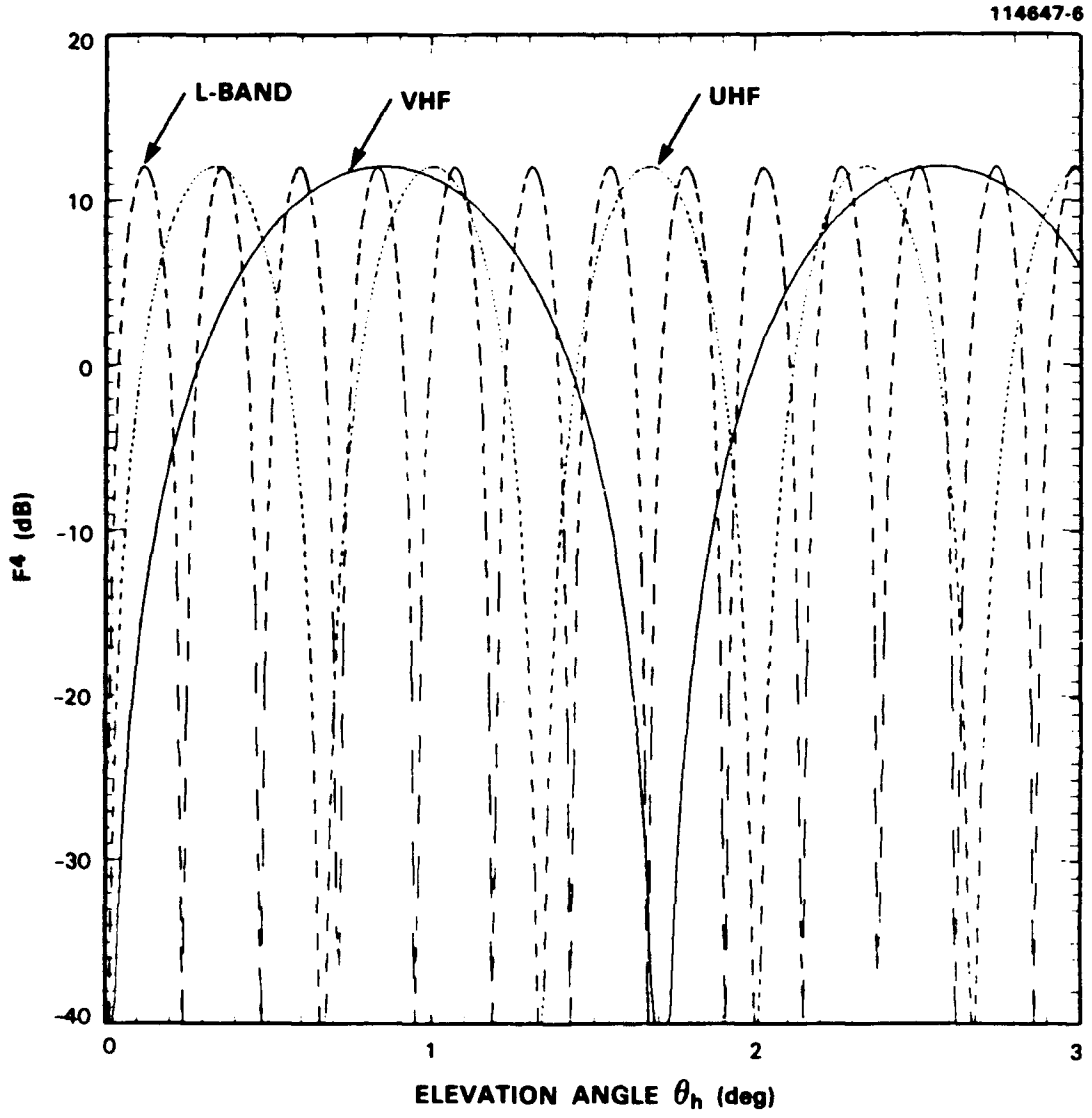

Figure B-5. Two-way multipath propagation loss F^4 versus hillside slope angle θ_h for the Phase One antennas with six tower sections extended. Computed by Equation (B.1), h_a = 29.6 m, 29.6 m, and 28.7 m for VHF, UHF, and L-band, respectively; see Table A-5.

Next, the question of estimating the slope of the ground on the hill running down from the antenna is addressed. This estimation is usually not as easy as it may at first appear. What we usually have is a contour topographic map, which in effect models the side of the hill in the direction of the repeat sector as a number of tilted straight line segments or facets, where each facet runs from one contour line to the next along the outward radial from the Phase One site position into the repeat sector. Each facet has a different tilt angle. This model creates the problem of having to decide which facet results in a horizontally reflected multipath ray. This is the active facet, which provides a first Fresnel zone of specular reflection in the horizontal direction, and at whose tilt angle we enter Figures B-4 and B-5 to determine multipath loss.

To determine which is the active facet, we run through an iterative procedure examining each facet. The geometry for this process is shown in Figure B-6. As is shown in Figure B-6, let the start range of the facet from the antenna position be r_1, the stop range of the facet be r_2, the decrease in terrain elevation from the antenna position to the beginning of the facet be y_1, the subsequent decrease in terrain elevation from the beginning of the facet to the end of the facet be y_2, and let the vertical antenna mast height be q. Let the slope of the facet with respect to horizontal be α, i.e., $\tan \alpha = y_2/(r_2-r_1)$. We imagine the planar facet surface to expand so as to be of infinite extent (i.e., the facet line is extended both to left and to right). We then ask, at what range r' on this infinite facet does the specular reflection point occur for an observer infinitely removed in the horizontal direction (i.e., horizontal specularly reflected ray). The condition for specular reflection is that the angle of incidence equals the angle of reflection from the tilted planar surface. The range to this specular point r' is given in Equation (B.3) by

$$r' = \cos 2\alpha \frac{Y_1 + h - r_1}{\tan \alpha} \quad . \tag{B.3}$$

So the test to determine the active facet is if $r_1 < r' < r_2$. That is, we compute r' for every facet down the side of the hill and find the one where $r_1 < r' < r_2$. The value of α from the active facet is what we use for θ_h to compute propagation loss in Equation (B.1).

One other task remains. The height of the antenna h_a in Equation (B.1) is the height of the antenna above the infinitely extended active facet surface in a direction normal to this surface (see Figure B-2). This height h_a may be significantly greater than or less than the actual antenna mast height q, depending on α and the details of the terrain profile out to the active facet. The quantity h_a is given by

$$h_a = (q + y_1) \cos \alpha - r_1 \sin \alpha \quad . \tag{B.4}$$

Thus, after the active facet is determined, its parameters are used to determine h_a by means of Equation (B.4), and then the active facet slope α and h_a are used in Equation (B.1) to determine multipath loss F^4. Figures B-4 and B-5 plot F^4 from Equation (B.1) as a function of facet slope but they do so only for values of h_a equal to antenna mast height q. However, in going from q to h_a, the only difference in Figures B-4 and B-5 is that the abscissa scale changes by a fixed multiplicative factor, according to the relationship $h_a\theta_h = q\theta_h'$, where θ_h is the new scale applicable for height h_a and θ_h' is the old scale as plotted in Figures B-4 and B-5 applicable for $h_a = q$. Thus, if $h_a > q$, the rate of lobing with increasing angle is faster by q_a/h_a, and vice versa if $h_a < q$. In this manner, Figures B-4 and B-5 may still be used to estimate a multipath loss for values of h_a different than the actual mast heights explicitly applicable in these figures.

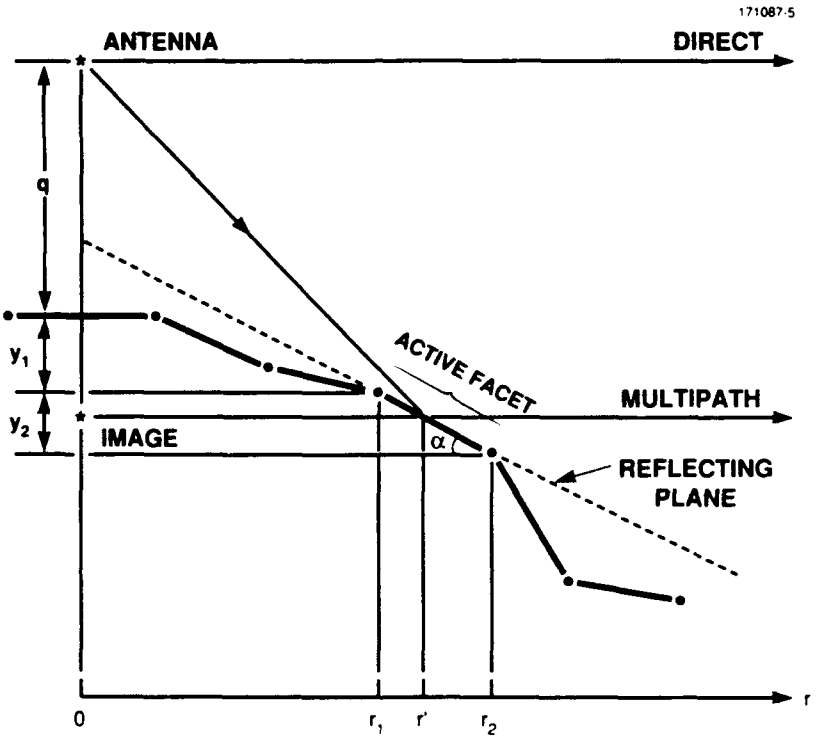

Figure B-6. Active facet geometry.

In this section, a simple method or model has been discussed for estimating the effects of multipath on observed clutter strength when Phase One is situated at a topographic high point in open low-relief terrain. The degree of this model's validity in any given situation is the extent to which it qualitatively explains observed features in the multifrequency characteristic of mean clutter strength versus frequency. That is, if features are explained, the simple model can be applied to the real situation; if features are not explained, the model oversimplifies the real situation. However, the simple model has proven useful to explain a number of singular features in our measurements. These include high VHF clutter at Strathcona, low UHF clutter at Beiseker, a UHF peak at Polonia, and different rates of falloff of clutter strength with decreasing frequency at a number of sites depending on particular terrain slope, for example, Picture Butte II, Rosetown Hill, and Spruce Home. In the next section, we use this model to understand long-range mountain clutter measured from open, low-relief prairie sites.

B.3 LONG-RANGE MOUNTAIN CLUTTER

When Phase One observed ground clutter from visible terrain at long ranges of 100 km or more, that clutter usually came from mountains because at most Phase One sites only mountains rise high enough to be visible at such long ranges. Even so, visible mountains at such long ranges barely rise above a distant horizon and are usually observed at elevation angles of considerably less than 1 deg above the local horizontal at the antenna. This being the case, one might assume that when such long-range mountains are observed from open, low-relief prairie sites, that their X-band clutter strengths would be substantially greater than their VHF clutter strengths, due to significant multipath propagation loss being expected at VHF at such low angles. In fact, our measurements of long-range mountain clutter from open, low-relief prairie sites show just the opposite — mountain clutter strength at VHF is 10 or 12 dB stronger than at X-band. The reason for this difference is that the inclined surface away from the topographic prairie high point upon which Phase One sets up rotates the VHF multipath pattern downwards and hence brings the long-range mountains at the horizon into stronger illumination, as discussed in the previous section.

In this section, we present multifrequency long-range mountain clutter strengths measured at three sites. Although constituting an aside from our principal interest in clutter at shorter ranges, these multifrequency long-range mountain data measured at three different sites are interesting in their own right and appear to point towards a general nonsite-specific frequency dependence in such data. In addition, these long-range mountain results provide examples of implementing the simple approximate technique for estimating dominant site-specific multipath effects presented in the previous section.

We now proceed to show long-range clutter strengths of high peaks and ranges in the Canadian Rocky Mountains as measured looking west from three different Phase One sites in Alberta. Two of these sites, Magrath and Lethbridge West, were on open, low-relief prairie in southern Alberta. The third site, Brazeau, was located farther north in Alberta in low-relief boreal forest. At each site, we reduce mountain clutter data from within a 45-deg azimuth sector to ranges extending well beyond 100 km. At each site, the mountain ranges observed within the sector include steep barren rock faces and snow-clad jagged peaks, as well as steep forested slopes at lower elevations. However, the specific mountain terrain from which clutter was measured was different for each site (i.e., there was no overlap on the ground in 45-deg sector coverage at the three sites). At each site, we compare multifrequency mean strengths at relatively near ranges (i.e., ≤ 24.7 km) within the 45-deg sector with multifrequency mean strengths at longer ranges (i.e., from 24.7 km out to more than 100 km) in the sector. At the near ranges, the mean clutter strengths so obtained are specific to the terrain type in which Phase One set up, either dense boreal forest or open prairie farmland and rangeland; whereas, at the long ranges, the mean clutter strengths are for mountainous terrain at all three sites.

All of the clutter results in this section are based on clutter data measured in survey mode (see Section 2.2.1 and Appendix A), in contrast to most other results in this report which come from our repeat sector data base. These survey mode data were acquired under continuous azimuth scan of the antenna, as opposed to the step scan of the antenna used in much of our repeat sector data, and with fewer pulses per cell recorded (typically 125) than in our repeat sector data (typically 1024). In these continuous scan data, we performed coherent integration over a period of time corresponding to antenna rotation of one-

eighth of the antenna beamwidth (typically 16 pulses) to arrive at each sample of clutter strength. Then, we assembled all of the clutter strengths over the 45-deg sector and specified range interval, either near or far, into a histogram of clutter strengths from which we obtained the mean clutter strength. Table B-1 shows some parameters associated with the scan mode survey data presented in this section. In these scan mode experiments, we emitted 500 pulses per second in all bands but recorded only one-out-of-N of these emitted pulses.

We now present multifrequency mean clutter strength results* as measured in our survey data to long ranges in 45-deg azimuth sectors at these three sites. These results are shown in Table B-2, both for the short-range interval at each site and the long-range interval containing mountains. The multifrequency mean clutter strength results for Brazeau (1) in Table B-2 are plotted in Figure B-7. In these Brazeau data of Figure B-7, the low-relief forest results measured at short range have the same inverse frequency dependence that is seen in our general low-relief forest, high depression angle, repeat sector results (e.g., see Table 11), except that these Brazeau survey data results are several decibels weaker in every band than our Brazeau repeat sector results because the depression angle is lower (i.e., longer range) in the survey data than in the repeat sector data. We attribute the decreasing strength with increasing frequency characteristic of these low-relief forest results to the RF absorption characteristics of the forest.

TABLE B-1
Survey Data Parameters

Parameter	VHF	UHF	L-Band	S-Band	X-Band
N (Record 1/N pulses)	16	8	4	2	2
Pulses/deg	15.6	31.25	62.5	125	125
Azimuth increment (deg)	10	4	2	1	1
Pulses/increment	156	125	125	125	125
~ 1/8 beamwidth coherent integration azimuth increment (deg)	1.25	0.5	0.25	0.125	0.125
Number of integrated pulses	20	16	16	16	16
Expected integration gain (dB)	13	12	12	12	12
Scan Data: 2 deg/s, 500 pulses/s, 1/N mode					

* These are mean upper bound values, including cells at noise level, see Appendix C.

TABLE B-2
Short- and Long-Range Multifrequency Mean Clutter Strengths* at Three Sites

	Mean Clutter Strength $\overline{\sigma^\circ F^4}$ (dB)				
	VHF	UHF	L-Band	S-Band	X-Band
Brazeau (1) 225° to 270°					
Forest (1 to 24.7 km)	–19.7	–21.7	–26.8	–33.3	–29.8
Mountains (24.7 to 143.0 km)	–19.3	–22.1	–29.0	–33.7	–31.5
Magrath 225° to 270°					
Open Prairie Farmland and Rangeland (1 to 24.7 km)	–55.3	–40.1	–35.5	–35.1	–31.6
Mountains (24.7 to 120.6 km)	–21.0	–20.9	–29.8	–32.6	–32.6
Lethbridge West 272° to 317°					
Open Prairie Farmland and Rangeland (1 to 24.7 km)	–53.0	–47.9	–35.9	–39.1	–31.8
Mountains (24.7 to 141.0 km)	——†	–21.0	–28.6	–36.7	–35.4

* Vertical polarization, 150-m pulse length.
† VHF mountain data were not collected at Lethbridge West.

The Brazeau long-range mountain results in Figure B-7 also have a similar inverse frequency dependence to that of our general mountain repeat sector results (see Table 11), except that the Brazeau long-range mountain results are 10 to 12 dB weaker in every band (specifically, weaker by 11.7, 11.5, 11.5, 12.3, and 9.9 dB at VHF, UHF, L-, S-, and X-band, respectively, than repeat sector mountain results in Table 11). This significant decrease in clutter strength of long-range mountains compared with short-range mountains is largely attributable, we believe, to a substantial diffraction loss occurring at the very long ranges and near grazing incidence illumination of the long-range mountains over this poorly reflecting forested terrain. At all three measurement sites under consideration here, although the terrain is of low-relief within the first 25 km, as range increases well beyond 25 km, the terrain becomes increasingly rough and ridged as the wooded foothills of the Rockies are encountered prior to the mountain peaks. Propagation paths near grazing incidence will suffer diffraction loss over these ridges. For example, the theoretical two-way diffraction loss along the shadow boundary of a single knife edge is 12 dB, which is very nearly the exact loss we observe above in the long-range mountain data of Figure B-7 compared with the short-range mountain data of Table 11.

We measured propagation characteristics over the Brazeau forest with our helicopter-borne propagation measurement equipment while we were there (see Table A-1), although not at the very long ranges to the mountains. At shorter ranges and higher angles, as would be expected, these propagation measurements indicated little or no forward multipath reflection from the forest at all five Phase One frequencies. The fact

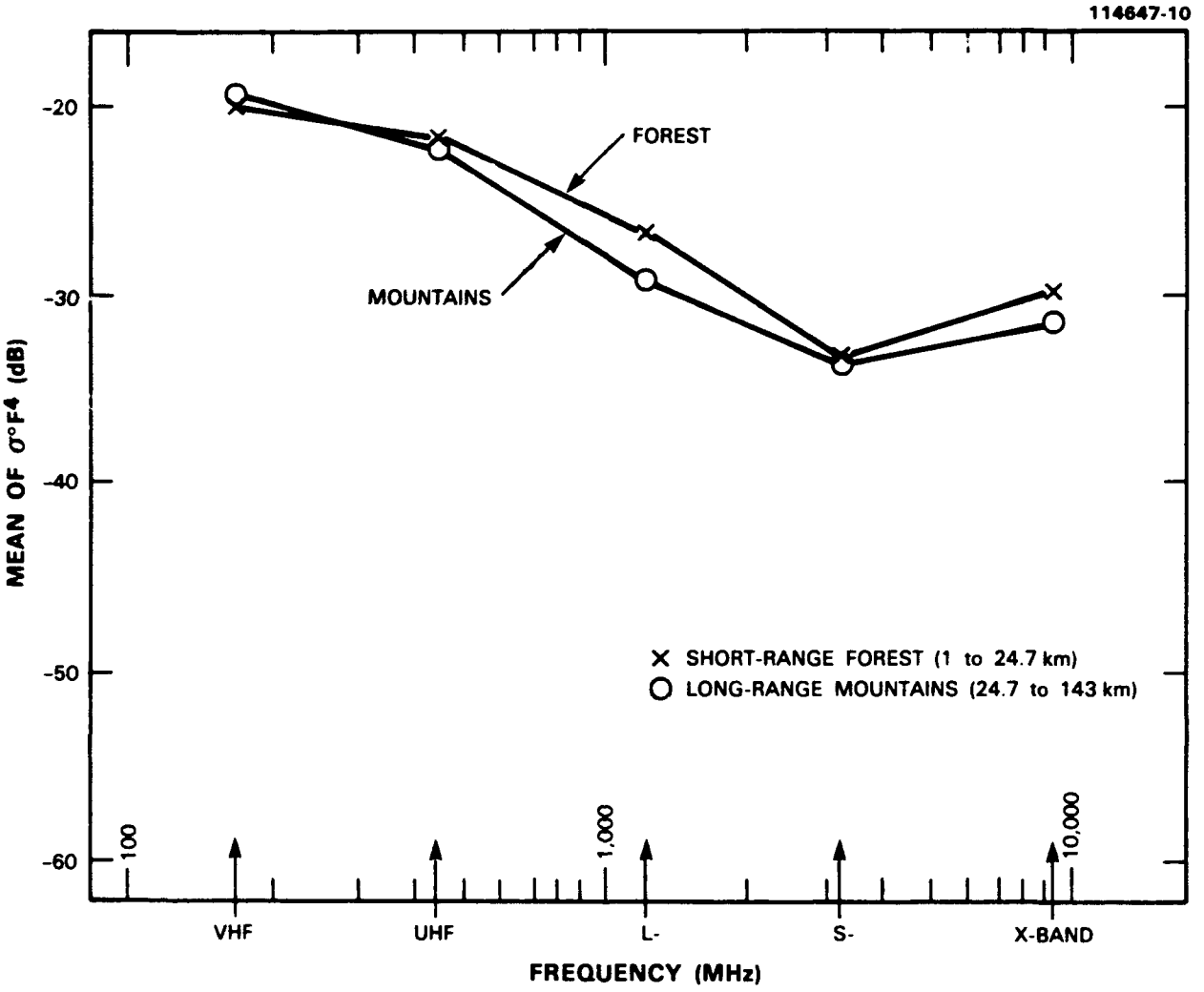

Figure B-7. Multifrequency mean clutter strengths from short-range forest and long-range mountains as measured at Brazeau (1). Azimuth interval = 225 to 270 deg; pulse length = 150 m; vertical polarization.

that this Brazeau terrain is substantially multipath-free has two ramifications for the clutter data in Figure B-7. First, the short-range forest results may be regarded as essentially intrinsic σ° results (i.e., $F \approx 1$ in these measurements). This is not a new observation here; from the same observation in our repeat sector results in the body of this report, we moved on to our association of the inverse frequency characteristic in such results with RF vegetative absorption properties of forest. Second, and more important to our discussion here, the decrease in strength of the long-range mountain data of Figure B-7 compared with our short-range repeat sector mountain measurements may be regarded as largely caused by diffraction, without any substantial accompanying multipath loss due to terrain reflections. This factor will be of significance next in this discus-

sion when we consider long-range mountain clutter measured from open prairie sites strongly supportive of multipath. Finally, concerning the Brazeau measurements of Figure B-7, we regard it as coincidental that the short-range forest and long-range mountain results are so similar.

We now go on to the Magrath and Lethbridge West results of Table B-2, which are plotted in Figures B-8 and B-9, respectively. It is apparent in Figures B-8 and B-9 that these survey data measurements obtained at these two sites provide very similar results both at short- and long-range. In addition, in comparing the data from both sites with the Brazeau data of Figure B-7, we observe that the long-range mountain data at all three sites are very similar but that the short-range data are very different at Brazeau from those at Magrath and Lethbridge West. At both Magrath and Lethbridge West, as at Brazeau, we also conducted propagation measurements (see Table A-1), which indicated that the open prairie farmland and rangeland terrain at both of these sites were strongly supportive of forward multipath reflections at all five Phase One frequencies. Hence, the short-range data in Figures B-8 and B-9 both show mean strengths that fall off rapidly with decreasing frequency due to increasing multipath loss with decreasing frequency, which is similar to our repeat sector results in very low-relief agricultural terrain. However, the long-range mountain clutter measured at Magrath and Lethbridge West appears to have no multipath loss on the basis of its being nearly equivalent to that measured at Brazeau in a multipath-free situation.

The mean strengths of long-range mountain clutter from all three sites are shown plotted together in Figure B-10. We find it remarkable that these three sets of multifrequency mean clutter strength measured from three different places on the surface of the earth are so nearly identical. Because we associate a substantial 12-dB diffraction loss with the Brazeau measurements of long-range mountain clutter in Figure B-10, we assume similar circumstances in the prairie measurements of long-range mountain clutter. That is, if multipath loss existed in these prairie measurements of long-range mountain clutter, it would cause them to be weaker than those obtained at Brazeau, increasingly so with decreasing frequency, and result in a different multifrequency characteristic. Thus, we conclude that relatively full illumination of the long-range mountains occurred in these prairie measurements in all bands, even though very large low-frequency multipath losses occurred at shorter ranges. This result seems somewhat counterintuitive. We next go on to show how this can, indeed, be the case, using our simple multipath model of the previous section to provide insight.

We begin with Magrath. Figure B-11 shows a terrain profile plotted from a 1:50,000 scale map in a direction centered within our long-range mountain sector. In Figure B-11, the active facet providing Fresnel reflection at 0-deg depression angle to the far-field, as found from Equation (B.3), is at a terrain slope of 1.85 deg. Also shown is the image of the Phase One antenna in the plane of this facet and a graphical indication of the direct ray from the actual antenna position and the multipath ray from the image position. Note that the effective height of the antenna h_a above the plane of the reflecting facet is substantially reduced from the mast height q. Table B-3 shows the heights of the long-range mountains seen from Magrath, in terms of height above sea level, effective height above the local horizontal incorporating the effects of curvature of a 4/3 radius earth, and in terms of elevation angle above the local horizontal.* Figure B-12 shows multipath lobing patterns F^4 at VHF, UHF, and L-band for the Phase One

* The depression angle below the local horizontal to the horizon on a 4/3 radius spherical earth is 0.12 deg for a 60-ft antenna mast and 0.15 deg for a 100-ft antenna mast

antennas above a reflecting plane tilted at $\alpha = 1.85$ deg, the angle of the reflecting facet in Figure B-11. In Figure B-12, the multipath loss F^4 is computed from Equation (B.1) using effective Phase One antenna heights h_a computed from Equation (B.4), where active facet slope α is 1.85 deg and mast heights q are provided in Table A-5.

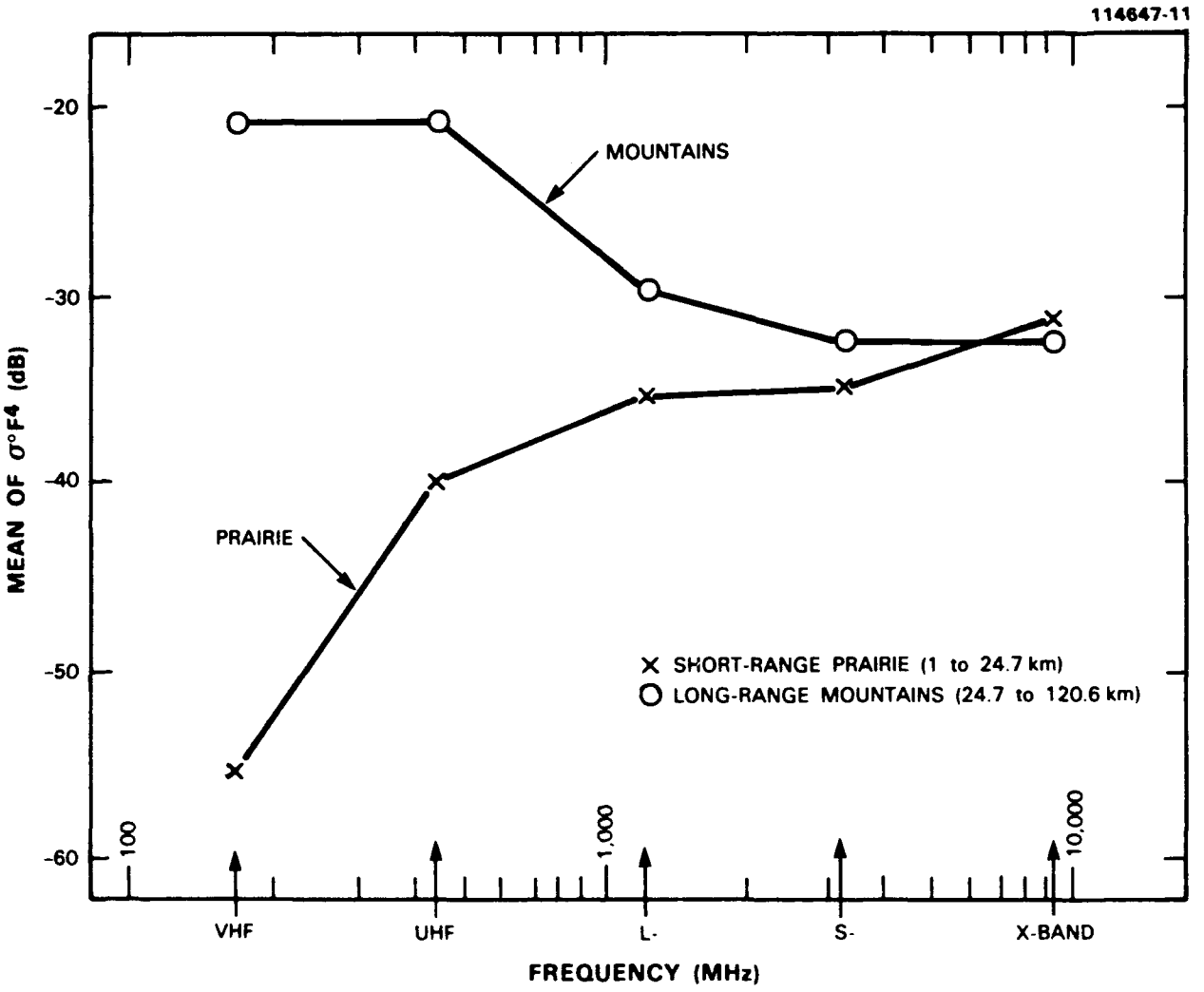

Figure B-8. Multifrequency mean clutter strengths from short-range prairie and long-range mountains as measured at Magrath. Azimuth interval = 225 to 270 deg; pulse length = 150 m; vertical polarization.

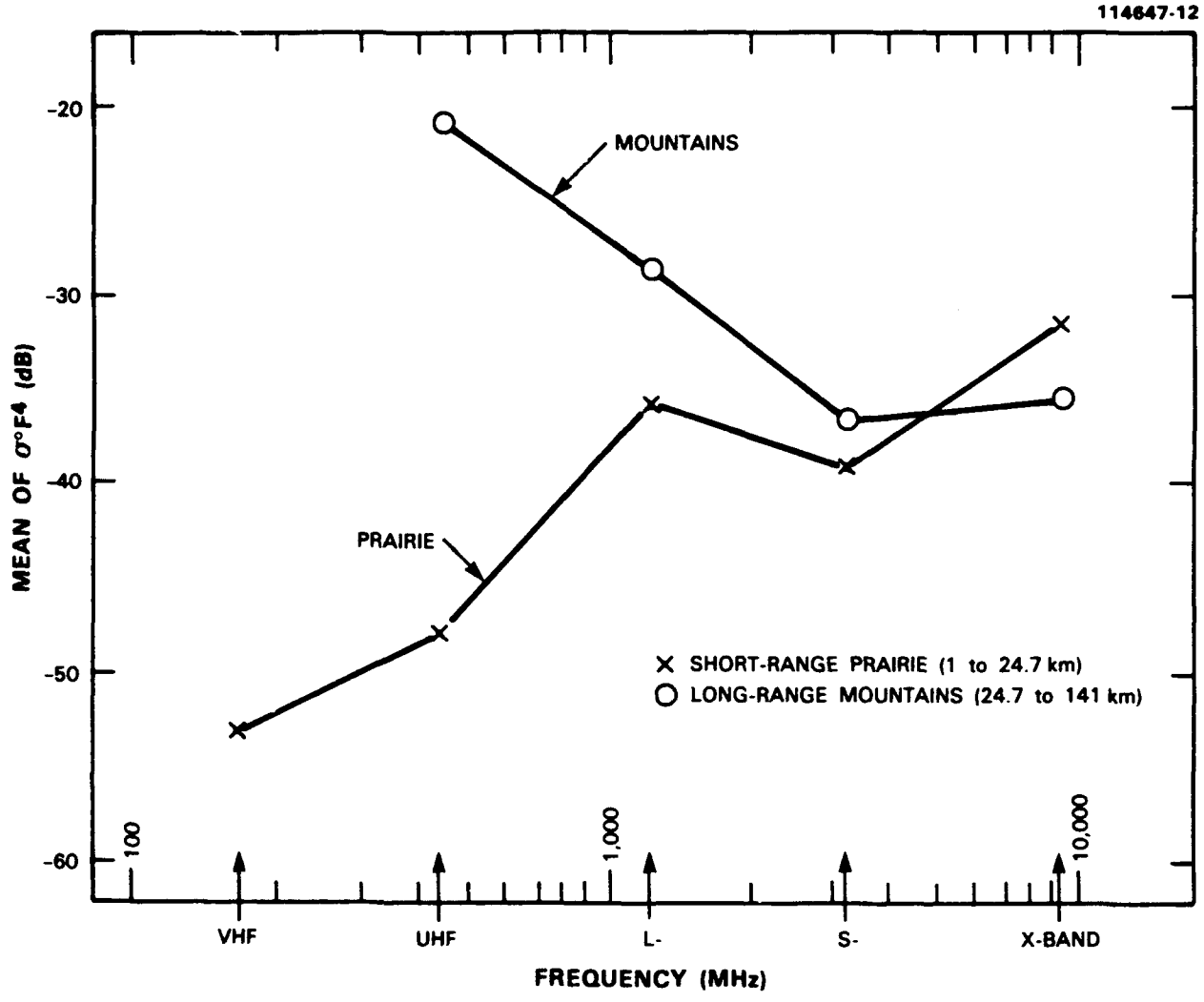

Figure B-9. Multifrequency mean clutter strengths from short-range prairie and long-range mountains as measured at Lethbridge West. Azimuth interval = 272 to 317 deg; pulse length = 150 m; vertical polarization.

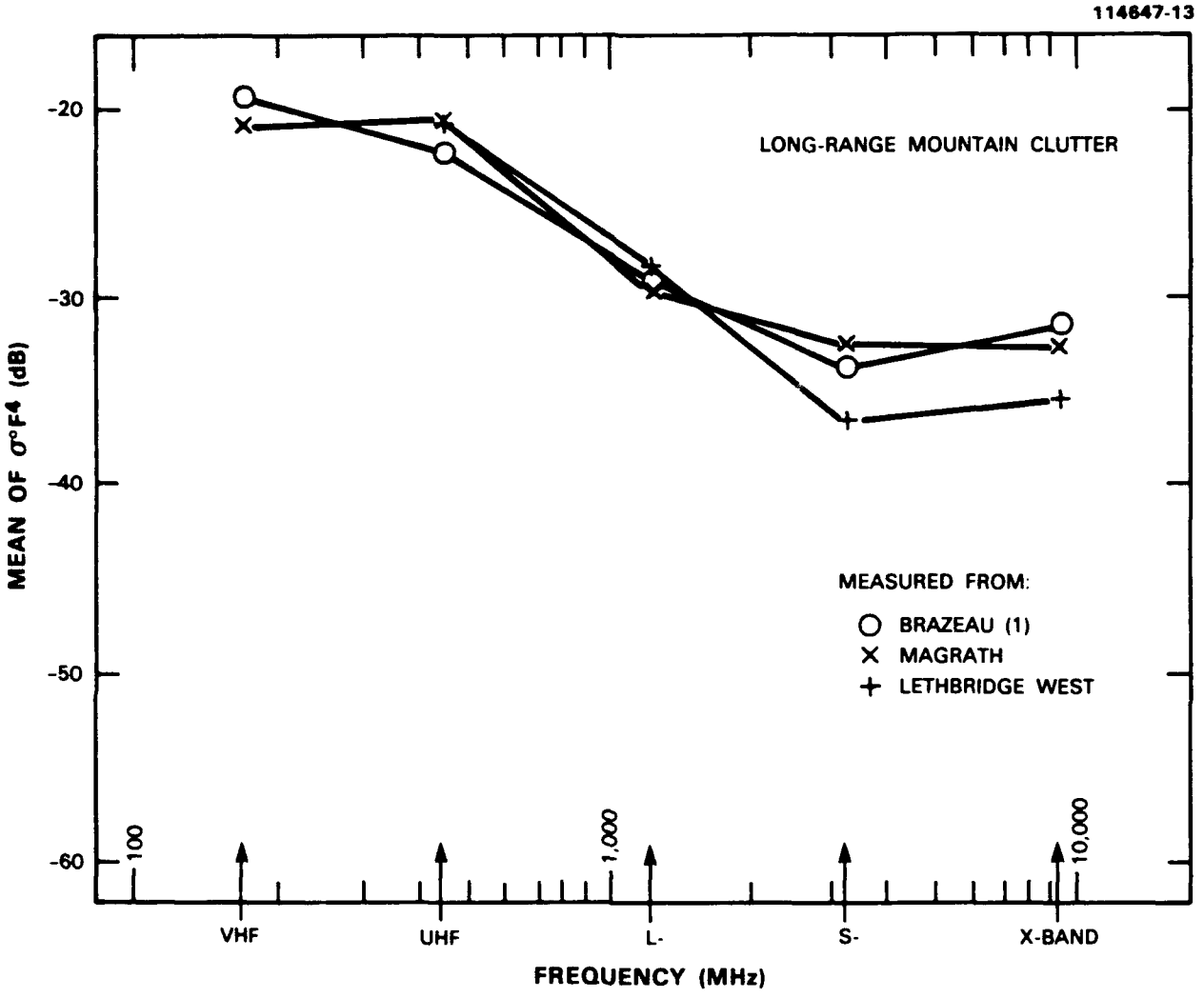

Figure B-10. Multifrequency mean clutter strengths from long-range mountains as measured from three sites. Brazeau (1), 25 to 143 km; Magrath, 25 to 121 km; Lethbridge West, 25 to 141 km. 45-deg azimuth sectors. Pulse length = 150 m, vertical polarization.

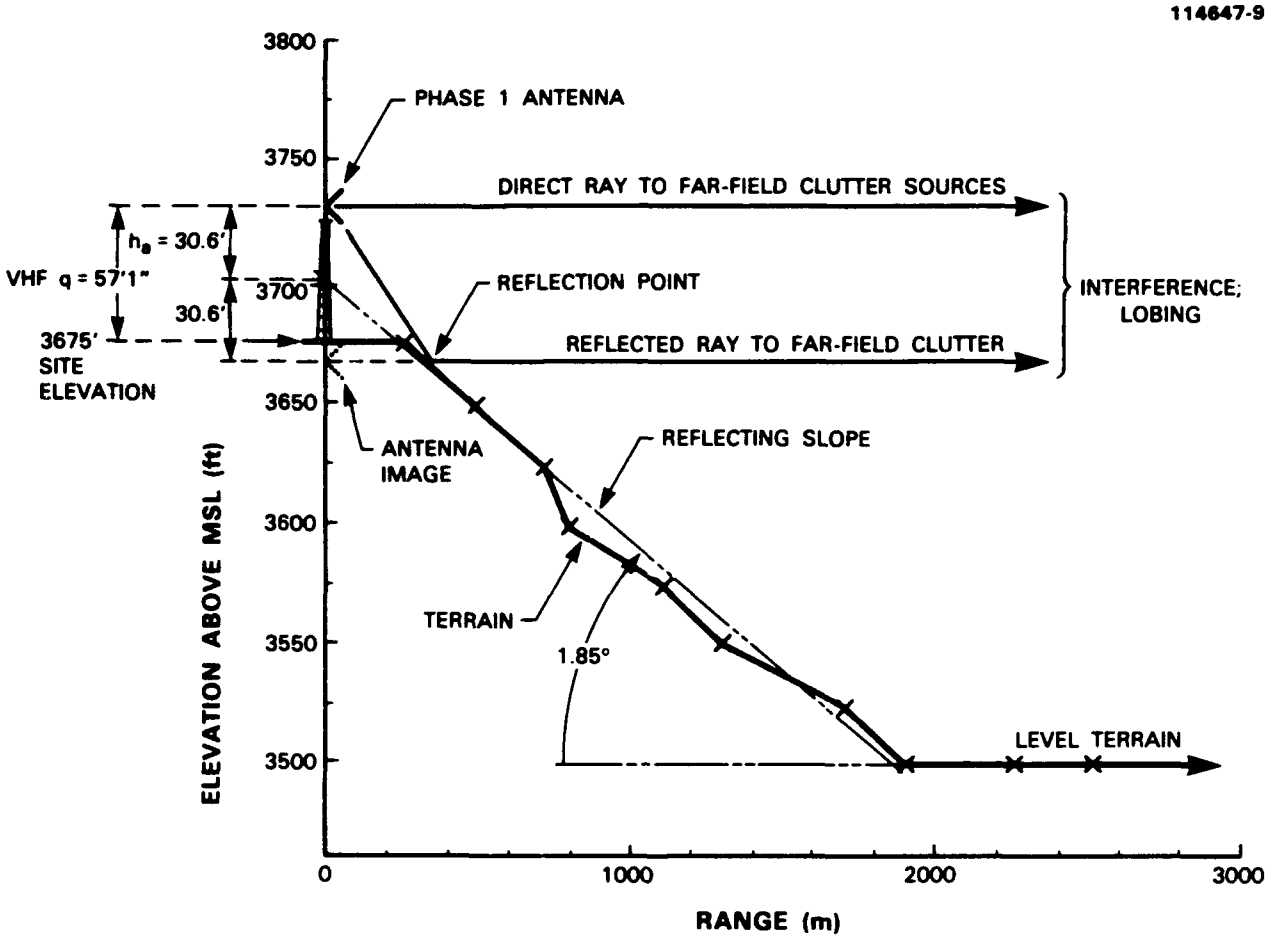

Fi· ·re B-11. Magrath terrain profile. Azimuth = 247.5 deg.

In Figure B-12, the bottom scale shows elevation angle above the tilted reflecting plane, whereas the top scale shows elevation angle above the local horizontal at the Phase One antenna. The elevation angles of the long-range mountain peaks above the local horizontal as computed in Table B-3 are indicated on the top scale. It is clear in Figure B-12 that, on the basis of a simple model of multipath from a tilted reflecting plane, the mountain peaks are illuminated well up on the lobing patterns in all bands. Even at VHF the mountain peaks reach to nearly the first maximum of the VHF lobing pattern. If we merely model the Magrath situation as multipath lobing above a level (i.e., not tilted) reflecting surface, the mountain peaks appear at elevation angles between 0.1 and 0.8 deg on the bottom scale in Figure B-12 (or, more accurately, in Figure B-4), which would lead to the expectation of significantly increasing strength of illumination of long-range mountain clutter, VHF to UHF to L-band, as F^4 monotonically rises with frequency on the underside of the first propagation lobe in much of this low-angle regime. There is no

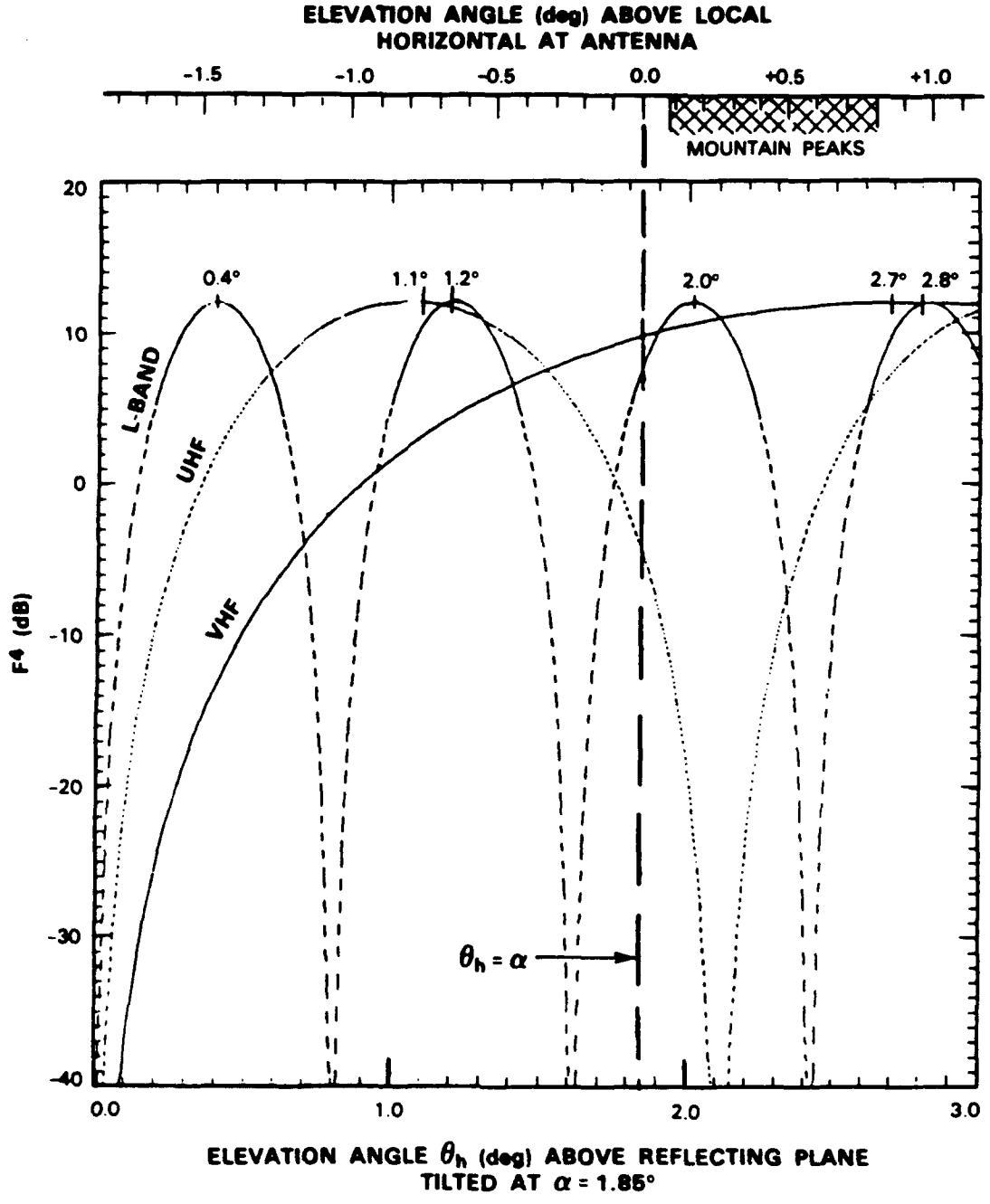

Figure B-12. Approximations to Phase One multipath lobing patterns at Magrath. Effective antenna heights h_a = 9.3 m, 9.3 m, and 8.5 m at VHF, UHF, and L-band, respectively. Azimuth = 247.5 deg.

evidence of such a countertrend of increasing clutter strength with increasing frequency due to multipath loss in the long-range mountain clutter measured at Magrath, especially when compared with the multipath-free mountain clutter measured at Brazeau. The Magrath measurement situation for these survey data in a 45-deg sector looking to long ranges is summarized in Table B-4.

TABLE B-3
Mountain Height Data at Magrath
WSW Octant (225 - 270 deg)

Range (km)	Mountain Peak Heights Above Sea Level (ft)	Net Mt. Peak Heights above Phase 1 Antennas (ft)*	Elevation Angles to Mt. Peaks from Phase 1 (deg)*
70	4500–5000	+322	+0.08
75	5000–6000	+1182	+0.28
80	6000–8000	+3032	+0.66
85	8000–9000	+3873	+0.80
90	6000–9000	+3704	+0.72

* Corrected for 4/3 earth curvature; Magrath site elevation was 3675 ft above sea level and VHF antenna height was 57 ft 1 in.

The Lethbridge West survey data results are now briefly discussed. Whereas at Magrath the visual impression was definitely that of being on a substantial hill, at Lethbridge West the terrain seemed to be locally more level. However, the Lethbridge West measurement scenario summary of Table B-5 does indicate that the local terrain in the direction of the mountains in our survey data sector inclines away from the site at a terrain slope α of 0.87 deg, and in fact at larger ranges out to 25 km, there is a greater terrain advantage at Lethbridge West than at Magrath. The terrain slope of 0.87 deg leads to the lobing patterns shown in Figure B-13. As is shown in the top scale of Figure B-13, the long-range mountain peaks are not illuminated as high in these lobing patterns as at Magrath but are still high enough to provide full illumination at gains higher than free space at all three bands according to this simple approximation. However, at VHF, the mountains, although well illuminated, do not reach the peak of the first multipath lobe; therefore, all else being equal, compared with Magrath we might expect the VHF mountain clutter measured from Lethbridge West to be slightly weaker than that measured from Magrath. Unfortunately, long-range mountain clutter was not measured at VHF at Lethbridge West, so this hypothesis cannot be checked. However, another hypothesis based on the lower terrain slope at Lethbridge West compared with Magrath can be checked. At Lethbridge West, the lower terrain slope is insufficient to bring the short-range terrain into illumination at UHF, so in Figure B-9 the short-range Lethbridge West clutter strengths at UHF stay down near the VHF levels. At Magrath, however, due to the higher terrain

TABLE B-4
Magrath Measurement Scenario

Mountain Peak Data

Range (km)	Peak Heights (kft)	Heights relative to Phase 1 Antennas (ft)	Elevation Angles Relative to Phase 1 Antennas (deg)
70 to 90	4.5 to 9.0	300 to 3900	0.08° to 0.80°

Terrain Profile Data

Site elevation: 3675' Azimuth: 247.5°

Reflection surface slope: 1.85° over 1650 m range (175' terrain fall-off)

Overall slope: 1.6° over 1900 m total range (same 175' fall-off); terrain is relatively flat beyond 1900 m range for a distance of >25 km, showing a dip to 3400' elevation across a deep river valley, followed by a gentle rise to 3600' on the prairie and across a major reservoir.

Effective Antenna Heights: 9.3 m for VHF and UHF; 8.5 m for L-band.

First Multipath Lobe Elevation Angles (see Fig. B-12):

VHF: 2.7° - 1.85° = +0.85° → full illumination of distant mountains; but limited illumination of short-range (< 25 km) farmland and rangeland.

UHF: 1.1° - 1.85° = -0.75° → full illumination of both distant mountains and short-range (< 25 km) terrain.

TABLE B-5
Lethbridge West Measurement Scenario

Mountain Peak Data

Range (km)	Peak Heights (kft)	Heights relative to Phase 1 Antennas (ft)*	Elevation Angles Relative to Phase 1 Antennas (deg)*
70 to 140	6 to 10	1900 to 3600	0.38° to 0.56°

Terrain Profile Data

Site elevation: 3100' Azimuth: 295°

Reflection surface slope: 0.87° over 2000 m range (100' terrain fall-off)

Overall slope: 1.6° over 3000 m range (175' fall-off); terrain is relatively flat beyond 3.0 km range for a distance of >25 km, rising to 3000' to 3100' elevation on the prairies and dipping to 2800' to 2900' across several more river valleys.

Effective Antenna Heights: 8.3 m for VHF and UHF; 7.4 m for L-band.

First Multipath Lobe Elevation Angles (see Fig. B-13):

VHF: 3.0° - 0.87° = +2.13° → good illumination of mountains; but very limited illumination of short-range (< 25 km) terrain.

UHF: 1.2° - 0.87° = +0.33° → full illumination of mountains; but limited illumination of level to rolling farmland out to 25 km range.

*Corrected for 4/3 earth curvature.

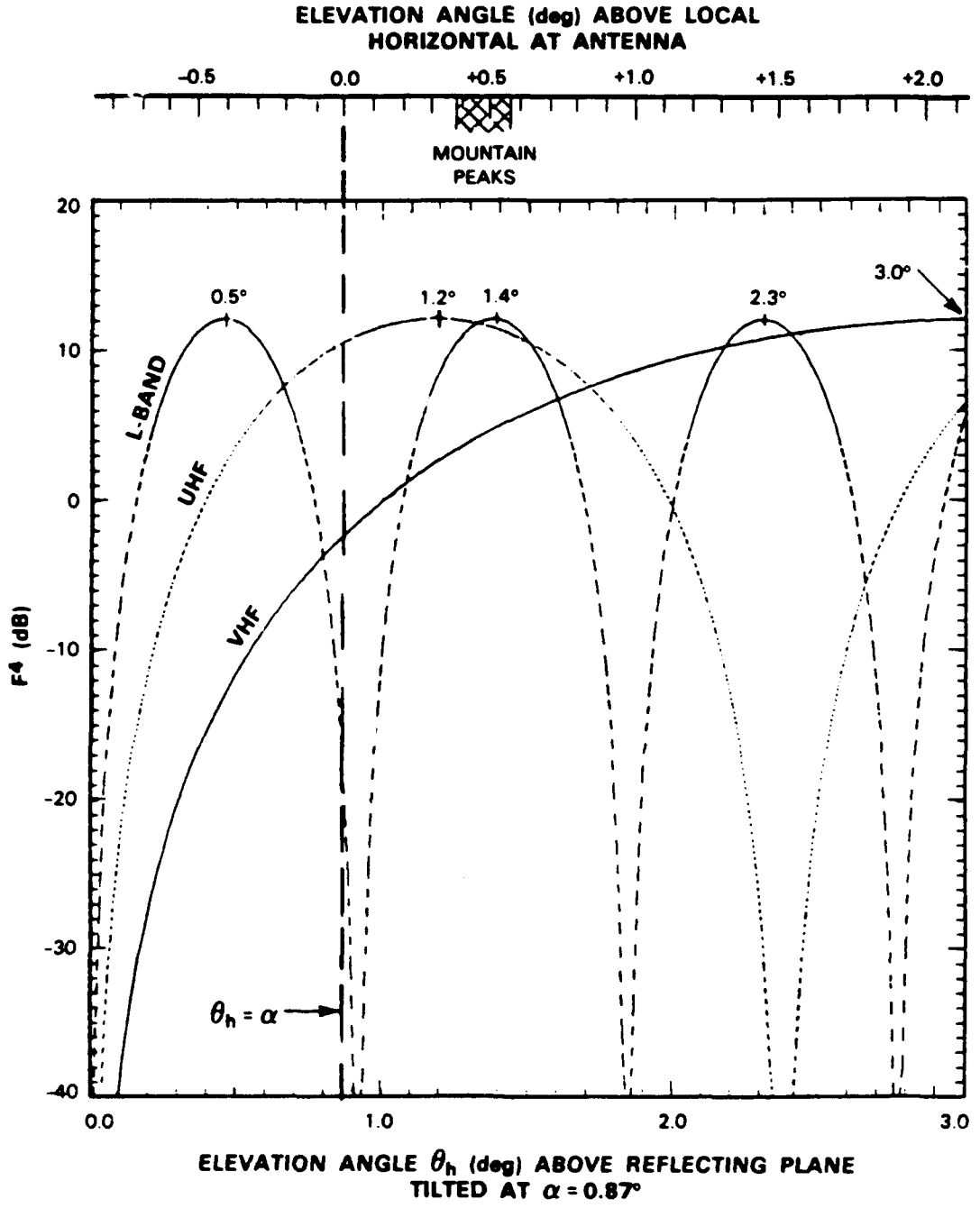

Figure B-13. Approximations to Phase One multipath lobing patterns at Lethbridge West. Effective antenna heights h_a = 8.3 m, 8.3 m, and 7.4 m at VHF, UHF, and L-band, respectively. Azimuth = 295 deg.

slope, the short-range terrain is much more strongly illuminated at UHF, so in Figure B-8 the short-range Magrath clutter strengths at UHF are much higher than the VHF levels and nearer the microwave band levels. Contributing to this effect is that the terrain advantage of the site position at Lethbridge West over the terrain looking out 25 km is greater than that at Magrath (see Tables B-4 and B-5), even though the local terrain slope is less at Lethbridge West than at Magrath. Thus, the 8-dB difference between Magrath and Lethbridge West short-range UHF mean clutter strength appears to be explainable based on differences in terrain specifics at these two low-relief prairie sites.

The long-range mountain clutter measurements from three different sites shown in Figure B-10 are now summarized. First, these long-range mountain data show a similar inverse frequency dependence, where mean clutter strengths decrease by 10 to 12 dB, from VHF to S- and X-bands, as do our short-range repeat sector measurements of mountain clutter. Taking local terrain slopes into account helps in understanding these measurements at the two sites locally situated in open low-relief terrain supportive of multipath. Second, the long-range mountain clutter is about 12 dB weaker in all bands than short-range mountain clutter. We attribute this 12-dB difference between short- and long-range mountain clutter to diffraction loss in the long-range data, even though the long-range mountains, although observed at near grazing incidence, were within direct line-of-sight visibility and were not beyond the radar horizon. Third, we mention once again the remarkable similarity in these long-range mountain clutter data measured at three, quite different sites. We have had a quick look at additional long-range mountain clutter data we measured from a number of other Alberta sites (e.g., Beiseker, Orion, Suffield, Pakowki Lake, Cochrane, Picture Butte II, and Woking), and in general these data seem to follow the same trend as shown in Figure B-10, although we have not reduced these data in detail.

APPENDIX C

CLUTTER COMPUTATIONS

TABLE OF CONTENTS

LIST OF TABLES

C.1 INTRODUCTION

The repeat sector at each site is a sector of concentration in which each measurement was repeated a number of times to provide a data base of increased parametric depth (i.e., more samples per cell, more variations in data collection parameters, such as data sampling rate and duration) than could be provided in our more spatially comprehensive survey data. As a result, the values of mean strength and other statistical attributes of repeat sector clutter amplitude distributions upon which this report is based may be thought of as being well understood, highly accurate, and reliable, based as they are on intensive in-house studies of repeat sector measurements at each site that were conducted as a logical way of gradually coming to grips with the voluminous Phase One data. In these studies, we generated the clutter amplitude distribution for each repeat sector measurement;* characterized the distribution in terms of its first four moments and various percentile levels including the median; provided goodness-of-fit information to standard distributions such as Weibull and lognormal; looked for modeling dependencies of the distribution on radar parameters, geometric parameters (e.g., range, illumination angle), and terrain descriptions; and explored effects of radar noise, integration gain, and correlation time in the data.

Detailed results of these site-by-site studies are available. A purpose of this appendix is to provide the flavor of these studies by showing selected groups of experiment-by-experiment repeat sector mean clutter strength at three sites, holding the main radar parameters of frequency, polarization, and resolution constant within each group. We begin by defining how we compute mean, standard deviation, and other attributes in measured clutter amplitude distributions. Then we discuss and illustrate effects of noise contamination on the computation of mean strength and the role of coherent integration in improving radar sensitivity to provide a valid computation of mean strength when the clutter returns are weak. Finally, we illustrate that typical effects of hour-to-hour and day-to-day variations, sampling rate variations, and antenna scan motion on the computations of mean strength are quite small.

This report provides values of mean strength for repeat sector clutter amplitude distributions measured across the 20-element Phase One radar parameter matrix (i.e., five frequencies, two polarizations, two range resolutions) at each site. Each value, which is tabulated in Appendix D, was selected as being centrally representative from a group of repeated measurements of the same frequency, polarization, and resolution. Thus, all values of mean strength and other attributes of repeat sector clutter amplitude distributions presented in this report are buttressed by underlying information in our measurement data base. This underlying information is illustrated by the results provided in Section C.5.

All computations involving $\sigma^{\circ}F^4$ data in this appendix are performed in units of m^2/m^2 but with subsequent conversion to decibels with respect to 1 m^2/m^2.

---

* Total repeat sector data base consists of 4465 measurements. Nominally, at each site, each of 20 different repeat sector experiments (i.e., five frequencies, two polarizations, two resolutions) was repeated about four times during the time on site with some variation in sampling rate (i.e., fast versus slow) and antenna scan motion (i.e., step scan versus continuous scan). At a few sites, we also varied antenna tower height and/or recorded a much larger than normal set of repeat data.

C.2 COMPUTATION OF MEAN STRENGTH, HIGHER MOMENTS, AND PERCENTILE LEVELS

Any statistical distribution has two basic parameters, which specify its central tendency and its dispersion, respectively. In this report, we describe clutter spatial amplitude distributions in terms of their important first two moments, namely, the mean (for describing central tendency) and the ratio of standard deviation to mean (for describing dispersion or spread), as well as their higher moments and percentile levels. These quantities are computed from a stored patch histogram in which the $\sigma°F^4$ bin size is always 1 dB. In each bin of this histogram, the number of samples at noise level and at saturation level are recorded, as well as the total number of samples. We have shown that the differences between statistical computations based on the actual array of non-rounded-off, individual pixel-level samples of $\sigma°F^4$, and the more efficient computations based on the rounded-off binned groups of the histogram are insignificant.

Let x represent clutter strength $\sigma°F^4$ in units of m^2/m^2. Let y represent the decibel value of $\sigma°F^4$, such that

$$y = 10 \log_{10} x. \tag{C-1}$$

In forming the histogram of spatial samples of clutter strength within a repeat sector clutter patch, measured values of y are sorted into bins 1 dB wide. In this histogram, let i be the bin index, which runs in increasing order from $i = 1$ at the minimum value of y in the histogram to $i = I$ at the maximum value of y in the histogram. The clutter strength in the i-th bin is x_i m^2/m^2, where $x_i = 10^{y_i/10}$. Let the number of samples in the i-th bin be n_i. Let the total number of samples in the histogram be N. Then

$$N = \sum_{i=1}^{I} n_i \quad . \tag{C-2}$$

Now we proceed to define mean and standard deviation in the histogram. These quantities are first computed from linear values x_i and subsequently converted to decibels. Thus,

$$\text{mean} = \bar{x} = \frac{1}{N} \sum_{i=1}^{I} n_i x_i \quad ; \tag{C-3}$$

and

$$\text{standard deviation} = \text{sd}(x) = \left[\frac{1}{N-1} \sum_{i=1}^{I} n_i (x_i - \bar{x})^2 \right]^{\frac{1}{2}} \quad . \tag{C-4}$$

In clutter amplitude statistics, these two quantities are almost always much less than unity. For convenience, we convert them to decibels units, as:

$$\bar{x}\big|_{\text{dB}} = 10 \log_{10}(\bar{x}) \quad ; \tag{C-5}$$

$$\text{sd}(x)\big|_{\text{dB}} = 10 \log_{10} [\text{sd}(x)] \quad . \tag{C-6}$$

Next, we define skewness and kurtosis in the histogram. Skewness is a measure of asymmetry in the distribution. Kurtosis is a measure of concentration about the mean, or, in other words, is a measure of the relative peakedness or flatness of the distribution. Let $g_3(x)$ be the coefficient of skewness and $g_4(x)$ be the coefficient of kurtosis. Then

$$g_3(x) = \frac{M_3(x)}{\left[M_2(x)\right]^{\frac{3}{2}}} \quad ; \tag{C-7}$$

$$g_4(x) = \frac{M_4(x)}{\left[M_2(x)\right]^2} \quad ; \tag{C-8}$$

where

$$M_q(x) = \frac{1}{N} \sum_{i=1}^{I} n_i (x_i - \bar{x})^q ; \quad q = 2,3,4 \quad . \tag{C-9}$$

When we provide values for the quantities $g_3(x)$ and $g_4(x)$ in the body of this report, it is subsequent to their conversion to decibel units in a manner similar to Equations (C-5) and (C-6) above.

For completeness, we also define the median level and other percentile levels in the histogram. Let P_i represent the probability that $y \le y_i$ (or, equivalently, that $x \le x_i$). Then

$$P_i = \frac{1}{N} \sum_{j=1}^{i} n_j \quad . \tag{C-10}$$

The median value of x is the value x_i corresponding to $P_i = 0.5$. Similarly, the 70- and 90-percentile values of x are the values x_i corresponding to $P_i = 0.7$ and 0.9, respectively. The assembling of our histogram of clutter amplitudes, and the computations made from this histogram are discussed more thoroughly elsewhere.

We now comment briefly on the interpretation of the above quantities. The standard deviation is meaningful only with respect to the mean. That is, it is the ratio of standard deviation to mean, namely, $\mathrm{sd}(x)/\bar{x}$, that is meaningful. We express this ratio as a decibel quantity, as:

$$10 \log_{10} \left[\mathrm{sd}(x) / \bar{x}\right] = 10 \log_{10} \left[\mathrm{sd}(x)\right] - 10 \log_{10}(\bar{x}) \quad . \tag{C-11}$$

It is this ratio, $10 \log_{10}[\mathrm{sd}(x)/\bar{x}]$, that we tabulate as a measure of spread in repeat sector clutter amplitude distributions throughout this report. Occasionally, we show this ratio as SD/MEAN (dB) or sd/mean (dB). In a Rayleigh* distribution, applicable to the theoretical situation of many randomly phased contributions in which no single contribution dominates, the ratio of standard deviation to mean is unity (i.e., $10 \log_{10}[\mathrm{sd}(x)/\bar{x}] = 0$ dB). Thus, the larger the empirical value of ratio of standard deviation to mean in decibels, the greater the degree of spread in the amplitude distribution beyond Rayleigh. Most of our

* By this, we mean the voltages are Rayleigh distributed. The powers are exponentially distributed.

measured clutter amplitude distributions have ratios of standard deviation to mean much greater than unity. Occasional repeat sector amplitude distributions occur, often at higher depression angles, that are close to Rayleigh with ratios of standard deviation to mean approaching unity (i.e., approaching 0 dB). In a Rayleigh distribution, the values of skewness and kurtosis are 2 and 9 or 3.01 dB and 9.54 dB, respectively; and the ratios of mean to median, 99- to 50-percentile, 90- to 50-percentile, and 70- to 50-percentile are 1.6, 8.2, 5.2, and 2.4 dB, respectively.

Elsewhere, we develop models of ground clutter spatial amplitude distributions using the analytic Weibull distribution function. Weibull statistics are convenient for this purpose because they can easily accommodate the wide spreads* existing in many of our measured distributions and because in the limiting, narrow spread case they degenerate to Rayleigh statistics as do our measured clutter spatial amplitude statistics. The Weibull cumulative distribution function may be written as:

$$P(x) = 1 - exp\left\{\frac{ln\ 2 \cdot x^b}{\left(x_{50}\right)^b}\right\} \quad . \tag{C-12}$$

where x_{50} = median value of x,

b = $1/a_{w}$, and

a_{w} = Weibull spread parameter.

This Weibull distribution degenerates to a Rayleigh distribution when $a_{w} = 1$. In the modeling studies referred to above, we characterize the spread in a clutter amplitude distribution by the Weibull spread parameter a_{w}. In this present report, which focuses more on careful representation of the measurement results behind the model rather than the model itself, we characterize the spread in a distribution by its ratio of standard deviation to mean as being more in keeping with statistical data reduction and less with extrapolation to a model. In a Weibull distribution, however, the Weibull spread parameter and ratio of standard deviation to mean are directly related as

$$\frac{\mathrm{sd}(x)}{\bar{x}} = \frac{\left[\Gamma\left(1+2a_{w}\right) - \Gamma^2\left(1+a_{w}\right)\right]^{\frac{1}{2}}}{\Gamma\left(1+a_{w}\right)} \quad \dagger \quad . \tag{C-13}$$

where Γ is the Gamma function. Furthermore, the mean-to-median ratio for Weibull statistics is

$$\frac{\bar{x}}{x_{50}} = \frac{\Gamma\left(1+a_{w}\right)}{(\ln 2)^{a_{w}}} \quad \dagger\dagger \quad . \tag{C-14}$$

---

* In contrast, the lognormal distribution usually overemphasizes the degree of spread required (i.e., our measured tails fall off more rapidly than do lognormal tails).

† An approximation for Equation (C-13) is $10\ log_{10}\left[\mathrm{sd}(x)/\bar{x}\right] \cong 0.1 + 3.5\left(a_{w} - 1\right) - \frac{a_{w}^2}{9} + \frac{a_{w}^3}{170}$.

†† An approximation for Equation (C-14) is $10\ log_{10}\left(\bar{x}/x_{50}\right) \cong -1.95 + 2.9\ a_{w} + 0.65\ a_{w}^2$.

Thus, the first two moments completely characterize a Weibull distribution. That is, to make use of the values of mean and ratio of standard deviation to mean provided in this report, we believe it is usually quite reasonable as a first approximation* to assume approximate Weibull statistics with a_w defined by Equation (C-13) and x_{50} subsequently defined by Equation (C-14). Then these values of a_w and x_{50} as computed from $\bar{x}$ and $\mathrm{sd}(x)/\bar{x}$ together completely define the distribution function given in Equation (C-12).

In this report we reduce clutter data within repeat sector patches. For convenience, each repeat sector patch is selected to be a range interval of an angular sector in a polar grid centered at the radar. The median repeat sector patch is 2.4 km in azimuth extent at its midrange point and 6 km in range extent. Repeat sector patches are selected only within terrain that is under general illumination by the radar. Thus, our data reduction avoids macroscale shadows cast by large terrain features. Nevertheless, the measurement of ground backscatter by means of a radar on the ground will almost always involve microscale shadowing as an important underlying phenomenon even within regions that are generally well illuminated. In fact, for low-relief terrain in which the radar wave skims the surface and backscatters significantly from vertical features only, even regions under general illumination will contain a high percentage of low return and/or shadowed cells at radar noise level. Our reduced data incorporate all the cells within our generally illuminated patches, including the cells at noise level.

We seldom use what we call "shadowless" statistics in which, within a repeat sector patch, only those clutter return samples above radar noise level are collected into histograms and distributions. Shadowless statistics are sensitivity dependent and are conditional, not absolute, measures of reflectivity. They are tempting to use, but our experience has been that they are often subsequently misinterpreted in analysis in ways which can misrepresent real system performance. A few examples of shadowless data are presented in Tables C-1 through C-4, but all of our major results in the main body of this report are based on computations involving all samples in the histogram, including those at radar noise level.

A major advantage of including all the samples within the distribution, including those at radar noise level, is that the resultant cumulative distributions, once they emerge from the noise, are independent of the sensitivity of the measurement radar. In other words, any percentile level in an amplitude distribution, to be an absolute measure, needs only to reflect how many samples exist below it, not the particular strengths of those samples. These matters of shadowing and sensitivity are discussed at greater length elsewhere.

In Section C.3, we discuss how we handle the contaminating influence of noise-level samples in our repeat sector ground clutter spatial amplitude distributions in computing their moments. In Section C.4, we discuss the computational ramifications of coherency in our measured data. In Section C.5, we expand upon these discussions by providing a number of examples of repeat sector mean clutter strength computed in various ways.

---

* Low-angle clutter is a messy statistical phenomenon. Our measured clutter distributions almost never pass rigorous statistical hypothesis tests (e.g., the Kolmogorov-Smirnov test) for belonging to Weibull, lognormal, or any other analytical distributions we have tried. Rather than dwell on statistical rigor, we emphasize engineering approximations to our distributions using Weibull statistics. Working in this manner, we do not guarantee rigorous Weibull statistics within specified confidence bounds, but we do, for example, provide the one-sigma variability of mean strength (an engineering indication of prediction accuracy) in our measured distributions within a given terrain type/relief/depression angle class, which is often on the order of 3 dB. We are less concerned with the exact shape of the distribution than in getting its level (i.e., first moment) right.

C.3 UPPER AND LOWER BOUNDS

The measured clutter amplitude distributions upon which this report is based include all of the clutter samples returned from within a repeat sector patch, including those at radar noise level. To determine the extent to which these noise samples contaminate our results, we compute the moments of these distributions in two ways: first, as an upper bound and second, as a lower bound. We compute the upper bound by assigning the measured noise power values to the noise level samples. That is, the actual clutter return for a noise level cell has to be less than or equal to the noise level; if it were greater, we would measure it above our noise floor. We compute the lower bound by assigning zero power to the noise level samples. That is, the actual clutter return for a noise level cell, even if only weakly illuminated through diffraction, theoretically has to be greater than zero. Every computation of repeat sector mean, standard deviation to mean, and higher moment in this report has been performed both ways, as an upper bound and as a lower bound. Almost all values provided are upper bounds (unless indicated otherwise).

Even when the amount of microshadowing within a patch is extensive (i.e., when a large percentage of returns are at radar noise level), it usually has very little effect on the estimates of these moments. Our upper and lower bounds to these quantities are usually within a tenth or even a few hundredths of a decibel of one another because these calculations are dominated by the strong returns from the discrete clutter sources within the patch. Examples of upper and lower bounds to mean patch clutter strength are provided in Tables C-1 through C-4.

The shadowless moments can be significantly higher than the upper and lower bounds to the moments including microshadow because the shadowless moments are computed over a conditional sample population of cells that can be much less than the total number of cells. If N is the total number of cells in the patch and N_c is the number of shadowless cells above radar noise level, then the shadowless mean is greater than the lower bound mean by $10 \log_{10}(N/N_c)$ dB. That is, the conditionally defined shadowless mean is highly sensitivity dependent because N_c is highly sensitivity dependent; whereas, the upper and lower bounds to the absolute mean (both normalized to the complete population of N cells) are usually not very sensitivity dependent. The shadowless mean is also provided in Tables C-1 through C-4. Note that the percentage of noise samples in each underlying histogram in these tables can be computed using the above relationship.

C.4 COHERENCY

The Phase One system measured radar reflections coherently. By this we mean that the radar return for each pulse from each resolution cell is available on our calibrated clutter tapes as an in-phase and quadrature number pair. A useful benefit of coherency in radar data is the increase in sensitivity that can be obtained by coherently integrating over a number of pulses. This sensitivity depends on the relative phase of the returned signal from the target remaining constant over the integration period while the pulse-to-pulse phase variation in the system noise is random. However, ground clutter is generally not a deterministic targetlike signal but is a noiselike random process.* Care must be taken in coherent integration of clutter returns to avoid unintentionally reducing the clutter as though it were noise while attempting to realize increased sensitivity to clutter returns.

* Clutter can be represented as correlated noise in space and time.

Let I_i and Q_i be the in-phase and quadrature samples for the i-th pulse on a given resolution cell in units of $\{\sigma^\circ\}^{1/2}$. Let the mean σ° of that cell, coherently averaged over N pulses, be $\sigma^\circ_{\text{coherent}}$. Then

$$\sigma^\circ_{\text{coherent}} = \frac{1}{N^2}\left[\left(\sum_{i=1}^{N} I_i\right)^2 + \left(\sum_{i=1}^{N} Q_i\right)^2\right] \quad . \tag{C-15}$$

Let the mean σ° of the same cell, noncoherently averaged over the N pulses, be $\sigma^\circ_{\text{noncoherent}}$. Then

$$\sigma^\circ_{\text{noncoherent}} = \frac{1}{N}\left[\sum_{i=1}^{N}(I_i)^2 + \sum_{i=1}^{N}(Q_i)^2\right] \quad . \tag{C-16}$$

It is apparent that coherent averaging sums voltagelike quantities; whereas, noncoherent averaging sums powerlike quantities. Furthermore, it is apparent that coherent averaging of a noncorrelated random clutter process will incorrectly reduce the estimated mean clutter strength by a factor of N.

We need to ensure that, if we wish to improve Phase One clutter sensitivity through coherent integration, we restrict the integration interval to be substantially less than the correlation time in the clutter process. Clutter correlation time is a strongly varying function of space and time, and, for example, can vary considerably from cell to cell within a repeat sector. Specification of correlation time statistics in our measured data can itself quickly become a major data reduction undertaking. Alternatively, and in fact what we did, was to observe the behavior of spatially averaged coherent mean clutter strength versus increasing number of pulses integrated over very long intervals in our long-time-dwell data, keeping the number of pulses integrated on each cell the same for a given computation of coherent mean strength spatially averaged over a set of cells. In this manner, we built up a base of information illustrating how spatially averaged coherent mean clutter strength could gradually diminish with increasing integration time, depending on parameters such as frequency band and terrain type. These results helped us proceed in repeat sector situations involving weak clutter backscatter where we needed integration gain to obtain accurate measures of mean, standard deviation, and other attributes in the resultant clutter amplitude distributions.

The foregoing discussion indicates that noncoherent computation of clutter strength is preferable if integration gain is not required because noncoherent computation avoids the complex issue of variable temporal correlation characteristics in a noiselike process. Therefore, as the baseline operation in obtaining all results for mean strength and other attributes in the repeat sector clutter spatial amplitude distributions of this report, we forego the coherency available in the data, and, for each return sample, we simply form the I_i^2 and Q_i^2 clutter strength estimate for that sample and bin it in a histogram containing all such samples* from the repeat sector. We then compute the mean and higher moments of the resultant

* The all-samples distribution is obtained by setting $N = 1$ in Equation (C-16); that is, each clutter return sample is individually binned in the histogram. Noncoherent averaging over a number N of return samples [$N > 1$ in Equation (C-16)] prior to assembling the histogram results in reduced spread in the distribution. Noncoherent averaging does not affect the mean of the resultant distribution compared with the all-samples distribution.

"all-samples" distribution, both as an upper bound and as a lower bound with respect to the noise level samples in the distribution. As long as these two bounds remain tight, within 0.1 dB or so, we regard the resultant all-samples values of mean and higher moments as definitive. As a standard procedure, we also routinely perform a coherent computation of the same results. In all cases where the all-samples clutter bounds were tight and the integration interval in the coherent computation was much less than the clutter correlation time, the coherent bounds were within a few tenths of a decibel of the corresponding all-samples bounds and provided an amplitude distribution with increased sensitivity at low levels.

At a very few sites, particularly with the reduced sensitivity of the high range resolution waveforms, repeat sector all-samples mean bounds diverged by many decibels. Such sites were characterized by being open (i.e., nonforested) and without large discrete clutter sources. Examples of such sites are our desert site of Knolls, Utah, and our wetland site of Big Grass Marsh, Manitoba. In both situations, we attempted to measure very weak backscatter at grazing incidence from what would be characterized more as a statistical rough surface and less as a sea of discretes. In these circumstances, particularly at high range resolution, the increased sensitivity available through integration gain is necessary for us to obtain accurate measures of mean and higher moments in the measured Phase One clutter amplitude distributions. At these sites, although the high resolution all-samples mean bounds diverged by many decibels, the high resolution coherent mean bounds remained relatively tight to within a few decibels, even at the weak mean clutter levels involved (e.g., -70 dB). As discussed above, tight coherent mean bounds do not necessarily indicate accuracy but only lack of degradation by noise samples. The further stipulation is that the coherent integration interval need be much less than the correlation times in the clutter processes. We ensured this through examination of the clutter data.

C.5 REPEAT SECTOR COMPUTATIONAL EXAMPLES

We now provide some examples of the set of results we obtain when we compute mean clutter strength within a repeat sector. As discussed previously, for each repeat sector clutter measurement, we compute upper and lower bounds to the absolute mean clutter strength in the repeat sector including noise-level cells, and also the shadowless mean clutter strength excluding noise-level cells, the latter being a conditional or nonabsolute measure of repeat sector mean clutter strength dependent on radar sensitivity. Furthermore, for each measurement we compute this set of three quantities two ways, first, as a noncoherent all-samples computation and second, as a coherent integration computation. Thus, for each repeat sector clutter measurement selected in this section, we show these six computed quantities for mean clutter strength.

At each site, for a given RF frequency band, polarization, and range resolution, we performed each repeat sector measurement a number of times during the period of time that the Phase One equipment was at the site. Although a major purpose of this procedure was to show day-to-day variations in clutter strength, within these repeated measurements we also varied underlying parameters involving data sampling rate and data acquisition interval or dwell time (see Table A-21). To briefly elaborate on this, on the one hand, we were motivated to use a relatively high data sampling rate (i.e., PRF) for the purpose of improving sensitivity through coherent integration. This procedure requires many samples within a clutter correlation period. On the other hand, we were motivated to use a low sampling rate so that our set of samples would cover many clutter correlation periods. This introduces a desirable element of temporal averaging in our statistics such

that the repeat sector spatial mean clutter strength is based on a temporal mean clutter strength in each spatial resolution cell within the repeat sector. One can imagine a burst mode of data collection that would provide the best of both worlds — fast sampling within a burst for coherent integration and slow sampling between bursts for time averaging. We did not implement such a burst mode of data collection because of the difficulties in data management and processing that an inconstant PRF within experiments would introduce.* Instead, we simply measured some repeat sector experiments with fast sampling and others with slow sampling but always with a constant sampling rate within each experiment.

We refer to repeat sector experiments with relatively high sampling rates as type 1 experiments, which were usually run using the Phase One beam step antenna azimuth positioning mode. In the beam step mode, the beam was held stationary at each azimuth during data collection and was then stepped to the next azimuth until complete coverage through the repeat sector was completed. Beam step experiments with low sampling rate for time averaging are referred to as type 2 experiments. In addition, we implemented type 3 experiments which, like type 2 experiments, also involved a low data sampling rate, but in conjunction with a continuous slow azimuth scan through the repeat sector during data collection to introduce continuous spatial averaging in the data stream.

We now show computations of mean clutter strength for the farmland repeat sector at the Beulah, North Dakota site. Table C-1 shows Beulah results at L-band; Table C-2 shows Beulah results at VHF. This site and these two bands are quite arbitrarily selected here to show typical examples of mean clutter strength computations as we observe them at most sites. Many of the effects discussed previously in Appendix C are quantified in the data of Tables C-1 and C-2. Thus, at Beulah, the all-samples mean bounds are always quite tight for all three experiment types. Further, in the high sampling rate type 1 experiments, the coherently integrated mean bounds are very close to the all-samples mean bounds. Theoretically, the coherently integrated result should always be less than or equal to the equivalent noncoherently integrated result. Occasionally, we observe that, in these type 1 experiments, the coherently integrated result can be very slightly (i.e., insignificantly) greater than the noncoherent all-samples result, an affect attributable to round-off as all the individual samples are individually binned in the histogram. That is, our noncoherent all-samples result is not averaged before binning.

The increase in sensitivity through coherent integration is observed in the data in Tables C-1 and C-2 in that the coherently integrated shadowless mean is much closer to the corresponding coherently integrated upper and lower bounds than is the noncoherent all-samples shadowless mean. This reflects the existence of fewer noise samples when coherent integration is employed. The number of noise samples may be calculated from the ratio of the shadowless mean to the mean lower bound (see Section C.3). In contrast to the high sampling rate type 1 experiments, in the low sampling rate experiments of type 2 or type 3, the coherently integrated mean is generally significantly less than the noncoherent all-samples mean, particularly at the higher frequencies (e.g., L-band), reflecting the fact that in these experiments the coherent integration interval can span many correlation periods.

* We did utilize a pseudo-burst-mode in time-hop data collection where we automatically repeated a standard, constant PRF experiment a number of times with a specified, long-term delay (usually 3 min) between experiments. See Table A-24, fields 100 and 102.

TABLE C-1

Computations of L-Band Repeat Sector Mean Clutter Strength at Beulah, North Dakota
(Repeat sector azimuth extent = 20 deg; range extent = 5.9 km; terrain type = farmland; see Table D-1)

Date/Time (hr:min)	Exp. Type†	$\overline{\sigma^\circ F^4}$ (dB)					
		Non-Coherent Binning of 128 samples/cell			Coherent Integration of 128 samples/cell		
		Upper Bound	Lower Bound	Shadowless	Upper Bound	Lower Bound	Shadowless
Range res = 150m; pol = hor							
7 June '84/09:29	1	-30.07	-30.07	-27.38	-30.08	-30.08	-29.81
14 June '84/15:10	3	-28.34	-28.35	-25.42	-28.90	-28.90	-28.52
14 June '84/15:48	2	-30.54	-30.55	-27.85	-30.83	-30.83	-30.50
14 June '84/16:22	1	-28.49	-28.50	-25.78	-28.46	-28.46	-28.05
Range res = 150m; pol = ver							
7 June '84/09:21	1	-30.64	-30.64	-28.40	-30.65	-30.65	-30.38
14 June '84/15:04	3	-27.76	-27.76	-25.41	-28.33	-28.33	-28.12
14 June '84/15:40	2	-28.20	-28.21	-25.81	-28.59	-28.59	-28.30
14 June '84/16:15	1	-27.72	-27.72	-25.43	-27.69	-27.69	-27.42
Range res = 15m; pol = hor							
7 June '84/09:43	1	-28.06	-28.09	-23.04	-28.09	-28.09	-27.07
14 June '84/14:59	3	-28.05	-28.11	-22.67	-28.61	-28.61	-26.94
14 June '84/15:16	2	-28.80	-28.87	-23.47	-29.29	-29.29	-27.81
14 June '84/16:04	1	-28.87	-29.25	-23.90	-28.86	-28.86	-27.35
Range res = 15m; pol = ver							
7 June '84/09:33	1	-28.18	-28.19	-24.20	-28.18	-28.19	-27.55
14 June '84/14:53	3	-28.01	-28.04	-23.93	-28.55	-28.55	-27.44
14 June '84/15:28	2	-28.60	-28.64	-24.45	-29.23	-29.24	-28.27
14 June '84/15:57	1	-28.85	-28.86	-24.56	-28.86	-28.86	-27.82

† Experiment Type

1. High sampling rate, step scan. Prf = 2000 Hz, 1024 pulses/step, dwell time = 0.512 s/step. Azimuth step size = 2°, azimuth re-position time = 15 s/step.
2. Low sampling rate, step scan. Prf = 31.25 Hz, 512 pulses/step, dwell time = 16.38 s/step. Azimuth step size = 2°, azimuth re-position time = 15 s/step.
3. Low sampling rate, continuous scan. Prf = 31.25 Hz, 500 pulses/beamwidth, scan rate = 0.125°/s, dwell time = 16 s/beamwidth.

TABLE C-2

Computations of VHF Repeat Sector Mean Clutter Strength at Beulah, North Dakota
(Repeat sector azimuth extent = 20 deg; range extent = 5.9 km; terrain type = farmland; see Table D-1)

Date/Time (hr:min)	Exp. Type†	$\overline{\sigma^\circ F^4}$ (dB)					
		Non-Coherent Binning of 128 samples/cell			Coherent Integration of 128 samples/cell		
		Upper Bound	Lower Bound	Shadowless	Upper Bound	Lower Bound	Shadowless
Range res = 150m; pol = hor							
10 June '84/05:58	1	-34.30	-34.30	-33.53	-34.18	-34.18	-34.13
10 June '84/07:18	3	-35.07	-35.07	-34.36	-35.12	-35.12	-35.10
10 June '84/07:49	2	-34.26	-34.26	-33.49	-34.42	-34.42	-34.42
13 June '84/10:44	1	-34.06	-34.06	-33.48	-34.12	-34.12	-34.12
13 June '84/18:40	1	-34.70	-34.71	-34.31	-34.72	-34.72	-34.61
Range res = 150m; pol = ver							
10 June '84/05:52	1	-26.73	-26.73	-26.73	-26.78	-26.78	-26.78
10 June '84/07:10	3	-27.43	-27.43	-27.34	-27.50	-27.50	-27.50
10 June '84/07:37	2	-26.90	-26.90	-26.79	-26.95	-26.95	-26.95
10 June '84/10:41	1	-27.16	-27.16	-27.11	-27.17	-27.17	-27.17
13 June '84/18:37	1	-27.35	-27.35	-27.24	-27.34	-27.34	-27.34
Range res = 36m; pol = hor							
10 June '84/05:55	1	-32.74	-33.11	-27.16	-32.98	-32.98	-32.30
10 June '84/07:14	3	-33.99	-34.82	-27.81	-34.34	-34.34	-33.21
10 June '84/07:42	2	-33.11	-33.59	-26.93	-33.49	-33.51	-31.28
10 June '84/10:38	1	-32.32	-32.73	-26.78	-32.65	-32.65	-30.91
Range res = 36m; pol = ver							
10 June '84/05:48	1	-26.81	-26.98	-22.64	-26.92	-26.92	-26.84
10 June '84/07:04	3	-27.91	-28.19	-23.74	-28.10	-28.10	-27.99
10 June '84/07:29	2	-26.85	-27.20	-20.64	-26.95	-26.95	-26.48
10 June '84/10:33	1	-27.24	-27.41	-23.13	-27.33	-27.33	-27.03

† Experiment Type

1. High sampling rate, step scan. Prf = 500 Hz, 1024 pulses/step, dwell time = 2.048 s/step. Azimuth step size = 10°, azimuth re-position time = 15 s/step.
2. Low sampling rate, step scan. Prf = 31.25 Hz, 1920 pulses/step, dwell time = 61.44 s/step. Azimuth step size = 10°, azimuth re-position time = 15 s/step.
3. Low sampling rate, continuous scan. Prf = 31.25 Hz, 2500 pulses/beamwidth, scan rate = 0.125°/s, dwell time = 80 s/beamwidth.

TABLE C-3

Computations of L-Band Repeat Sector Mean Clutter Strength at Peace River South II, Alberta (Repeat sector azimuth extent = 10 deg; range extent = 5.9 km; terrain type = forested river valley and farmland; see Table D-1)

Date/Time (hr:min)	Exp. Type†	$\overline{\sigma^\circ F^4}$ (dB)					
		Non-Coherent Binning of 128 samples/cell			Coherent Integration of 128 samples/cell		
		Upper Bound	Lower Bound	Shadowless	Upper Bound	Lower Bound	Shadowless
Range res = 150m; pol = hor							
15 Oct '83/17:22	1	-19.73	-19.73	-19.53	-19.74	-19.74	-19.74
18 Oct '83/14:40	1	-20.44	-20.44	-20.21	-20.46	-20.46	-20.46
19 Oct '83/13:38	1	-19.78	-19.78	-19.60	-19.80	-19.80	-19.77
20 Oct '83/15:04	1	-20.23	-20.23	-20.07	-20.21	-20.21	-20.21
21 Oct '83/15:44	1	-20.28	-20.28	-20.14	-20.28	-20.28	-20.28
22 Oct '83/14:57	1	-19.58	-19.58	-19.30	-19.62	-19.62	-19.59
28 Oct '83/11:32	1	-20.24	-20.24	-20.13	-20.25	-20.25	-20.23
28 Oct '83/14:51	1	-19.68	-19.68	-19.45	-19.66	-19.66	-19.66
29 Oct '83/14:06	1	-20.36	-20.36	-20.13	-20.35	-20.35	-20.35
31 Oct '83/14:39	1	-19.17	-19.17	-19.04	-19.18	-19.18	-19.18
2 Nov '83/18:57	1	-20.47	-20.47	-20.29	-20.46	-20.46	-20.46

† Experiment Type
1. High sampling rate, step scan. Prf = 2000 Hz, 1024 pulses/step, dwell time = 0.512 s/step. Azimuth step size = 2°, azimuth re-position time = 15 s/step.

In general, in all of the data in Tables C-1 and C-2, there is good repeatability in the results from hour to hour and day to day, and little noticeable effect with increased temporal (type 2 experiments) or spatial (type 3 experiments) averaging.

At occasional sites, we recorded more repeat sector experiments than we allowed ourselves at typical sites such as Beulah. One such site was Peace River South II, a river valley site in northern Alberta. Table C-3 shows mean clutter strength computations for the Peace River repeat sector for all the L-band experiments at 150-m range resolution and horizontal polarization. Across this larger set of repeated experiments we continue to see very close hour-to-hour and day-to-day repeatability in mean clutter strength. For example, the one-sigma value for the noncoherent, all-samples, mean upper bound in Table C-3 is 0.17 dB. The variations in these data include variations in calibration accuracy as well as true variations in the clutter (for example, due to weather-related effects). Day-to-day calibration variations could be studied further through examination of the measured returns from the discrete reference target of opportunity selected at Peace River. Our standard procedures called for the reference target return to be measured each day in each band that was used that day. We do not proceed here with such further investigation of calibration variations in the Peace River data in Table C-3, partly because the variations in Table C-3 are so small. The Phase One history of returns from daily reference targets (often water towers) across all sites is discussed in Appendix A.

Big Grass Marsh, Manitoba, was one of our weak clutter sites where Phase One sensitivity needed to be increased by means of coherent integration to obtain accurate values of repeat sector mean clutter strength. This is illustrated by the L-band data in Table C-4. We see that at low range resolution, the Phase One sensitivity before improvement through integration provides mean bounds separated by as much as 5 dB, but after improvement through integration this separation reduces to 0.13 dB. More dramatically, however, at high range resolution, before integration gain the mean bounds were separated by as much as 22.5 dB, which reduces to 2.8 dB after integration.

TABLE C-4

Computations of L-Band Repeat Sector Mean Clutter Strength at Big Grass Marsh, Manitoba (Repeat sector azimuth extent = 20 deg; range extent = 5.9 km; terrain type = wetland; see Table D-1)

Date/Time (hr:min)	Exp. Type†	$\overline{\sigma^\circ F^4}$ (dB)					
		Non-Coherent Binning of 128 samples/cell			Coherent Integration of 128 samples/cell		
		Upper Bound	Lower Bound	Shadowless	Upper Bound	Lower Bound	Shadowless
Range res = 150m; pol = hor							
4 Feb '84/16:04	1	-66.94	-71.73	-62.59	-69.60	-69.73	-68.97
Range res = 150m; pol = ver							
4 Feb '84/15:59	1	-67.84	-69.15	-63.04	-68.69	-68.71	-68.11
Range res = 15m; pol = hor							
4 Feb '84/16:19	1	-50.97	-73.50	-53.69	-63.38	-66.17	-62.04
Range res = 15m; pol = ver							
4 Feb '84/15:54	1	-55.51	-71.36	-54.22	-66.00	-67.32	-63.53

† Experiment Type
1. High sampling rate, step scan. Prf = 2000 Hz, 1024 pulses/step, dwell time = 0.512 s/step. Azimuth step size = 2°, azimuth re-position time = 15 s/step.

APPENDIX D

TABULATED VALUES OF MEAN AND RATIO OF STANDARD DEVIATION TO MEAN IN REPEAT SECTOR CLUTTER AMPLITUDE DISTRIBUTIONS FOR 49 PHASE ONE SETUPS

LIST OF TABLES

In this appendix, we tabulate values of mean and ratio of standard deviation to mean in repeat sector clutter amplitude distributions across our complete set of 49 Phase One site visits. The results are presented in Tables D-1 through D-6. Table D-1 lists our measurement sites in chronological order of measurement and includes a capsule description of the repeat sector measurement scenario at each site. The five following tables, Tables D-2 through D-6, list the values of mean and ratio of standard deviation to mean in repeat sector clutter amplitude distributions at each of our five Phase One radar frequencies, VHF, UHF, L-, S-, and X-band, respectively. Within each of these five tables, the values of mean and ratio of standard deviation to mean are listed in the same chronological site order as given by Table D-1. For each site visit, values are provided for all Phase One waveforms, that is, at all four combinations of polarization and pulse length where polarization is either horizontal (H) or vertical (V) and pulse length is either long (150 m) or short (15 m or 36 m).

Each pair of numbers for mean and ratio of standard deviation to mean in Tables D-2 through D-6 comes from a repeat sector measurement that has been selected as best (i.e., central) from a group of identically repeated measurements. Elsewhere in this report, we refer to this centrally selected measurement or experiment as the digest experiment, and hence the set of numbers in Tables D-2 through D-6 as our digest repeat sector data set. Most of the values in Tables D-2 through D-6 were obtained from coherent integration of 128 pulses in our pulse-by-pulse calibrated data, collected with the antenna stationary in each beam position (i.e., step scan through the repeat sector). The values provided in Tables D-2 through D-6 are what we refer to as "shadowed upper bound" values that include all samples within the sector including those at radar noise level. These values are almost always identical to two decimal places to lower bound values, so we may almost always regard the values in these tables as not bounds at all but as being precisely accurate to the two decimal places shown and unaffected by included samples at radar noise level. The method of computing these values is explained in detail in Appendix C.

One purpose in presenting the numbers in Tables D-2 through D-6 in chronological order of measurement is that consecutive groups of sites with common hardware problems or data acquisition limitations stand out. For example, in Table D-5 at S-band, in setups 2 through 4 no data were collected because the S-band transmitter was not installed for these site visits; in setups 6 through 11 the data are questionable because of a faulty RF circulator and limiter in the S-band receiver; in setups 13 through 16 no data were collected while replacement parts for this receiver circuitry were being acquired; and in setups 39 through 45 a universal calibration adjustment of +4 dB was required because a broken cable shield caused high VSWRs. Although S-band was our most troublesome frequency band, similar sequences may be observed elsewhere in Tables D-2 through D-6. Usually in this report we present data within groups of sites by common terrain type. In these nonchronological groupings, missing data points can appear to occur rather haphazardly. Reference to Tables D-2 through D-6 can provide contextual information on missing data.

We now explain why there are no results in Tables D-2 through D-6 for setup numbers 1 and 5. First, the purpose of setup number 1, Katahdin Hill (1) at Lincoln Laboratory, was as much to initially check out the Phase One equipment and develop data acquisition procedures as it was to measure clutter. Although we have available calibrated clutter data from Katahdin Hill (1), its formats differ from our standard formats instituted subsequently; and therefore, it has not been convenient for us to analyze these data as yet. However, we revisited Katahdin Hill as our last setup [viz., setup 49, Katahdin Hill (2)], for which we have analyzed the data. Thus, the penalty to this report in not analyzing Katadhin Hill (1) data

is that we did not lose the site but did lose a seasonal revisit. Like Katahdin Hill (1), setup number 5, North Truro, also has no numbers entered in Tables D-2 through D-6. North Truro was principally a sea clutter measurement site on a Cape Cod beachfront cliff overlooking the Atlantic Ocean. Although we acquired ground clutter measurement data in addition to sea clutter, we have not calibrated most of these North Truro ground clutter data. Offsetting the lack of data at North Truro, however, is the fact that, for setup number 21, Plateau Mountain, we have two repeat sectors. Thus, in total we have results tabulated from 42 different repeat sectors, with six seasonal revisits, in Tables D-2 through D-6.

Tables D-2 through D-6 nominally contain 960 (i.e., 48 setups × 20) accurately calibrated and consistently reduced pairs of numbers for mean and ratio of standard deviation to mean in ground clutter spatial amplitude distributions. In totality these numbers provide a wealth of information descriptive of ground clutter amplitude distributions over large spatial regions at near grazing incidence. It is clear from this set of numbers that low-angle ground clutter constitutes a phenomenon of extreme variability. The purpose of this report is to sort through this variability to find general parametric trends that bring order and predictability to the phenomenon.

Repeat sector results from Tables D-2 through D-6 are plotted in various combinations throughout this report. Individual plots of mean strength for each repeat sector (including repeated visits) are provided in Appendix E.

TABLE D-1

Terrain Descriptions of Repeat Sectors in Chronological Order of Measurement

Set-Up No.	Site Name	Dep Ang (deg)	Land-form	Land Cover	Range (km)	Azimuth (deg)
1	Katahdin Hill, Mass.	0.4	5-4	43-21-52	1-6.9	220-250
2	Shilo, Man.	0.2	1-3	21-31	1-10	228-258
3	Neepawa, Man.	-0.9	7-2	21-41	1-10	287-307
4	Polonia, Man.	2.0	7-2	21-41	1-10	107-127
5	North Truro, Mass.	Sea clutter measurement site				
6	Cochrane, Alta.	1.7	7-2	31/32-21/22-41/43-11	1-10	220-240
7	Strathcona, Alta.	1.5	3-2	11-12-51	1-10	62- 82
8	Penhold II, Alta.	0.1	4-2	21-41-11	15-24	54- 74
9	Beiseker, Alta.	0.4	3-2	21-31	8-17	150-170
10	Westlock, Alta.	0.4	3	43-21-62	8-13.9	42- 52
11	Cold Lake, Alta.	0.2	3-7	43-21	5-10.9	120-130
12	Suffield, Alta.	0.3	3-5-9	31-62-52-12	7-12.9	125-135
13	Pakowki Lake, Alta.	0.3	1-3	21-31	1-10	6- 16
14	Orion, Alta.	1.2	3-1	21-31	1-10	186-196
15	Beiseker (2), Alta.	Seasonal revisit				
16	Cochrane (2), Alta.	Seasonal revisit				
17	Brazeau, Alta.	1.2	3	42-62-41	4-9.9	170-180
18	Lethbridge W., Alta.	0.3	3-8	11-12-21	6-11.9	92-102
19	Magrath, Alta.	0.7	3-2	21-33	5-10.9	125-135
20	Waterton, Alta.	-1.8	8-7	42-7-41	9-14.9	175-185
21(a)	Plateau Mt., Alta.	2.3	4	31-32-21	20-40	40- 50
21(b)	Plateau Mt., Alta.	1.2	8	42-7	11-16.7	255-265
22	Picture Butte II, Alta.	0.1	3-8	11-12	22-27.9	172-182
23	Beiseker (3), Alta.	Seasonal revisit				
24	Brazeau (2), Alta.	Seasonal revisit				
25	Puskwaskau, Alta.	2.1	2	43	1-6.9	230-240
26	Peace River S.II, Alta.	-0.1	2-7	21-41	12-17.9	348-358
27	Woking, Alta.	0.2	2-7	43	4-9.9	118-136
28	Beiseker (4), Alta.	Seasonal revisit				
29	Wolseley, Sask.	0.5	3-1	21	6-10	301-311
30	Headingley, Man.	0.04	1	11-12-41	14-19.9	82- 92
31	Altona II, Man.	0.2	1	21-11-14	2.5-8.4	262-272
32	Big Grass Marsh, Man.	0.2	1	62-22	1-6.9	350- 10
33	Gull Lake W., Man.	1.0	1	61-52-43	1-6.9	300-320
34	Spruce Home, Sask.	0.3	1	21-41	3-8.9	40- 50
35	Rosetown Hill, Sask.	0.4	1	21	4-9	45- 65
36	Wainwright, Alta.	0.6	5-3	41-32-31	1-6.9	120-150
37	Dundurn, Sask.	0.2	5	32-41-31	1-6.9	295-325
38	Corinne, Sask.	0.15	1	21	1-8.9	330- 30
39	Gull Lake W. (2), Man.	Seasonal revisit				
40	Sandridge, Man.	0.3	1	41-62-22	1-6.9	298-318
41	Turtle Mt., Man.	0.5	5	41-52	2-7.9	102-122
42	Beulah, N.D.	1.2	2	21	1-6.9	50- 70
43	Knolls, Utah	0.3	1	7-33	3.0-6.5	290-307
44	Booker Mt., Nev.	1.8	3	7-33	12-17.9	125-145
45	Vananda E., Mont.	1.0	3-5	31-32	3.6-9.5	40- 60
46	Wachusett Mt., Mass.	2.1	5-4	43-21-11	8-13.9	156-176
47	Scranton, Penna.	1.0	7-4-3	43-12-11	8-13.9	300-320
48	Blue Knob, Penna.	1.6	4	21-43-11	16-21.9	80-100
49	Katahdin Hill (2), Mass.	Seasonal revisit				

TABLE D-2

Mean and Ratio of Standard Deviation to Mean in VHF Measurements of Repeat Sector Ground Clutter Amplitude Distributions for 49 Phase One Setups

		MEAN (dB)				SD/MEAN (dB)			
No.	SITE NAME (VISIT)	150H	150V	36H	36V	150H	150V	36H	36V
1.	Katahdin Hill(1)[1]	-	-	-	-	-	-	-	-
2.	Shilo	-57.40[2]	-54.10[2]	N/A	-43.66[2]	4.40	4.42	N/A	4.62
3.	Neepawa	-35.19	-30.36	-32.50	-28.21	5.29	4.55	5.97	4.75
4.	Polonia	-40.29	-32.20	-36.71	-29.52	6.60	7.98	10.18	10.77
5.	No. Truro[1]	-	-	-	-	-	-	-	-
6.	Cochrane(1)	-21.00	-13.18[2]	-17.53[2]	N/A	5.60	5.33	6.16	N/A
7.	Strathcona	-5.74	-5.38	-0.76	-3.61	8.69	5.46	7.50	6.54
8.	Penhold II	-24.31	-18.64	-22.77	-15.25	6.34	5.19	5.60	6.14
9.	Beiseker(1)	-29.17	-28.90	-28.62	-26.16	7.15	6.89	8.54	8.22
10.	Westlock	-21.89	-25.38	-20.75	-21.29	0.60	0.06	2.03	3.05
11.	Cold Lake	-20.28	-16.35	-18.72	-15.40	5.67	4.82	7.08	5.77
12.	Suffield	-51.28	-52.85	N/A[3]	-48.27[3]	2.97	2.02	N/A	4.07
13.	Pakowki Lake	-58.67	-60.15	-57.21[3]	-56.11[3]	4.89	4.04	5.79	4.88
14.	Orion	-46.80	-49.48	-46.94[3]	-46.09[3]	3.51	3.08	5.39	5.11
15.	Beiseker(2)	-31.86	-28.96	-30.49[3]	-27.47[3]	7.66	7.69	8.92	9.38
16.	Cochrane(2)	-22.69	-14.38	-21.03[3]	-16.11[3]	5.70	4.38	5.47	5.20
17.	Brazeau(1)	-15.89	-11.51	-12.50	-13.14	1.99	4.10	2.99	2.61
18.	Lethbridge West	N/A[6]	-34.02[4]	N/A[6]	-32.31[4]	N/A	5.33	N/A	8.27
19.	Magrath	-25.28[5]	-32.94	-27.55[5]	-29.62[5]	5.63	4.06	7.02	5.56
20.	Waterton	-9.14[5]	-1.58	-6.45[5]	-2.33[5]	0.86	1.19	2.03	1.78
21A.	Plateau Mountain	-35.42	-27.33	-33.36	-26.48	4.12	4.56	4.80	5.63
21B.	Plateau Mountain	-15.64	-8.45	-14.41	-6.69	2.40	2.60	3.94	3.88
22.	Picture Butte II	-20.92	-19.88	-20.34	-18.73	6.40	6.98	10.00	10.34
23.	Beiseker(3)	-29.33	-29.59	-28.59	-27.72	8.10	7.57	8.77	8.15
24.	Brazeau(2)	-16.50	-15.50	-13.87	-11.55	2.92	1.23	3.68	2.43
25.	Puskwaskau	-14.45	-18.77	N/A[3]	N/A[3]	5.46	6.73	N/A	N/A
26.	Peace River So. II	-20.77	-17.08	-17.87	-15.48	2.27	1.95	1.51	3.48
27.	Woking	-25.50	-24.32	-22.86	-22.12	0.25	2.20	1.13	2.90
28.	Beiseker(4)	-28.30	-24.08	-27.40	N/A	8.23	7.95	8.91	N/A
29.	Wolseley	-66.30	-64.29	-60.54	-58.46	3.20	2.13	2.10	1.89
30.	Headingley	-35.57	N/A[6]	N/A[6]	N/A[6]	5.69	N/A	N/A	N/A
31.	Altona II	-31.46	-31.30	-29.38	-30.29	5.28	5.75	8.66	9.18
32.	Big Grass Marsh	-68.60	-70.48	-66.74	-66.84	1.90	1.49	0.49	1.79
33.	Gull Lake West(1)	-25.21	-28.33	N/A[3]	N/A[3]	3.01	2.75	N/A	N/A
34.	Spruce Home	-49.15	-36.83	-46.89	-35.77	2.66	3.43	2.31	4.22
35.	Rosetown Hill	-55.98	-50.15	-51.81[3]	-46.75[3]	4.58	4.44	5.31	4.76
36.	Wainwright	-27.10	-33.32	-28.59	-29.91	7.04	3.65	4.97	3.20
37.	Dundurn	-42.66	-43.88	-41.68	-41.88	7.05	7.78	7.22	8.07
38.	Corinne	-54.85	-58.52	-52.54	-57.60	8.20	6.62	8.85	7.80
39.	Gull Lake West(2)	-24.73	-30.97	-19.93	-26.93	2.25	2.38	2.39	3.11
40.	Sandridge	-46.08	-45.96	-43.35	-43.87	1.68	3.52	1.86	4.87
41.	Turtle Mountain	-32.80	-31.50	-31.47	-28.95	3.08	2.36	4.40	4.56
42.	Beulah	-34.30	-26.73	-32.98	-26.92	5.82	5.75	6.70	7.97
43.	Knolls	-71.02	-66.63	-63.36	-63.22	-0.10	1.88	5.45	1.48
44.	Booker Mountain	-38.24	-31.51	-35.68	-29.88	3.47	2.94	4.87	5.34
45.	Vananda East	-41.74	-39.21	-38.90	-38.23[3]	6.37	4.09	9.28	5.66
46.	Wachusett Mountain	-17.96	-17.18	-18.09[3]	-16.25[3]	1.97	1.09	2.85	1.65
47.	Scranton	-10.59	-10.48	-7.16	-8.79	4.67	2.09	4.98	2.19
48.	Blue Knob	-10.76	-10.93	-10.99	-9.78	2.54	3.31	3.92	4.49
49.	Katahdin Hill(2)	-23.00	-24.26	-20.30	-21.83	4.58	4.03	7.70	3.91

N/A = Data not available

1. Equipment test sites; ground clutter data not yet analyzed.
2. Survey data used.
3. VHF external interference; data may be questionable.
4. Antenna drive motor interference; questionable data.
5. Inconsistent clutter data; questionable.
6. Hardware problems.

TABLE D-3

Mean and Ratio of Standard Deviation to Mean in UHF Measurements of Repeat Sector Ground Clutter Amplitude Distributions for 49 Phase One Setups

		MEAN (dB)				SD/MEAN (dB)			
No.	SITE NAME (Visit)	150H	150V	36H	36V	150H	150V	36H	36V
1.	Katahdin Hill(1)[1]	-	-	-	-	-	-	-	-
2.	Shilo	-46.48	-40.29[2]	-45.24[2]	-53.89	6.48	6.25	8.97	6.44
3.	Neepawa	-26.15	-20.68	-24.13	-18.98	5.43	5.67	7.19	7.51
4.	Polonia	-32.24	-25.83	-28.49	-21.81	5.93	6.81	8.38	8.06
5.	No. Truro[1]	-	-	-	-	-	-	-	-
6.	Cochrane(1)	-18.80	-21.26[2]	-19.19[2]	Q[2]	6.89	5.27	10.58	-
7.	Strathcona	-15.87	-13.73	-13.05	-12.61	7.78	9.18	8.33	8.58
8.	Penhold II	-15.44	-16.27	-13.71	-13.82	5.74	4.81	8.58	6.25
9.	Beiseker(1)	-39.00	-36.81	-38.71	-35.05	5.36	6.62	7.79	7.97
10.	Westlock	-27.15	-25.34	-25.78	-25.28	4.15	6.16	4.40	5.68
11.	Cold Lake	-21.41	-18.45	-18.94	-16.65	4.93	4.08	4.73	4.25
12.	Suffield	-36.80	-33.22	-35.16	-32.39	6.04	6.34	7.59	8.25
13.	Pakowki Lake	-46.35	-39.59	-43.18	-37.15	4.07	7.69	5.78	10.43
14.	Orion	-38.68	-34.90	-38.46	-35.18	6.71	6.67	8.13	7.06
15.	Beiseker(2)	-40.91	-35.30	-38.37	-34.21	5.15	6.45	7.30	8.07
16.	Cochrane(2)	-20.80	-19.14	-18.71	-18.20	6.17	5.65	7.27	6.73
17.	Brazeau(1)	-15.86	-16.13	-15.54	-13.45	3.27	2.26	5.27	5.08
18.	Lethbridge West	-12.15	-13.52	-11.74	-12.87	8.69	9.06	11.80	11.93
19.	Magrath	-30.20	-28.72	-26.54	-29.54	5.12	5.53	8.72	7.50
20.	Waterton	-11.97	-10.15	-9.92	-7.69	2.39	1.73	3.48	3.74
21A.	Plateau Mountain	-33.11	-31.07	-32.33	-30.36	5.85	5.76	7.15	7.24
21B.	Plateau Mountain	-14.15	-11.11	-13.50	-8.38	4.94	5.54	7.12	6.54
22.	Picture Butte II	-17.10	-14.76	-16.13	-13.66	7.73	7.45	10.51	10.13
23.	Beiseker(3)	-38.45	-33.62	-36.52	-31.67	5.49	6.14	6.70	8.17
24.	Brazeau(2)	-15.02	-14.74	-12.87	-11.68	3.74	3.66	5.56	5.17
25.	Puskwaskau	-22.24	-19.14	-22.48	-18.41	3.73	4.07	4.74	5.32
26.	Peace River So. II	-21.10	-17.70	-17.65	-15.69	2.93	3.53	4.60	4.26
27.	Woking	-15.22	-18.71	-15.48	-17.01	2.40	2.63	4.49	4.00
28.	Beiseker(4)	-37.26	-34.45	-35.29	-32.98	5.49	5.35	9.10	7.53
29.	Wolseley	-44.19	-39.54	-42.82	-37.38	4.74	4.53	6.51	6.43
30.	Headingley	-25.66	-20.47	-20.83	-18.76	7.29	7.42	11.86	11.79
31.	Altona II	-28.76[3]	-31.64[3]	-25.34[3]	-27.95[3]	5.43	5.91	7.67	8.15
32.	Big Grass Marsh	-76.12	-74.36	-73.75	-73.51	3.37	4.39	4.05	3.67
33.	Gull Lake West(1)	-31.61	-27.64	-30.65	-27.17	3.49	4.16	4.33	5.53
34.	Spruce Home	-32.32	-27.32	-31.27	-27.12	5.50	5.47	7.19	6.00
35.	Rosetown Hill	-41.32	-37.35	-40.95	-35.50	7.43	8.72	9.59	10.01
36.	Wainwright	-31.99	-31.48	-29.07	-29.18	4.37	3.68	8.16	6.45
37.	Dundurn	-48.33	-47.69	-47.07	-46.87	6.43	4.82	6.46	5.94
38.	Corinne	-46.09	-48.69	-45.46	-46.72	11.33	10.67	13.27	12.56
39.	Gull Lake West(2)	-25.63	-27.05	-26.54	-20.98	5.30	3.88	4.56	5.49
40.	Sandridge	-38.66	-41.30	-34.18	-37.34	2.59	2.46	2.96	3.14
41.	Turtle Mountain	-30.80	-29.69	-29.68	-29.75	6.08	5.44	6.82	6.93
42.	Beulah	-29.93	-31.46	-31.27	-30.51	6.90	5.69	8.25	7.22
43.	Knolls	-74.39	-74.29	-73.26	-72.56	1.77	2.10	3.36	1.65
44.	Booker Mountain	-44.30	-38.29	-42.62	-37.04	5.54	4.44	9.95	7.83
45.	Vananda East	-38.89	-40.77	-38.12	-39.87	6.58	5.87	8.55	7.79
46.	Wachusett Mountain	-24.59[3]	-23.91[3]	-24.88[3]	-23.61[3]	2.87	2.17	3.23	2.59
47.	Scranton	-13.01	-12.93	-14.17	-12.87	3.67	3.09	4.19	3.02
48.	Blue Knob	-18.61	-18.70	-18.13	-18.06	2.97	3.00	5.36	4.42
49.	Katahdin Hill(2)	-32.13	-33.97	-29.12	-29.67	4.39	3.71	5.72	4.76

N/A = Data not available

Q = Questionable data.

1. Equipment test sites; ground clutter data not yet analyzed.
2. Survey data used.
3. UHF external interference; data may be questionable.

TABLE D-4

Mean and Ratio of Standard Deviation to Mean in L-Band Measurements of Repeat Sector Ground Clutter Amplitude Distributions for 49 Phase One Setups

		MEAN (dB)				SD/MEAN (dB)			
No.	SITE NAME (Visit)	150H	150V	15H	15V	150H	150V	15H	15V
1.	Katahdin Hill(1)[1]	-	-	-	-	-	-	-	-
2.	Shilo	-34.05	-31.09	-33.01	-29.54	9.18	8.55	14.50	12.96
3.	Neepawa	-25.96	-21.19	-22.87	-20.28	6.69	7.49	9.84	9.08
4.	Polonia	-30.83	-28.42	-25.97	-27.76	5.58	5.00	7.22	8.07
5.	No. Truro[1]	-	-	-	-	-	-	-	-
6.	Cochrane(1)	-24.91	-26.15	-21.95[4]	-24.31	6.12	5.05	7.31	6.62
7.	Strathcona	-16.89	-11.80	-14.30	-15.81	8.24	7.18	10.14	8.92
8.	Penhold II	-27.94	-25.85	-26.24	-25.61	5.06	4.78	6.39	6.54
9.	Beiseker(1)	-29.00	-27.90	-28.42	-26.53	6.53	11.08	10.66	14.80
10.	Westlock	-29.00	-28.13	-25.63	-27.24	2.98	4.22	5.15	4.72
11.	Cold Lake	-25.62	-24.71	-22.68	-22.93	3.74	3.32	4.20	4.22
12.	Suffield	-24.96	-26.12	-23.92	-22.29	9.83	10.69	12.55	13.65
13.	Pakowki Lake	-29.34	-30.05	-25.98	-25.60	6.39	6.68	9.22	8.90
14.	Orion	-32.11	-33.93	-30.53	-30.97	10.71	7.60	12.03	9.07
15.	Beiseker(2)	-34.50	-32.51	-28.79	-29.45	9.04	9.90	10.73	15.67
16.	Cochrane(2)	-19.28	-20.11	Q[2]	-19.19	5.75	5.20	-	7.07
17.	Brazeau(1)	-23.28	-20.54	-22.55	-20.99	3.73	3.71	3.89	3.21
18.	Lethbridge West	- 4.27	- 8.94	- 5.16	- 8.29	9.14	9.55	13.05	13.10
19.	Magrath	-25.92	-28.01	-27.40	-29.94	7.63	7.80	10.03	9.39
20.	Waterton	-16.38	-17.14	-14.57	-15.06	1.69	2.44	2.85	2.66
21A.	Plateau Mountain	-29.56	-31.94	N/A[3]	N/A[3]	7.03	4.42	N/A	N/A
21B.	Plateau Mountain	-18.98	-19.32	-18.36	-17.83	4.25	4.41	4.02	4.66
22.	Picture Butte II	- 9.92	- 9.39	- 9.69	- 8.76	8.80	8.23	10.93	10.73
23.	Beiseker(3)	-31.92	-29.34	-31.42	-29.39	6.90	10.62	8.47	13.12
24.	Brazeau(2)	-19.70	-19.11	-19.54	-19.14	3.66	3.53	5.20	3.91
25.	Puskwaskau	-20.66	-24.86	-24.81	-22.76	2.96	1.29	3.90	4.01
26.	Peace River So. II	-19.73	-20.41	-20.97	-20.95	3.61	4.72	5.74	6.01
27.	Woking	-22.57	-21.67	-21.85	-20.63	3.08	3.07	2.85	2.51
28.	Beiseker(4)	-28.21	-25.44	-27.39	-26.05	7.10	9.83	10.93	14.49
29.	Wolseley	-38.03	-37.10	-38.35	-36.88	4.82	5.64	8.00	8.51
30.	Headingley	-16.07	-15.67	-16.20	-13.45	6.69	6.91	10.71	11.28
31.	Altona II	-16.04	-20.32	-10.40	-16.42	6.25	6.16	9.95	9.33
32.	Big Grass Marsh	-69.60	-68.69	-63.38	-66.00	5.67	6.20	3.20	8.41
33.	Gull Lake West(1)	-30.37	-27.87	-28.21	-26.60	3.91	4.11	7.24	7.65
34.	Spruce Home	-24.75	-25.47	-24.07	-24.77	4.69	4.83	6.25	6.30
35.	Rosetown Hill	-30.97	-30.67	-29.86	-29.55	7.89	7.48	11.37	10.79
36.	Wainwright	-30.37	-29.66	-27.78	-27.49	2.85	2.96	3.98	3.85
37.	Dundurn	-42.55	-43.65	-42.63	-43.50	7.04	5.38	8.92	7.63
38.	Corinne	-33.85	-35.15	-32.26	-34.13	10.34	10.41	12.66	11.70
39.	Gull Lake West(2)	-22.30	-24.08	-27.98	-24.27	5.31	4.04	6.09	5.72
40.	Sandridge	-37.71	-40.19	-33.76	-38.33	3.87	3.13	6.51	9.04
41.	Turtle Mountain	-33.10	-31.48	-31.30	-30.08	5.47	4.49	5.90	6.14
42.	Beulah	-30.07	-30.64	-28.06	-28.18	6.29	5.24	8.27	7.16
43.	Knoils	-71.52	-74.90	-63.96	-68.61	4.41	8.29	0.20	-0.24
44.	Booker Mountain	-39.86	-39.49	-39.90	-38.98	6.41	6.98	10.34	11.12
45.	Vananda East	-39.50	-40.34	-39.17	-39.76	4.80	3.64	7.99	6.72
46.	Wachusett Mountain	-26.75	-26.10	-26.62	-25.68	2.09	1.86	2.62	2.73
47.	Scranton	-16.83	-16.81	-16.74	-16.29	5.02	3.28	5.16	3.90
48.	Blue Knob	-20.60	-20.34	-20.15	-19.48	6.74	3.16	10.43	7.04
49.	Katahdin Hill(2)	-30.70	-30.88	-30.63	-28.91	4.43	5.88	6.13	6.26

N/A = Data not available

1. Equipment test sites; ground clutter data not yet analyzed.
2. Hardware problem; data questionable.
3. Data not collected with this waveform.
4. Survey data used.

TABLE D-5

Mean and Ratio of Standard Deviation to Mean in S-Band Measurements of Repeat Sector Ground Clutter Amplitude Distributions for 49 Phase One Setups

No.	SITE NAME (Visit)	MEAN (dB)				SD/MEAN (dB)			
		150H	150V	15H	15V	150H	150V	15H	15V
1.	Katahdin Hill(1)[1]	-	-	-	-	-	-	-	-
2.	Shilo	N/A	N/A	N/A	N/A	N/A	N/A	N/A	N/A
3.	Neepawa	N/A	N/A	N/A	N/A	N/A	N/A	N/A	N/A
4.	Polonia	N/A	N/A	N/A	N/A	N/A	N/A	N/A	N/A
5.	No. Truro[1]	-	-	-	-	-	-	-	-
6.	Cochrane(1)	Q[2]	Q[2]	Q[2]	Q[2]	-	-	-	-
7.	Strathcona	Q[2]	Q[2]	Q[2]	Q[2]	-	-	-	-
8.	Penhold II	Q[2]	Q[2]	Q[2]	Q[2]	-	-	-	-
9.	Beiseker(1)	Q[2]	Q[2]	N/A[2]	Q[2]	-	-	-	-
10.	Westlock	Q[2]	Q[2]	Q[2]	Q[2]	-	-	-	-
11.	Cold Lake	Q[2]	Q[2]	Q[2]	Q[2]	-	-	-	-
12.	Suffield	-25.25	-29.86	-22.76	-27.80	9.98	9.87	15.86	13.90
13.	Pakowki Lake	N/A[2]	N/A[2]	N/A[2]	N/A[2]	N/A	N/A	N/A	N/A
14.	Orion	N/A[2]	N/A[2]	N/A[2]	N/A[2]	N/A	N/A	N/A	N/A
15.	Beiseker(2)	N/A[2]	N/A[2]	N/A[2]	N/A[2]	N/A	N/A	N/A	N/A
16.	Cochrane(2)	N/A[2]	N/A[2]	N/A[2]	N/A[2]	N/A	N/A	N/A	N/A
17.	Brazeau(1)	-29.42	-26.93	-31.17	-29.25	3.55	4.71	4.58	4.82
18.	Lethbridge West	-10.05	-8.19	-12.65	-10.07	8.03	8.63	12.08	11.25
19.	Magrath	-35.43	-30.57	-36.41	-32.54	5.90	6.95	7.78	8.50
20.	Waterton	-18.08	-17.23	-19.54	-19.02	3.22	3.15	4.17	3.82
21A.	Plateau Mountain	-37.37	-32.24	N/A[3]	N/A[3]	5.86	6.91	N/A	N/A
21B.	Plateau Mountain	-24.65	-23.29	-25.30	-24.76	7.25	6.30	6.94	7.01
22.	Picture Butte II	-15.08	-10.08	-14.90	-9.78	9.45	9.42	14.11	14.43
23.	Beiseker(3)	-30.57	-29.02	-32.85[4]	-30.43[4]	5.50	5.37	6.37	6.99
24.	Brazeau(2)	-28.67	-27.72	-29.23	-28.13	3.48	4.63	5.99	4.86
25.	Puskwaskau	-34.27	-31.71	-35.29	-32.58	2.53	2.99	3.99	3.57
26.	Peace River So. II	-24.88	-22.91	-25.22	-24.40	4.59	4.84	9.24	6.56
27.	Woking	-25.60	-21.27	-25.24	-24.07	2.35	1.77	3.03	2.41
28.	Beiseker(4)	-30.62	-27.20	-35.37[4]	-31.57[4]	10.25	10.66	8.36	9.45
29.	Wolseley	-28.99	-26.30	-30.55	-29.24	8.10	7.89	11.97	10.78
30.	Headingley	-15.09	N/A[2]	-16.73	N/A[2]	11.15	N/A	14.95	N/A
31.	Altona II	-9.20	-7.72	-10.83	-9.38	11.47	11.04	15.27	14.11
32.	Big Grass Marsh	-49.15	-48.71	-51.99	-52.81	7.34	6.97	12.21	11.98
33.	Gull Lake West(1)	-36.16	-33.98	-35.68	-31.81	5.91	5.19	7.00	8.55
34.	Spruce Home	-26.67	-23.72	-26.60	-24.94	6.78	8.06	9.11	8.66
35.	Rosetown Hill	-34.20	-33.55	-34.97	-33.21	9.13	9.48	13.69	13.41
36.	Wainwright	-32.04	-29.52	-30.81	-28.18	3.86	3.66	5.30	4.99
37.	Dundurn	-40.70	-40.45	-43.59	-41.36	6.55	6.27	8.27	8.09
38.	Corinne	-26.95	-25.95	-33.37[4]	-31.32[4]	12.50	12.41	13.99	13.75
39.	Gull Lake West(2)	-32.16[5]	-31.42[5]	-32.42[5]	-30.15[5]	9.26	4.48	8.34	7.88
40.	Sandridge	-37.28[5]	-34.76[5]	-36.64[5]	-34.63[5]	4.06	3.67	7.13	6.80
41.	Turtle Mountain	-35.36[5]	-32.67[5]	-34.78[5]	-31.68[5]	4.62	4.14	6.14	6.15
42.	Beulah	-32.91[5]	-30.11[5]	-34.67[5]	-32.37[5]	5.71	6.43	8.32	7.48
43.	Knolls	-56.05[5]	-56.82[5]	-57.43[5]	-58.45[5]	8.71	7.10	11.14	7.41
44.	Booker Mountain	-41.23[5]	-37.78[5]	-41.86[5]	-39.11[5]	1.78	1.46	3.00	2.12
45.	Vananda East	-38.09[5]	-35.76[5]	-37.50[5]	-35.09[5]	2.93	2.66	5.14	4.38
46.	Wachusett Mountain	-27.70	-25.42	-28.98	-26.10	2.68	3.16	4.49	3.78
47.	Scranton	-20.53	-20.22	-23.05	-20.44	4.68	3.30	7.36	5.93
48.	Blue Knob	-27.99	-24.15	-28.59	-24.46	4.61	4.59	7.15	9.56
49.	Katahdin Hill(2)	-32.97	-29.93	-32.49	-29.23	4.85	5.62	6.72	6.25

N/A = Data not available.

Q = Questionable data.

1. Equipment test sites; ground clutter data not yet analyzed.
2. Hardware problem.
3. Data not collected with this waveform.
4. S-band thin-pulse range extent shorter than all other waveforms.
5. S-band means adjusted by +4dB (calibration shift because of hardware problem).

TABLE D-6

Mean and Ratio of Standard Deviation to Mean in X-Band Measurements of Repeat Sector Ground Clutter Amplitude Distributions for 49 Phase One Setups

No.	SITE NAME (Visit)	MEAN (dB)				SD/MEAN (dB)			
		150H	150V	15H	15V	150H	150V	15H	15V
1.	Katahdin Hill(1)[1]	-	-	-	-	-	-	-	-
2.	Shilo	-34.88	-32.28	-32.52	-29.00	6.76	2.62	10.01	11.45
3.	Neepawa	-28.21	N/A	N/A	N/A	6.38	N/A	N/A	N/A
4.	Polonia	-28.77[3]	-27.28[3]	-29.41[3]	-36.00[3]	8.26	7.08	10.46	8.20
5.	No. Truro[1]	-	-	-	-	-	-	-	-
6.	Cochrane(1)	Q[2]	N/A[2]	N/A[2]	N/A[2]	-	N/A	N/A	N/A
7.	Strathcona	Q[2]	Q[2]	N/A[2]	N/A[2]	-	-	N/A	N/A
8.	Penhold II	Q[2]	N/A[2]	N/A[2]	N/A[2]	-	N/A	N/A	N/A
9.	Beiseker(1)	-31.61	-29.50	-32.07	-29.24	5.49	5.30	7.53	13.08
10.	Westlock	-30.45	-28.60	-29.87	-29.14	5.05	4.26	7.59	6.62
11.	Cold Lake	-24.97	-23.94	-24.01	-23.61	4.39	5.15	4.90	5.30
12.	Suffield	-21.85	-23.97	-23.13	-21.49	10.57	11.00	15.44	15.75
13.	Pakowki Lake	-29.30	-28.48	-27.93	-26.41	7.39	5.73	9.67	8.52
14.	Orion	-33.97	-32.35	-33.44	-31.63	6.07	6.68	10.10	11.28
15.	Beiseker(2)	-30.34	-28.18	-28.97	-27.45	5.27	5.44	6.64	8.59
16.	Cochrane(2)	-20.84[3]	-20.51[3]	-20.53[3]	-19.37[3]	7.32	7.47	9.51	6.37
17.	Brazeau(1)	-26.86	-26.08	-27.17	-25.94	3.60	3.90	5.20	5.54
18.	Lethbridge West	-11.86	-10.75	-10.32	-9.46	7.18	6.97	11.26	11.45
19.	Magrath	-32.41	-28.47	-33.08	-28.69	5.06	5.27	6.31	5.95
20.	Waterton	-21.91	-21.30	-22.10	-21.14	3.63	3.60	4.05	4.20
21A.	Plateau Mountain	N/A[2]	N/A[2]	N/A[2]	N/A[2]	N/A	N/A	N/A	N/A
21B.	Plateau Mountain	N/A[2]	N/A[2]	N/A[2]	N/A[2]	N/A	N/A	N/A	N/A
22.	Picture Butte II	N/A[2]	N/A[2]	N/A[2]	N/A[2]	N/A	N/A	N/A	N/A
23.	Beiseker(3)	N/A[2]	N/A[2]	N/A[2]	N/A[2]	N/A	N/A	N/A	N/A
24.	Brazeau(2)	N/A[2]	N/A[2]	N/A[2]	N/A[2]	N/A	N/A	N/A	N/A
25.	Puskwaskau	N/A[2]	N/A[2]	N/A[2]	N/A[2]	N/A	N/A	N/A	N/A
26.	Peace River So. II	-26.54	-24.83	-27.09	-25.06	4.06	4.38	6.13	7.58
27.	Woking	-26.33	-23.93	-27.34	-25.68	1.45	1.46	2.33	2.41
28.	Beiseker(4)	-30.96	-28.30	-32.04	-28.29	6.06	5.49	7.40	6.92
29.	Wolseley	-34.16	-31.46	-34.78	-31.02	5.71	5.30	8.69	8.84
30.	Headingley	-9.11	-4.83	-8.89	-6.55	9.40	8.72	15.45	13.48
31.	Altona II	-13.40	-13.35	-15.39	-13.24	9.00	8.58	12.34	12.58
32.	Big Grass Marsh	-44.70	-40.70	-42.73	-41.32	6.23	8.19	10.46	10.22
33.	Gull Lake West(1)	-32.32	-31.37	-31.50	-30.96	5.71	5.47	7.27	6.68
34.	Spruce Home	-26.76	-25.13	-26.39	-24.78	8.24	8.59	9.40	9.84
35.	Rosetown Hill	-34.37	-32.96	-34.70	-30.65	9.96	9.55	10.67	11.94
36.	Wainwright	-30.02	-27.48	-29.07	-27.31	3.03	2.80	4.90	5.03
37.	Dundurn	-35.73	-34.62	-36.94	-35.13	6.08	5.25	7.70	7.56
38.	Corinne	-22.55	-26.50	-27.74	Q	14.04	10.52	15.95	-
39.	Gull Lake West(2)	-26.13	-26.51	-26.86	-26.30	7.41	3.99	9.14	6.05
40.	Sandridge	-37.64	-35.49	-35.31	-33.77	3.35	3.97	5.42	5.55
41.	Turtle Mountain	-30.14	-29.07	-29.55	-27.94	4.08	4.55	5.69	5.53
42.	Beulah	-27.04	-24.75	-27.52	-25.01	7.88	6.62	10.88	8.52
43.	Knolls	-42.48	-41.38	-43.13	-41.48	2.89	1.92	4.30	4.20
44.	Booker Mountain	-25.65	-23.05	-26.72	-24.20	0.29	0.29	0.64	0.63
45.	Vananda East	-27.71	-25.45	-27.47	-25.57	1.51	1.56	3.19	2.74
46.	Wachusett Mountain	-21.69[3]	-20.10[3]	-22.05[3]	-19.62[3]	3.68	2.81	4.01	3.83
47.	Scranton	-19.98	-17.91	-19.85	-18.27	4.13	3.58	6.09	6.10
48.	Blue Knob	-24.50	-19.00	-23.48	-20.75	4.51	4.83	7.82	7.29
49.	Katahdin Hill(2)	-31.46	-30.60	-32.57	-31.47	4.90	4.69	5.91	6.20

N/A = Data not available

Q = Questionable data

1. Equipment test sites; ground clutter data not yet analyzed.

2. Hardware problem.

3. Two-way vertical beam correction > 10 dB

REFERENCES

1. J.B. Billingsley and J.F. Larrabee, "Measured spectral extent of L- and X-band radar reflections from wind-blown trees," MIT Lincoln Laboratory, Lexington, Mass., Project Report CMT-57 (6 February 1987). DTIC AD-A179942/8.

2. S. Ayasli, "Propagation effects on radar ground clutter," *Proc. IEEE National Radar Conference*, IEEE Aerospace and Electronic Systems Society and the IEEE Los Angeles Council, Los Angeles, Calif. (12–13 March 1986).

3. H.C. Chan, "Radar sea-clutter at low grazing angles," *Proc. Inst. Electr. Eng.* **137,** 102–112 (1990).

4. S. Ayasli, (private communication, 1990).

5. E. Jakeman, "On the statistics of K-distributed noise," *J. Phys. A* **13,** 31–48 (1980).

6. S. Watts and K.D. Ward, "Spatial correlation in K-distributed sea clutter," *Proc Inst. Electr. Eng.* **134,** 526–531 (1987).

7. S. Ayasli, "SEKE: A computer model for low-altitude radar propagation over irregular terrain," *IEEE Trans. Antenna Propag.* **AP-34,** 1013–1023 (1986).

REPORT DOCUMENTATION PAGE

Form Approved
OMB No. 0704-0188

1. AGENCY USE ONLY (*Leave blank*)	2. REPORT DATE	3. REPORT TYPE AND DATES COVERED
	15 November 1991	Technical Report

4. TITLE AND SUBTITLE

Multifrequency Measurements of Radar Ground Clutter at 42 Sites

5. FUNDING NUMBERS

C — F19628-90-C-0002

6. AUTHOR(S)

J. Barrie Billingsley and John F. Larrabee

7. PERFORMING ORGANIZATION NAME(S) AND ADDRESS(ES)

Lincoln Laboratory, MIT
P.O. Box 73
Lexington, MA 02173-9108

8. PERFORMING ORGANIZATION REPORT NUMBER

TR-916
Volume 2: Appendices A through D

9. SPONSORING/MONITORING AGENCY NAME(S) AND ADDRESS(ES)

Department of the Air Force
SAF/AQL
The Pentagon
Washington, D.C. 20330

10. SPONSORING/MONITORING AGENCY REPORT NUMBER

ESD-TR-91-175

11. SUPPLEMENTARY NOTES

None

12a. DISTRIBUTION/AVAILABILITY STATEMENT

Approved for public release; distribution is unlimited.

12b. DISTRIBUTION CODE

13. ABSTRACT (*Maximum 200 words*)

This report determines how ground clutter strength varies with RF frequency from VHF to X-band in ground-sited radar. This determination is accomplished by providing extensive empirical results from multifrequency clutter measurements conducted at 42 different sites widely dispersed over the North American continent. These results indicate that the frequency dependence of ground clutter strength depends upon terrain type and can vary, for example, from a strongly decreasing function of frequency in forest to a strongly increasing function of frequency in farmland. Five major terrain categories are defined that encompass this dependence, namely, urban, mountains, forest, farmland, and desert. Within each terrain category, results are also shown to be dependent upon the relief or roughness of the terrain and upon the depression angle at which the terrain is illuminated. The depression angle dependence is important, even for the very low angles (typically within a degree of grazing incidence) and small (typically fractional) variations in angle that occur in ground-sited radar. This report presents specific clutter strength results at each of five frequencies (VHF, UHF, L-, S-, and X-band) from each of the 42 sites at which measurements were conducted. The report then combines results from similar sites to obtain the general dependence of clutter strength versus frequency for each terrain category. Clutter strengths are described in terms of moments (including the mean) and percentile levels (including the median) in measured clutter amplitude distributions resulting from cell-by-cell spatial variation over a selected large kilometer-sized macroregion of terrain at each site called the repeat sector. Measurements over the repeat sector at each site were repeated a number of times to increase the reliability of the results. In addition to determining the frequency dependence of ground clutter strength in various terrain types, this report determines dependencies of clutter strength with radar polarization and resolution and specifies long-term temporal variability of clutter strength with weather and season. The report includes descriptions of the clutter measurement equipment and measurement procedures, provides calibration results, and describes the resultant multifrequency ground clutter measurement data bases that are now maintained at Lincoln Laboratory.

14. SUBJECT TERMS				15. NUMBER OF PAGES
radar ground clutter	terrain reflectivity	land clutter	radar clutter	758
clutter measurements	low-angle	backscatter	electromagnetic propagation	16. PRICE CODE
clutter models	multifrequency	multipath		

17. SECURITY CLASSIFICATION OF REPORT	18. SECURITY CLASSIFICATION OF THIS PAGE	19. SECURITY CLASSIFICATION OF ABSTRACT	20. LIMITATION OF ABSTRACT
Unclassified	Unclassified	Unclassified	None